Long-pulse Supercontinuum Light Sources

Moselund, Peter M.

Publication date:
2009

Document Version
Publisher's PDF, also known as Version of record

Long-pulse Supercontinuum Light Sources

Peter M. Moselund

July 31st 2009

DTU Fotonik
Department of Photonics Engineering

DTU Fotonik
Department of Photonics Engineering
Technical University of Denmark
Ørsteds Plads 345V
DK-2800 Kgs. Lyngby
Denmark

Contents

Preface

The present thesis describes the results of scientific research carried out as part of my Ph.D. project in the period April 1st 2006–August 14th 2008 and December 14th 2008–July 31st 2009. From August 14th 2008 to December 14th 2008 I was on leave while working at NKT Photonics as a research engineer in the supercontinuum development group.

The research took place at DTU Fotonik - Department of Photonics Engineering, Technical University of Denmark, and at NKT Photonics A/S. The project was financed by the Photonics Academy Denmark and supervised by

- Ole Bang, Head of Fiber Sensors & Supercontinuum, Associate Professor, Ph.D., DTU Fotonik, Technical University of Denmark, Kgs. Lyngby

- Carsten L Thomsen, Product Development Manager, Ph.D., NKT Photonics A/S, Birkerød

Acknowledgements

I would first like to thank my supervisors, Ole Bang, DTU Fotonik, Carsten L. Thomsen, NKT Photonics, and Claus F. Petersen, who was my supervisor at NKT Photonic during the first year of my project, for support, guidance, advice, and help in many ways throughout this project.

I would also like to thank the many others who have helped and supported me in my work. At NKT Photonics, where most of the practical work took place, I thank the supercontinuum development team for much help and support, particularly Frederik D. Nielsen for help with building a solid state laser in the beginning of the project and solving all sorts of practical problems since then, and Thomas Feuchter and especially Thomas Vestergaard Andersen for many fruitful discussions and help in the laboratory. I also thank Danny Noordegraaf, also at NKT Photonics, for help with using the tapering equipment, Lars H. Frandsen, now at NKT Photonics, for taking scanning electron images for me, while he was at DTU Fotonik, until I was trained to do it myself, and everyone else at NKT Photonics for

helping me and being great colleagues. From DTU, I thank Peter Tidemand-Lichtenberg, DTU Physics, for help with building a solid state laser in the beginning of this project, Lara Scolari for introducing me to the process of tapering PCFs on a Vytran machine and shared my frustrations with the many hardware problems, Peter John Roberts for assistance in calculating the mode mixing in tapered PCFs, Kristian Nielsen and Michael H. Frosz for introducing me to COMSOL calculation of fiber characteristics and Per D. Rasmussen, who did great work on the development of the supercontinuum simulation code and developed the Comsol scripts used for calculation of fiber dispersion profiles. Everyone else at DTU Fotonik who has helped me and made my working life happier also deserve thanks, especially the people at the DTU Fotonik Friday Bar, who were always easy to convince to stay for a late night beer and a long talk if I made out of the labs on a Friday. Finally Michael H. Frosz again deserves a special thanks for countless discussions on supercontinuum generation and for continuously supporting my experimental investigations with numerical simulations. I thank those, whom I have forgotten here, but whose contribution has nonetheless helped me in my daily life and work. A special thanks goes to Rebecca B. Ettlinger for loving support throughout this project and extensive proof-reading of this thesis as well as all the papers which I have published as part of the PhD. Also a special thanks goes to my family and my friends who have supported me through the project and put up with my being mostly stressed and busy for the last three years.

Note for the reader

Many acronyms are used in this document, and I would therefore like to call the reader's attention to the list of acronyms on page 114, which may be an aid to the reader. An electronic version of document is available by request to `pmm@com.dtu.dk`.

Peter M. Moselund, July 31st 2009

Abstract

A wide and continuous optical spectrum generated from a spectrally narrow light source through nonlinear effects is known as a supercontinuum (SC). This thesis describes how a SC can be generated in a photonic crystal fiber (PCF) using picosecond pump pulses and how one may modify its spectral shape by either seeding the generation with other wavelengths or modifying the dispersion properties of the PCF.

Seeding is performed by sending back part of the output continuum and time matching it with the pump pulse. Using this method we show that a higher order four-wave mixing gain band can be seeded in order to produce strong peaks in the output SC. We investigate how this effect depends on the spectrum of the seed and exact time matching with the pump as well as on pump power and find that seeding also can modify the dispersive wave generation in the SC. We show that at low pump powers the seed can be used to greatly reduce amplitude noise in the SC but that this noise reduction is relatively small at high pump powers. We also investigate seeding of modulation instability (MI) with a Raman gain peak at high powers and show that this does not reduce amplitude noise.

Subsequently we investigate how the dispersion profile of the PCF affects the spectrum and noise in the SC. We show that the extent of the visible end of the generated SC depends on the extent of the infrared end and that this can be limited by a second zero dispersion wavelength (ZDW), a slow-down of the soliton red shift, or the infrared absorption edge of silica. It is shown that in order to maximize the extension of the visible spectrum, the group velocity at the infrared end has to be as low as possible. However, designs which achieve this have low conversion efficiency from pump light to visible light because the ZDW is shifted away from the pump. Long tapered PCFs may improve the conversion efficiency but their production has previously been expensive. We demonstrate how an SC may be generated in short tapers, made using compact equipment and off-the-shelf PCFs. We investigate what design parameters of the taper affects the spectrum, noise and efficiency of the generated SC and show that a short PCF taper in a 50 cm fiber can generate light down to 400 nm with considerably lower noise and much shorter output pulses than a conventional SC source based on longitudinally uniform PCFs.

Resumé (Danish abstract)

Superkontinuum lyskilder med lange pulser

Fra en spektralt smal lyskilde kan der gennem ikke-liniære effekter opstå et bredt kontinuert spektrum af lys; dette kaldes et superkontinuum (SK). I denne afhandling beskriver vi, hvordan et SK kan skabes i en fotonisk krystalfiber (FKF) ved hjælp af pikosekund-pulset pumpe laser, og hvordan man kan ændre den spektrale form ved enten at pode genereringen med bælgelængder væk fra laser pumpen eller ændre dispersionsegenskaberne af FKF'en. Podningen virker ved, at en del af superkontinuumet sendes tilbage og bliver tidsafstemt med pumpe pulsen. Ved brug af denne metode viser vi, at et højere ordens forstærkningsbånd for firebølgeblanding kan podes, så det opbygger kraftige toppe i det endelige superkontinuum. Vi undersøger, hvordan denne effekt er afhængig af det spektrum, der podes med, og af den præcise tidsafstemning med pumpen. Ved højere pumpe effekter kan podningen også bruges til at ændre på genereringen af dispersive bølger i kontinuumet. Vi viser, at podningen kraftigt kan reducere støjen i SK'et ved lav pumpeeffekt, men at denne reduktion er relativt lille ved høj pumpe effekt. Vi undersøger også podning af modulationsinstabilitet ved hjælp af en Ramantop ved høj pumpe effekt og viser, at dette ikke reducerer amplitude støjen.

Efterfølgende undersøger vi, hvordan dispersionsprofilen af FKF'en påvirker spektrum og støj i det genererede SK. Vi viser, at udbredelsen af den synlige del af det genererede SK er afhængig af udbredelsen af den infrarøde del, og at denne kan begrænses af tilstedeværelsen af en ekstra nuldispersionsbølgelængde (NDB), en nedbremsning af solitonernes rødforskydning eller den infrarøde absorptionskant i silika. Det vises, at hvis man vil maksimere den spektrale udbredelse af det synlige spektrum, skal gruppehastigheden ved den infrarøde kant være så lav som muligt. Konverteringseffektiviteten fra pumpe til synligt lys falder dog i de fiberdesigns hvor dette er opfyldt, fordi NDB'en samtidig flyttes væk fra pumpen. For at øge effektiviteten kan man benytte lange tilspidsede FKF'er, men deres produktion har hidtil været dyr. Vi demonstrerer, hvordan man kan generere et SK i korte tilspidsede fibre, som kan produceres ved hjælp af kompakt udstyr og frit tilgængelige FKF'er. Vi undersøger, hvilke designparametre

for de tilspidsede fibre, der påvirker spektret, støjen og effektiviteten af det genererede SK, og viser, at korte tilspidsede fibre i et 50 cm langt stykke FKF kan producere lys ned til 400 nm med betydeligt mindre støj og meget kortere udgangspulser end en konventionel SK kilde baseret på fibre, som er uniforme i længderetningen.

List of publications

The following publications form the basis of this thesis:

Journal Publications

[1] P. M. Moselund, M. H. Frosz, C. L. Thomsen and O. Bang "Back-seeding of higher order gain processes in picosecond supercontinuum generation," Opt. Express **16**(16), 11,954–11,968 (2008).

[2] M. H. Frosz, P. M. Moselund, P. D. Rasmussen, C. L. Thomsen, and O. Bang, "Increasing the blue-shift of a supercontinuum by modifying the fiber glass composition," Opt. Express **16**(25), 21,076–21,086 (2008). Also included in Virtual J. Biomed. Opt. **4** 2, (2009).

[3] P. M. Moselund, C. L. Thomsen, T. V. Andersen, T. Feuchter, and O. Bang, "Raman seeding of high power picosecond supercontinuum generation," Optics Lett. Submitted.

In addition an article will be submitted in August 2009 on the basis of the material presented in chapter 5:

P. M. Moselund, M. H. Frosz, C. L. Thomsen and O. Bang "Supercontinuum generation in short PCF tapers", Opt. Express (2009). To be submitted.

Conference contributions

[4] P. M. Moselund, M. H. Frosz, C. L. Thomsen, and, O. Bang, "Back seeding of picosecond supercontinuum generation in photonic crystal fibres", *SPIE Europe Photonics Europe* Proceedings of SPIE (2008), 6990–24.

[5] P. M. Moselund, M. H. Frosz, C. Thomsen, and O. Bang, "Picosecond supercontinuum generation with back seeding of different spectral parts", *Australian Conference on Optical Fibre Technology* (2008).

[6] P. M. Moselund, M. H. Frosz, C. L. Thomsen, and O. Bang, "Noise Reduction of High-power Supercontinuum sources by Back Seeding," in *Proceedings of Conference of Lasers and Electro Optics (CLEO Europe)* CD4.2 (2009).

In addition the following has been published during the Ph.D. Project (April 1st 2006 – July 31st 2009) However, this work is outside the scope of this thesis:

Journal Publications

- R. B. Ettlinger and P. M. Moselund, "Superkontinuum - et glimt fra en eksperimentel ph.d", Gamma (150), 18–29 (2008). `http://www.gamma.nbi.dk/Galleri/gamma150/superkontinuum.ps.gz`. Gamma is a popular science magazine in Danish published by the Niels Bohr institute at the University of Copenhagen.

- P. M. Moselund, M. H. Frosz, C. L. Thomsen, and O. Bang, "Back-seeded Higher-Order Parametric Gain in Supercontinuum Generation," Optics and Photonics News: Optics In 2008, Nonlinear Optics **19**(12), 35 (2008).

Conference contributions

- C. L. Thomsen, Q. Yujun, M. Pedersen, F. D. Nielsen, T. Andersen, P. M. Moselund, T. Feuchter, C. Agger, K. E. Mattsson, C. Pedersen, K. G. Jespersen, and B. Andersen, "High brightness visible supercontinuum source", EPS-QEOD Europhoton Conference p. TuB3 (2006).

- M. Ø. Pedersen, F. D. Nielsen, Y. Qian, P. M. Moselund, C. F. Pedersen, and C. L. Thomsen, "High power tunable multi-line supercontinuum source", Focus on Microscopy (2007), `http://www.focusonmicroscopy.org/2007/PDF/019_Pedersen.pdf`.

- P. M. Moselund, O. Bang, and C. L. Thomsen, "Supercontinuum broad-band light sources for bio-optics", Biophotonics 07 Summerschool, poster presentation (2007), `http://http://www.biop.dk/biophotonics07/poster/PMM_Biop07_poster.pdf`.

- C. L. Thomsen, M. O. Pedersen, F. D. Nielsen, Y. Qian, P. M. Moselund, and C. F. Pedersen, "High power tunable multi-line supercontinuum source", Nanooptik - Kleine Dimension Grosse Wirkung, GMM-Workshop (2007).

Chapter 1

Introduction

A supercontinuum is a broad continuous spectrum of light generated from an intense narrow band light source through nonlinear interaction with the propagation medium. It is one of the most spectacular phenomena in optics and involves a large number of nonlinear processes. These nonlinear processes, which are caused by the nonlinearity of the interaction between an intense optical field and the bound electrons of a dielectric medium, give rise to changes in the frequency and phase of the optical field during its propagation. Supercontinuum generation was first reported in 1970 by Alfano and Shapiro who saw a 400 – 700 nm continuum generated by filamentation of picosecond pulses in bulk borosilicate glass [7]. From the beginning it was clear that the processes generating the continuum required some interaction length to be efficient. In the first experiments this interaction length was ensured by the self focussing of the pump light which created filaments that confined the light sufficiently to provide a significant interaction length. This, however, required very high peak power in the pump pulses. The use of optical fibers was the first great simplification in supercontinuum generation because the optical fiber could confine light over long distances allowing greatly increased interaction lengths. The second large step forward occured with the introduction of photonic crystal fibers in which the temporal walk-off between different wavelengths of light could be controlled with great freedom. One could say that after the conventional optical fibers had ensured spatial confinement over long distances the PCFs allowed temporal confinement and thus greatly enhanced the efficiency of nonlinear processes. The first demonstration of supercontinuum generation in PCFs in 2000 by Ranka et al. [8] sparked a strong renewal of interest in supercontinuum generation and this has lead to huge advances in the understanding and application of supercontinua in the following decade.

Today supercontinuum generation is a mature technology and the most significant processes responsible for the generation of the continua have been explained [9]. Supercontinuum sources have been used for a large variety

of applications including optical coherence tomography (OCT) [10], optical mammography [11], confocal microscopy [12], stimulated emission depletion (STED) [13, 14] fluorescence microscopy and fluorescence lifetime microscopy (FLIM) [14], and wavelength division multiplexing in optical communication [15]. In fact the 2005 Nobel Prize in Physics was awarded for work on supercontinuum based frequency metrology [16, 17]. Meanwhile the assembly of supercontinuum sources have moved out of the university labs and onto the industrial production lines with a handful of commercial suppliers of supercontinuum products [18] fighting for their bit of the market. The part of the existing laser market that is potentially replaceable by white light sources was estimated to be around 130 million Euro in 2007 [19], so supercontinuum generation is rapidly becoming big business. Supercontinuum generation is so far the main application of photonic crystal fibers and the photonic crystal fibers have in turn been described as the first commercially successful photonic crystal technology. Development of supercontinuum sources can thus be seen as the vanguard of a significant part of the field of photonics and the heavy impact that they are starting to make on the field of optical analysis sets a high standard for other technologies which will follow them.

The focus of this PhD project was to test and develop methods to control the spectra of supercontinua generated using high power picosecond pump pulses and especially on how one could reduce amplitude noise and extend the spectrum to shorter wavelengths. The goal was to do this using methods that could relatively easily be transferred to commercially viable supercontinuum source designs in order to ensure that the progress achieved could benefit the many users of supercontinuum sources. The work is built upon observations made during practical experiments run in the laboratories at NKT Photonics and at DTU Fotonik. Where necessary numerical simulations run by Michael H. Frosz have been included in order to be able to explain the results. This approach has been used because the numerical modeling of wide supercontinua generated by high power picosecond pulses is still a computationally very demanding task and the results of single simulations are very sensitive to input noise. In addition many assumptions and simplifications have to be made to model a system and this means that the results from numerical simulations never quite match experiments. Basing the investigation on experiments avoided these problems, thereby increasing the likelihood that results could easily be reproduced in systems designed for production.

1.1 Outline of this thesis

Supercontinuum generation is a complicated phenomenon which relies on the interplay between many nonlinear effects but is still heavily affected by several linear effects. In order to provide a framework of theory within which the measurements can be explained, chapter 2 will give a short introduction to optical guiding and the linear and nonlinear effects that are important in supercontinuum generation before summarizing how these effects come together in picosecond based supercontinuum generation. Following this, the experimental results will be described. These have been split into three main areas.

The first part, in chapter 3, focuses on the effect of seeding a supercontinuum with part of its own output radiation. The importance of the temporal matching of the seed with the pump pulse is covered along with the effects of the spectrum of the seed and the power of the pump on the supercontinuum spectrum and amplitude noise. The measurements are subsequently compared to numerical simulations. It was found that this type of seeding could produce strong local peaks in the supercontinuum while simultaneously increasing the spectral broadening of the continuum. It was also found that the seeding could considerably reduce the pulse to pulse amplitude noise in the outer parts of the spectrum at low powers but that noise reduction was relatively small at high pump powers. The section on seeding is finished off with a description of how a Raman peak from the pump system can be used to seed a supercontinuum spectrum to shift energy from the short wavelength to the long wavelength part of the continuum without affecting the amplitude noise.

The seeding had a very significant effect at low powers, but the main focus of this PhD was high power supercontinua and at high pump powers seeding had little effect. In addition the seeding scheme investigated would require significant alterations to be implemented for it to be used in normal supercontinuum generation systems. It was therefore decided to investigate other technologies, which were more suited for implementation in systems. The short second part in chapter 4 covers research on how the fiber design can be optimized to generate light deeper in the blue-violet part of the visible spectrum. It was found that by increasing the size of the air holes of a fiber and reducing the core the spectrum could be extended significantly. In addition it was found that as the visible spectrum was extended, the amplitude noise in the visible part of the spectrum could be pushed to lower wavelengths and reduced in a large part of the visible spectrum. However, it was found that the cost of generating light at shorter and shorter wavelengths was that the efficiency of light generation in the visible spectrum was reduced and the necessary core sizes became so small that it became difficult to efficiently couple light into them. In order to overcome the limitations imposed by a fixed fiber design the focus shifted to investigating the

use of a tapered fiber.

It had earlier been demonstrated in the literature that very long tapers can be used to generate extremely wide supercontinua. However, such tapers had to be produced directly on a draw tower. This would make a large scale production of such tapers very costly and this technology was therefore not likely to be available for many of the applications which could greatly benefit from its impressive results. Chapter 5 describes our investigation into the use of short tapers for which established production technologies and equipment already existed. We investigated how the length, width and transition region affects the spectrum and amplitude noise of the generated supercontinuum. We showed that short tapers can be used to generate light at least down to 400 nm with very low pulse-to-pulse amplitude noise and very short continuum pulses. Although the efficiency of the visible light generation is still low, it is believed that with continued development the efficiency can become comparable to that of present supercontinuum sources or better. If the problem of low efficiency is overcome it is believed that the short continuum pulses and low noise that the tapers can generate could make this the technology of choice for picosecond supercontinuum generation in the future.

Chapter 2

Theory

Supercontinuum generation is, as already stated, a very complicated physical phenomenon and the understanding of it requires the understanding of a wide range of optical terms and effects. This chapter is devoted to briefly explaining the theoretical concepts required for understanding the work described in the rest of this thesis. The chapter begins with an introduction of the linear effects of refraction, dispersion, attenuation and wavelength dependence of fiber modes and the effective core area. Then nonlinear concepts will be explained starting with self phase modulation and cross-phase modulation followed by the inelastic scattering processes of Raman and Brillouin scattering and the elastic parametric processes in modulation instability or four-wave mixing. Section 2.2.4 will explain what solitons are and the many effects in supercontinuum generation which they are responsible for. Section 2.3 will consider the relationship between the pump peak powers and the breakdown threshold of silica fibers and finally section 2.4 will give a brief explanation of how all these nonlinear phenomena interact when a supercontinuum is generated using high power picosecond pulses.

2.1 Linear effects

2.1.1 Refraction and the guidance of light

Refraction occurs when light travels from one medium to another in which it propagates at a different speed. This is the basic effect underlying optical guiding and the workings of lenses. The speed of light in a medium is described by its refractive index, which is the relation between the velocity of light in the medium compared to the velocity of light in a vacuum. Generally the refractive index is higher the more dense a material is. The law of refraction states that if light moves from a medium with a high refractive

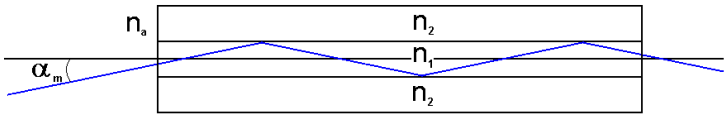

Figure 2.1: Light which enters a fiber with an angle, which is smaller than the acceptance angle α_{m} will experience total internal reflection at all sides of the high index media n_1 and thus be guided

index to a medium with a low refractive index with a sufficiently low angle of incidence it will be totally reflected as has been illustrated in fig. 2.1. Using this principle one is able to guide light over long distances with only very small losses. The effect is first documented by the Swiss and French physicists Colladon and Babinet in 1842 [20, 21] who described how a jet of water can guide light. Today it is the principle behind optical fibres which form the basis of optical communications.

In a conventional fibre, a medium with a higher refractive index, n_1, called the core, is surrounded with a medium with a lower index, n_2, normally called the cladding. The maximum input angle, α_{m}, with which light will be guided by the core is

$$\sin(\alpha_{\mathrm{m}}) = \frac{\sqrt{\mathrm{n}_1^2 - \mathrm{n}_2^2}}{\mathrm{n}_{\mathrm{a}}} \tag{2.1}$$

where n_a is the refractive index in the area from which the light is being coupled in as seen in fig. 2.1. Conventional fibers are based on silica doped with various elements in order to raise the refractive index of the core so that it guides the light. This approach, however, does put some limitations on the index contrasts and core sizes one can produce, which strongly limits the flexibility of the fiber design for nonlinear applications. In the late nineties the photonic crystal fiber (PCF) was introduced [22]. The solid core PCF, which is the only kind which will be used in this work, uses a pattern of rods with different material in the cladding to lower the average index of the cladding and confine the light to the core of the fiber. In the most common configuration the rods are air holes arranged in a triangular pattern around the core, as seen on fig. 2.2. This type of structure is normally characterized by its pitch, Λ, which is the average distance between the centers of the air holes, and the relative hole size, d/Λ, which is the diameter of the holes divided by the pitch.

It should be noted that the above explanation of guiding is based on the somewhat simplified ray-tracing model, which is not valid once the length scales approach the wavelength of light as is the case in single mode fiber optics. However, this model is much simpler to explain and the conclusions

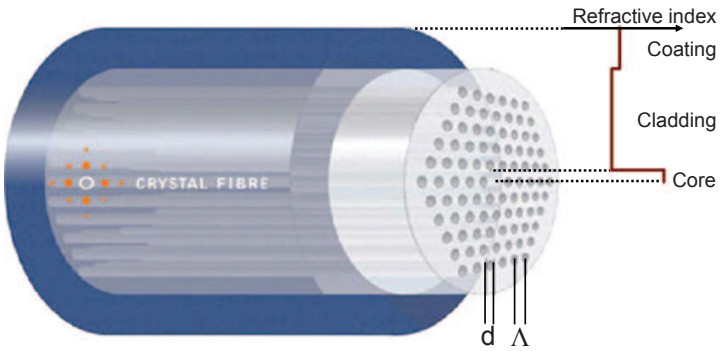

Figure 2.2: Solid core photonic crystal fiber. The air holes reduce the effective index of the cladding below that of the core which can then guide light. Figure curtesy of NKT Photonics

drawn are still valid. For an analysis which more closely matched the physics behind the effects one should base the argument on the propagation of the electromagnetic field and Maxwell's equations.

2.1.2 Chromatic dispersion

The refractive index of a material will vary for different colors of light, and this variation is referred to as chromatic dispersion. The chromatic dispersion in optical fibers is made up of two components, the material dispersion, which dominates for short wavelengths, and the waveguide dispersion, which dominates for long wavelengths. The material dispersion is caused by the variation of the way in which the electromagnetic field interacts with the electrons of a dielectric medium depending on the frequency of the electromagnetic field. This is related to the absorption of electromagnetic radiation at certain resonance frequencies by oscillating of bound electrons in the medium. Far from these resonance frequencies this can be modeled by the Sellmeier equation [23]

$$n^2(\lambda) = 1 + \sum_{j=1}^{m} \frac{B_j \lambda^2}{\lambda^2 - \lambda_j^2} \tag{2.2}$$

where λ_j is the resonance wavelength, B_j is the weight of the jth resonance, and $n(\lambda)$ is the wavelength dependent refractive index. The Sellmeier coefficients for silica, B_j and λ_j, used in this work were obtained from Malitser [24] in the case of the simulations performed by Michael H. Frosz, and Okamato [25] for the dispersion calculations performed by the author. The differences between the two dispersion profiles predicted based on the two sets of parameters were negligible. The two sets of values were:

	Malitson (1965) [24]	Okamoto (1980) [25]
B_1	0.6961663	0.6965325
B_2	0.4079426	0.4083099
B_3	0.8974794	0.8968766
λ_1	0.0684043 μm	0.06609318 μm
λ_2	0.1162414 μm	0.1181101 μm
λ_3	9.896161 μm	9.896160 μm

The dispersion of fibers will be different from that of bulk silica described by the Sellmeier equation. This is because dielectric waveguiding of the fiber structure modifies the effective index to be different from the material index. In PCF this difference, which is known as the waveguide dispersion, can be much greater than in conventional fibers. Indeed, the heavy modification of the fiber dispersion which can be achieved in PCFs and which was first shown by Mogilevtsev et al. [26] is one of the main advantages of PCFs for supercontinuum generation.

The mode propagation constant, β, is used in order to numerically describe the effect of the chromatic dispersion. It is normally expanded in a Taylor series around the center frequency $\omega_o = \frac{2\pi c}{\lambda_0}$ of the pulse spectrum, as in [23]:

$$\beta(\omega) = n(\omega)\frac{\omega}{c} = \beta_0 + \beta_1(\omega - \omega_0) + \frac{1}{2}\beta_2(\omega - \omega_0)^2 + \cdots , \tag{2.3}$$

where

$$\beta_m = \left(\frac{d^m\beta}{d\omega^m}\right)_{\omega=\omega_0} \qquad (m = 0, 1, 2, ...). \tag{2.4}$$

The first β terms are related to the refractive index through the relations:

$$\beta_1 = \frac{1}{v_g} = \frac{n_g}{c} = \frac{1}{c}\left(n + \omega\frac{dn}{d\omega}\right)_{\omega=\omega_0}, \tag{2.5}$$

$$\beta_2 = \frac{1}{c}\left(2\frac{dn}{d\omega} + \omega\frac{d^2n}{d\omega^2}\right)_{\omega=\omega_0}, \tag{2.6}$$

where n_g is the group index and v_g is the group velocity. Thus β_1 is the inverse of the group velocity, while β_2 is the group velocity dispersion (GVD) which describes temporal broadening of the pulse relative to its spectral width. Another parameter which is commonly used in place of β_2, is the dispersion parameter D. D is related to β_2 by the relation

$$D = \frac{d\beta_1}{d\lambda} = -\frac{2\pi c}{\lambda^2}\beta_2 \approx \frac{\lambda}{c}\frac{d^2n}{d\lambda^2} \tag{2.7}$$

For supercontinuum generation a very critical parameter for a fiber design is the wavelength at which β_2 and D become zero. This is known as

the ZDW and it separates the normal dispersion region, where D is negative, from the anomalous dispersion region, where D is positive. The zero dispersion wavelength of bulk glass is 1.27 μm while waveguide dispersion due to doping and dielectric waveguiding shifts that of conventional single mode fibers (SMFs) to about 1.31 μm. In PCFs the presence, number of and position of the ZDW(s) is heavily dependent on the fiber structure. In traditional fibers the waveguide dispersion is dominated by the coresize and the difference in refractive index, Δn, between the core and the cladding. Similarly, in PCFs the coresize and index difference are controlled by the pitch (Λ) and relative hole size (d/Λ) of the cladding but these can be used to control the dispersion to a much larger degree so that the ZDW of PCFs can be pushed below 500 nm [27]. This characteristic of PCFs meant that their invention brought about a revival in nonlinear fiber optics and especially the field of supercontinuum generation.

The dispersion profiles used in this work were modeled using either a fully-vectorial plane-wave expansions model [28] implemented in the the open source software package called MIT Photonic Bands (MPB) or using a mode solver based on the finite element method implemented in the commercial program COMSOL Multiphysics 3.4. The MPB software relies on the assumption that the structure is periodic, which is an advantage when calculating the fundamental space-filling mode of the cladding but a disadvantage when calculating the modes of the whole fiber as it allows the theoretic possibility of resonances with the with field in the fictive fibers repeated beside it. The COMSOL model avoids this and in addition also makes it possible to estimate leakage losses, which will be discussed in the next section. The dispersion profiles of the fiber used in this work will be presented where relevant, but a greater selection of dispersion curves are presented in fig. A.1 in appendix A in order to illustrate the connection between fiber structure and dispersion curves.

2.1.3 Attenuation

When supercontinuum spectra spanning about two and a half octaves are to be generated in fibers one has to have low losses over a very broad band of wavelengths. Like the dispersion, the attenuation of the signal in the fiber varies with wavelength. The attenuation of fibers is normally defined using the following relation and noted in dB/km using the second relation [23]:

$$P_T = P_0 \exp(-\alpha L) \qquad \alpha_{dB} = -\frac{10}{L} \log\left(\frac{P_T}{P_0}\right) = 4.343\alpha \tag{2.8}$$

where P_T is the transmitted power, P_0 is the launched power, L is the fiber length, α is the attenuation constant and α_{dB} is the attenuation in dB

per fiber length. The SC spectrum extends far outside the low loss spectrum normally used in telecom fibers and the losses in PCFs are therefore also frequently noted in dB/m. There are six main attenuation mechanisms governing the spectral loss in a PCF and these are incorporated in the calculation of the attenuation coefficient as follows [29]:

$$\alpha(\lambda) = A_{Ray}/\lambda^4 + A_{ip}(\lambda) + A_{uv}\exp(\lambda_{uv}/\lambda) + A_{ir}\exp(-\lambda_{ir}/\lambda) + A_{im}(\lambda) + A_{leak}(\lambda) \tag{2.9}$$

where A_{Ray} represents the Rayleigh scattering loss, A_{ip} represents the imperfection scattering loss, A_{uv} represents the strength of the ultraviolet absorption loss with the λ_{uv} wavelength of resonance, A_{ir} represents the strength of the infrared absorption loss with the λ_{ir} wavelength of resonance, A_{im} represents the absorption loss due to impurities, and A_{leak} represents the confinement loss. The contribution from each of these mechanisms has been plotted in fig. 2.1.3. All the numeric values to be inserted in the equation for PCFs has not been found collected in any single previous paper and thus it was deemed relevant to cover the loss mechanisms in somewhat greater detail here.

The six basic loss mechanisms in silica fibers can be split into the three categories: scattering, absorption and confinement loss. Scattering is the transmission losses arising from the deflection of light by inhomogeneities in the fiber which largely arise from the fabrication of the fiber. Absorbtion loss comes from the vibrational resonances of the fiber material and the impurities in the fiber. Confinement loss is light leaking out through the microstructured cladding.

Scattering loss (2.1.3 pink line) is a combination of Rayleigh scattering and Imperfection scattering. Rayleigh scattering loss is caused by density fluctuations in the refractive index, which are much smaller than the optical wavelength ($< \lambda/10$) and is inversely proportional to the fourth power of the wavelength. Imperfection scattering is due to inhomogeneity of the fiber and is largely wavelength independent [31]. A PCF from NKT Photonics A/S has here been chosen to represent the state of the art in commercial PCFs. Its Rayleigh loss was estimated to be 1.3 dB/km/μm^4 and the imperfections loss about 1 dB/km/μm^4. This fits well with the Rayleigh loss of 1.08–1.36 dB/km/μm^4 and imperfections loss of 0.83–1.81 dB/km found in [29] for optimized and standard production processes. The scattering loss can be minimized by smoothing the interior surface of the holes by polishing, washing and etching and tightly controlling the drawing process to minimize irregularities in the fiber [29]. It has been found in a theoretical study that Rayleigh loss should decrease with increasing pitch and increasing relative hole size [32]. As an example it has been calculated that in a fiber with large air holes the Rayleigh scattering loss doubled with a decrease in pitch of 22% [32]. However, the connection between the fiber

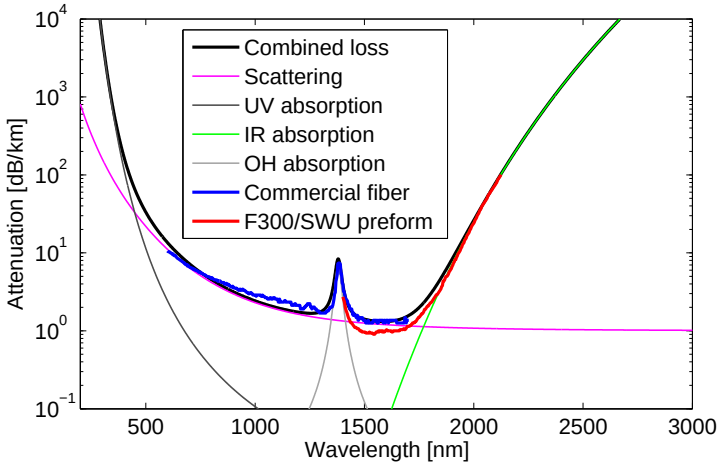

Figure 2.3: The losses of a PCF profile calculated using eq. 2.9 (black) and the relative contribution of the most important loss sources. Leakage loss has not been included in this figure because it is insignificant for all of the fibers discussed in this work. The attenuation of a PCF from NKT Photonics A/S (blue) [30] and a fiber preform made from F300/SWU silica [2](red) has been included for comparison.

structure and the scattering loss has not been thoroughly quantified experimentally and since the rayleigh losses should be below 0.1 dB/m above 500nm it is of little importance for supercontinuum generation (SCG). The structure dependence of scattering losses will therefore not be considered here.

The ultra-violet (UV) and infrared (IR) absorption losses (2.1.3 black and green lines) are intrinsic to the silica material and are caused by electronic resonances in the UV region and vibrational resonances in the far-infrared (FIR) region. The absorption arising from these absorption peaks are exponentially dependent on the photon energy and the relationship of this dependence, which is normally called the Urbach law [31], can be expressed as

$$\alpha_{uv} = A_{uv} \exp(\frac{\lambda_{uv}}{\lambda}) \qquad \alpha_{ir} = A_{ir} \exp(\frac{-\lambda_{ir}}{\lambda}) \tag{2.10}$$

where the UV constants $A_{uv} \simeq 0.001$ dB/km, $\lambda_{uv} \simeq 4.67$ μm were found in [31] and the IR constants $A_{ir} \simeq 6 \times 10^{11}$ dB/km, and $\lambda_{ir} \simeq 478$ μm were obtained from fitting to a loss measurement on a pure silica fiber preform [2]. Since these losses arise from the silica material itself they can only be altered

by altering the material. The limited transmission window of silica will always set a limit on the possible extent on the supercontinuum spectrum by absorbing blue light or infrared light. When one considers the normal fiber lengths used for picosecond supercontinuum generation which is 5-15 m the attenuation would have to be in the order of 0.1–1 dB/m in order to heavily affect the generated spectrum. In normal silica the absorption reaches 1 dB/m at around 340 nm and 2365 nm (see fig. 2.1.3). This fits well with the infrared limit of picosecond generated supercontinua reported to date which normally end at a wavelength of approximately 2350 nm or shorter. If the SC generation process could be accelerated so that the SC could be generated in 0.5-1.5 m of fiber it is possible that one could tolerate an attenuation one magnitude higher, which would increase the usable transmission window to approx 290-2670 nm.

The impurity attenuation is similar to the UV and IR absorption, in that it is due to material resonances, but as the term suggests the vibrations are in this case not due to the silica itself but due to its interaction with other basic elements. There are many possible impurities but in normal PCFs by far the most important is hydrogen from water which attaches itself to defects in the glass in the form of OH. OH has a strong vibration at 2730 nm and its second harmonic, which lies at 1385 nm, is the cause of a dominant attenuation peak (2.1.3 gray line). It also causes minor absorption peaks at 950 nm and 1250 nm but these are normally so weak that they will be ignored here. The content of OH in the final fiber comes both from the original content of the glass as well as from OH which diffuses into the core later in the fiber drawing process [33]. The holey structure of PCFs combined with the strain under which they are drawn means that there is a large number of defects in the fiber glass [34]. Because of this and because of insufficient drying of the glass, early PCF fibers had an extremely strong absorption peak of about 500-600 dB/km [35] at 1385 nm. However, in approximately the last five years production processes have been improved by e.g. using high purity vaporphase axial deposition (VAD) glass [29, 33], dehydrating the glass before drawing [29, 35] and purging the fibers with inert gasses during drawing [29, 35] and fibers can now be produced with attenuation below 0.5 dB/km at 1385 nm [29], even though most commercially available fibers still have absorption above 15 dB/km [30] and the PCF from NKT Photonics A/S used as example here has a OH loss peak of about 7 dB/km. However, this is still low enough to make OH absorption insignificant for most SCG applications where only 5-20 m of fiber are used. It has been speculated that drawing induced defects may also cause absorption bands in different parts of the transmission spectrum, particularly at 630 nm, [34] as these have been found in conventional pure silica fibers [36]. However, they will not be considered here since they have not been documented in PCFs.

It should be noted that the storage and handling of PCF fibers subse-

quent to their fabrication can also seriously affect their impurity loss. It has thus been reported that the loss of a PCF fiber was increased from 3 dB/km to over 300 dB/km by the infiltration of the holes with water saturated gas [34]. In the same study it was also found that the tensile strength of fibers was reduced in the course of a few days after infiltration due to corrosion caused by the water saturated gas.

Since it the OH absorption can be very strong it is important to include it in the calculation of the fiber attenuation and we have found that its shape in dB could approximately be fitted to a Lorentzian profile with the shape

$$\alpha_{OH}(\lambda) = \frac{A_{OH}}{1 + \left(\frac{\lambda - 1385\ \text{nm}}{16\ \text{nm}}\right)^2} \qquad [dB/km] \tag{2.11}$$

Where A_{OH} is the peak value of the loss.

Confinement loss is attenuation due to light leaking out from the core and through the microstructured cladding which surrounds it and subsequently being stripped off by the coating. This loss is always strongest at long wavelengths and is generally characterized by having a strong cut-on wavelength above which the loss increases sharply. The confinement loss is dependent on the PCF structure and increases with decreasing core size and decreases with increasing relative hole size and increasing number of rings of holes in the structure [37]. However, when the pitch of the structure becomes lower than or equal to the wavelength ($\Lambda \leq \lambda$) it has been found that the increase in hole size has little effect on the confinement loss and the confinement loss is then mainly controlled by the finite extent of the cladding structure $\Lambda(N_r + 0.5)$ where N_r is the number of rings of air holes surrounding the core [37, 38]. The confinement loss can be calculated from the imaginary part of the effective refractive index of a PCF with equation 2.12 [37, 39]:

$$\alpha_{leak} = \frac{20}{ln(10)} \frac{2\pi}{\lambda} Im(n_{eff}) \qquad [dB/m] \tag{2.12}$$

where λ is the wavelength in meters. The confinement loss in all PCFs used in this work was found to be insignificant compared to the absorption loss and is not considered further. Confinement loss curves of other PCF designs where the confinement loss does become important can bee found in appendix A in fig. A.6.

2.1.4 Fiber modes and effective area

The refractive index of glass is wavelength dependent, and since a difference in refractive index is responsible for the guiding of light in a fiber, the way the light is guided will also be wavelength dependent. In optical fibers this can affect the spatial distribution of the light in the fiber, the

so-called mode structure, which will be investigated further in sec. 5.4 in the context of tapered PCFs. A mode can be seen as a standing wave of the transverse field in the core, which has nodes at the boundaries of the core. This criteria can only be fulfilled for certain energy distributions, depending on the wavelength of the light. In many applications including nonlinear optics one is normally interested in only having a single mode in the fiber because different modes will experience different waveguide dispersion and thus separate temporally. This single mode is the fundamental mode which represents an single rotationally symmetric intensity peak in the fiber. Only the light from a fundamental mode can be properly collimated or focussed down to a diffraction limited spot, which is important for many SC applications, and higher order modes are also for this reason undesired. For a conventional fiber one can calculate whether the fiber supports propagation of modes other than the fundamental mode by calculating its V parameter [31]:

$$V = \frac{\pi d}{\lambda}\sqrt{n_{core}^2 - n_{cladding}^2} \tag{2.13}$$

where λ is the wavelength, d is the core diameter, n_{core} is the refractive index of the core, and $n_{cladding}$ is the refractive index of the cladding. If $V \leq 2.405$ the fiber supports only the fundamental mode. As the inclusion of the wavelength in the equation, indicates a conventional single mode fiber will always be multimoded if the wavelength becomes sufficiently short. A similar V parameter has been found for PCFs given by [40]:

$$V_{PCF} = \frac{2\pi\Lambda}{\lambda}\sqrt{n_{core}^2(\lambda) - n_{cladding}^2(\lambda)} \tag{2.14}$$

where Λ is the pitch of the PCF structure, $n_{core}^2(\lambda)$ is the wavelength dependent effective refractive index of the core (n_{eff}) and $n_{cladding}^2(\lambda)$ is the wavelength dependent refractive index of the free space filling mode of the triangular lattice structure which makes up the cladding. The PCF is single mode if $V_{PCF} \leq \pi$. It has been found that the wavelength dependence of both the core and cladding indexes makes it possible to produce PCFs which are single mode for all wavelengths, or endlessly single mode (ESM) as they have been called [41]. This is one of the unique characteristics of PCF fibers. In a fiber one may also have what is know as cladding modes, which are modes not confined to the core but which spread through the whole cladding region. However, commercial fibers normally have a coating surrounding the cladding, as seen in fig. 2.2, which has a higher index than the cladding and thus the cladding modes will leak into the coating and have a high attenuation so they are normally not important.

Even when light is guided in the fundamental mode in the core, the area over which the light is distributed, called the effective area (A_{eff}), will change to some degree due to the wavelength dependence of the refractive

index and since the nonlinear effects responsible for supercontinuum generation are strongly dependent on the local field strength, the variation of this with wavelength is an important parameter. The effective area is therefore connected with the nonlinearity parameter (γ) of a fiber which describes the power which is necessary in order to produce nonlinear effects in a fiber and which will be discussed in sec. 2.2. The effective area definition used in this work is

$$A_{eff} = \frac{(\int_S |E^2|)^2}{\int_S |E^4|} \tag{2.15}$$

where S is the fiber cross section and E is the electric field. For all fibers used in this work, the area over which the light is distributed increases with wavelength. The ratio with which the area increases is dependent on the relative hole size and pitch of the fiber and may vary from a 40% increase in area for one PCF to a 700% increase in area in another PCF over the wavelength interval of 300-2300 nm. The effective areas of the fibers used in this work have been calculated using a fully-vectorial plane wave expansion [28] and will be noted when they are considered important to the understanding of the propagation dynamics.

The linear effects described above will affect the propagation of all light no matter its intensity, but there are a number of effects which will only have significant impact on light with high intensities; these are the nonlinear effects which will be described in the next section.

2.2 Nonlinear effects

As for other dielectrics, the response of silica to strong electromagnetic fields is nonlinear due to the interaction between the field and the bound electrons in the material. This means that the polarization ($\boldsymbol{P}$) which the field ($\boldsymbol{E}$) induces in the electric dipoles of the material will not be linear in the field but will instead be a product of the field ($\boldsymbol{E}$), the permittivity (ϵ_0) and the susceptibility $\chi^{(j)}$. The susceptibility is a tensor from which the three lowest orders are normally considered. $\chi^{(1)}$ represents the linear contribution to ($\boldsymbol{P}$) and its effect is included through the chromatic dispersion and the refractive index described above in sec. 2.1.2. $\chi^{(2)}$ governs nonlinear effects such as second harmonic and sum-frequency generation but it is zero in symmetric molecules such as silica [23]. However, it should be noted that defects and other color centers which locally break the glass symmetry may still contribute to second harmonic generation under some circumstances. $\chi^{(3)}$ is the nonlinearity which is responsible for the effects that lead to supercontinuum generation and which include four-wave mixing and nonlinear

refraction. The effect of $\chi^{(3)}$ is included through the introduction of the nonlinear refractive index (n_2) and the nonlinearity parameter (γ) which are defined as

$$\tilde{n}(\omega, |\boldsymbol{E}|^2) = n(\omega) + n_2|\boldsymbol{E}^2| \qquad \text{and} \qquad \gamma = \frac{2\pi n_2}{A_{eff}\lambda} \tag{2.16}$$

where $\tilde{n}(\omega, |\boldsymbol{E}|^2)$ is the intensity dependent refractive index, $n(\omega)$ is the linear part of the refractive index given by eq. 2.2 and (A_{eff}) is the effective area. Note that the nonlinear refractive index is here assumed not to have a wavelength dependence even though it is known that it has one [42]. The wavelength dependence of the nonlinearity has here been ignored because of lack of data. The wavelength dependence of n_2 is generally ignored in studies regarding supercontinuum generation even though it might have significant effect when very wide spectra are generated. The nonlinearity increases sharply at short wavelengths [43] and since one of the prediction models used for the nonlinearity relates it to the material losses through a Kramers - Kronig transformation it may also change considerably at the long wavelengths when the silica absorption increases. In this work the nonlinear refractive index value of $n_2 = 2.6 * 10^{-20}\text{m}^2/\text{W}$ [23] was used. It should be noted that in this work we only consider the nonlinearity of the glass because the nonlinearity of air is three orders of magnitude lower than that of silica [37] and most of the optical effect in a solid core PCF is confined in the glass.

2.2.1 Self phase modulation and cross-phase modulation

As discussed above the refractive index of silica is dependent on the electric field, with the refractive index being higher for more intense electric fields. The envelope of an optical pulse will have a varying field intensity and therefore also a varying local refractive index and this will modify the phase of the light. In effect the central part of the pulse, which has the highest intensity will be moving slower than the front and back edge of the pulse and this will cause the wavelengths in the front edge to be stretched or spectrally red-shifted and the wavelengths at the back edge to be compressed or spectrally blue-shifted. In isolation this effect, which is called self-phase modulation (SPM), will therefore cause the spectrum of the pulse to broaden while the temporal shape remains unchanged. In a normal dispersion regime the spectrally broadened pulse will disperse temporally and ripples become apparent on the spectrum. In the anomalous dispersion region SPM leads to the formation of solitons, which will be discussed below.

The explanation above considers the propagation of only a single wavelength, but often more than one wavelength is propagating through the same fiber and the local refractive index felt by all light will then be deter-

mined by their combined field intensity at any given time and place. Two or more waves which propagate simultaneously will therefore affect each other's phases and in this case the effect is known as cross-phase modulation (XPM). This effect is only efficient if there is good velocity matching between the interacting waves because the phase shift caused by XPM is dependent on the gradient in intensity felt by the wave integrated over the time that it has felt it. If two pulses pass each other the total sum of the positive intensity gradient felt when the other pulse is approaching will be canceled by the negative gradient felt when the other pulse is receding and the net effect will be zero. The effect of XPM is important in supercontinuum generation as will be discussed in the context of soliton trapping in sec. 2.2.4.

2.2.2 Stimulated inelastic scattering

Scattering processes which convert light to other frequencies in optical fibers can be either the inelastic or elastic scattering processes. The inelastic processes lead to a loss of optical energy as some power is converted to phonon vibrations in the fiber. Among these processes are Raman and Brillouin scattering. The elastic processes on the other hand maintain energy conservation through the scattering and among these are four-wave mixing (FWM) and harmonic generation.

Raman Scattering

Raman scattering is a process whereby light is inelastically scattered by interacting with the vibrations of the molecules it propagates through. This leads to some of the light being converted to a lower frequency wave, called the Stokes wave, and vibrations in the fiber molecules, known as phonons. It was initially discovered in 1928 [44] but only demonstrated in optical fibers in 1972 [45]. The phonon vibrations which are created are dependent on the molecular bindings in the material and can be used for label free analysis of chemical substances. In the silica glass of the PCF fibers the Raman effect causes a gain whose peak is down shifted 13.2 THz but the gain stretches out more than 20 THz from the pump due to the crystalline nature of silica [46]. When a strong pump is generated at 1064 nm a Raman peak will gradually develop around 1114 nm and as it develops the pump peak is depleted. The effect of this on supercontinuum generation will be investigated further in sec. 3.7. The Raman effect is also important in supercontinuum generation as it shifts energy toward the longer wavelengths. Thus it depletes wavelengths around 1014 nm to give gain to the pump which in turn is depleted to give gain at 1114 nm and so forth. The most important

effect of Raman gain is, however, that it causes soliton red shift, which will be discussed in sec. 2.2.4 and which produces most of the supercontinuum bandwidth.

Stimulated Brillouin scattering

A strong electromagnetic field can create an acoustic wave in the fiber through the process of electrostriction. This acoustic wave will propagate through the fiber at low velocities and modulate the refractive index of the fiber creating a grating which reflects light back toward the pump. This effect is called Brillouin scattering. Brillouin scattering is not generally a problem in picosecond SC generation because the pulse length is too short to allow a build up of the grating and indeed no reference has been found of picosecond SC generations attempts being limited by stimulated Brillouin scattering. The Brillouin gain peak frequency of PCF fibers depends on their structural parameters. The measurement of the Brillouin scattering has actually been proposed as a method for measuring structural variations along the fiber [47]. Since there are small variations in the structure along the PCF, the gain peak frequency of the PCF will also vary along the length. This means that the longer the fiber is the wider its Brillouin gain band. Since a wide gain band lowers the efficiency of the gain, the PCFs also have significantly higher Brillouin threshold than conventional fibers. One 73.5 m PCF was measured to have an approximately seven times higher Brillouin threshold than a comparable dispersion shifted conventional fiber [48]. However, the increase in Brillouin threshold will be dependant on the structural uniformity of the fiber.

2.2.3 Parametric processes

The elastic scattering processes in silica are also called parametric processes because unlike in the inelastic processes, which are dependent on interaction with the glass itself, the parametric processes are only dependent on the modulation of a medium parameter, e.g. the refractive index. Two important parametric processes are harmonic generation, which is dependent on the second order susceptibility and four-wave mixing (FWM), which is dependent on the third order susceptibility. However, since only the third order susceptibility is important in pure silica fiber, only FWM will be discussed here.

Modulation instability and four-wave mixing

Ideally the intensity profile of a long pulse or continuous wave should always be smooth, but in reality there will always be some measure of noise which imposes many small local peaks and dips on the smooth intensity profile of the pulse envelope. When these local peaks induce SPM, the leading edge of a local peak will be red-shifted and the rear edge will be blue-shifted. If this takes place in a normal dispersion region, this means that the local peak will gradually be broadened temporally and smoothed out and the propagation is stable. However, if the dispersion is anomalous, the red-shifted front edge of the local peak will move slower than the central part of the pulse and the blue-shifted back edge will move faster. This means that the local peak will be temporally compressed and sharpened and experience more SPM. The result of this is that any long pulse propagating in a medium with anomalous dispersion is inherently unstable against noise and will eventually break up into a train of pulses. This phenomenon is known as modulation instability (MI) and may be found in many areas of physics such as water surface waves [49] and plasma cyclotron waves [50]. It was first observed in fibres in 1986 [51] after being theoretically predicted in 1980 [52]. Due to the interplay between SPM and anomalous dispersion, the pulse breakup will generate sub pulses most efficiently at certain frequencies, which depend on the pump power, and since the spectrum of the pulses is a transform of the temporal shape, the temporal breakup causes spectral side lobes to grow from the spectrum of the pump. The frequency shift between the pump line and the MI gain frequencies is equal to the repetition rates of the pulses created in the breakup of the original pulse. If the higher order dispersion and wavelength dependence of the nonlinearity is ignored, one can make a simple estimate of the frequency shift of the peak of the MI gain using the equation [23]:

$$\Omega_{max} = \pm\sqrt{\left(\frac{2\gamma P_0}{|\beta_2|}\right)} \tag{2.17}$$

where Ω_{max} is the angular frequency shift of the maximum gain from the pump peak, γ is the nonlinearity parameter of the fiber, P_0 is the peak power, and β_2 is the group velocity dispersion parameter discussed in sec. 2.1.2.

Thus the MI gain peak will move away from the pump line proportionally to the square root of the pump peak power and the square root of the nonlinearity while the frequency shift will be reduced proportionally to an increase in $\sqrt{\beta_2}$. However, in order to determine the gain peak more exactly and to determine the full MI gain spectrum, one can use a more complex equation which includes the higher order dispersion and the Raman response. The gain is proportional to g=2 Im(K), with K given by the equation [53]:

$$K = \sum_{m=1}^{\infty} \frac{\overline{\beta}_{2m+1}}{(2m+1)!}\Omega^{2m+1} \pm \sqrt{\left[\sum_{m=1}^{\infty} \frac{\overline{\beta}_{2m}}{(2m)!}\Omega^{2m} + 2\gamma P_0(1 - f_R + f_R\tilde{h}_R\right] \sum_{m=1}^{\infty} \frac{\overline{\beta}_{2m}}{(2m)!}\Omega^{2m}} \tag{2.18}$$

where Ω is the angular frequency, $f_R = 0.18$ is the fractional contribution of the delayed Raman response, and $\tilde{h}_R$ is the Fourier transform of the delayed Raman response given by [53]:

$$\tilde{h}_R(\Omega) = \frac{\tau_1^2 + \tau_2^2}{\tau_2^2 - \tau_1^2(i + \tau_2\Omega)^2} \tag{2.19}$$

where $\tau_1 = 12.2$ fs and $\tau_2 = 32$ fs.

In order to illustrate the contribution to the MI gain from the various effects, the gain spectrum has been calculated for a fiber with $\Lambda = 3.7\ \mu m$ and $d/\Lambda = 0.79$ at two different pump powers, as seen on fig. 2.4. It is

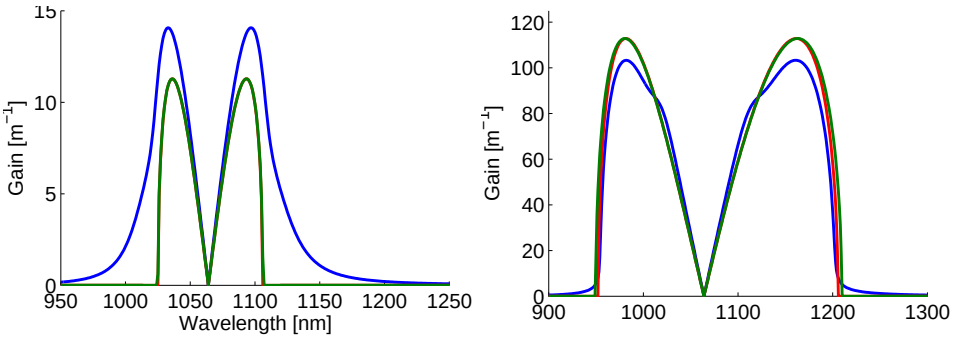

(a) $P_0 = 1$ kW **(b)** $P_0 = 10$ kW

Figure 2.4:

The MI gain with wavelength in a fiber with $\Lambda = 3.7$ and d/Λ=0.79 at 1kW (left) and 10 kW (right) The curves show the gain calculated from the whole K equation (blue), the gain calculated from K without the Raman effect i.e. assuming $\tilde{h}_R = 0$ (red), and finally the MI gain disregarding the Raman effect and all β_m elements except β_2 (green). At 1 kW the higher order β terms have very little effect and the gray and black dotted curves overlap. Note the different Y-scales on the two figures.

interesting to note that the effect of the inclusion of the Raman gain changes as the peak power is increased. At low pump powers, when the MI gain peak is inside the Raman peak gain wavelength of 1114 nm, the Raman response increases the MI gain, but at higher pump powers, when the MI gain peak is outside the Raman gain peak, the inclusion of the Raman response lowers the MI gain. The MI gain normally builds up from noise, creating a random breakup of the pulse, but it has recently been shown that if the MI gain region is seeded, the MI breakup can be controlled so that it follows a more deterministic pattern and the noise in the final continuum is reduced [54–56].

While the term MI is usually only used to describe the breakup of a pump into a train of short pulses, the same mechanism is also behind the effect known as four-wave mixing (FWM), which as mentioned is normally the only type parametric gain occurring in pure silica. It occurs when one wave with frequency ω_1 beats with another with frequency ω_2. If they have good phase matching and a long interaction length, a frequency down shifted Stokes wave with frequency ω_3 and a frequency upshifted anti-Stokes wave with frequency ω_4 are created. Due to momentum conservation the frequencies must satisfy the following condition

$$\omega_1 + \omega_2 = \omega_3 + \omega_4 \tag{2.20}$$

and must satisfy the phase matching condition

$$\Delta k = \beta(\omega_1) + \beta(\omega_2) - \beta(\omega_3) - \beta(\omega_4) + 2\gamma P_0 = 0 \tag{2.21}$$

The gain spectra of these new waves can be calculated with equations similar to 2.18. The $2\gamma P_0$ accounts for the intensity dependence of the refractive index, but it will have relatively little influence if the group velocity curve is steep.

2.2.4 Solitons and soliton effects

Solitons

In anomalous dispersion the shortest wavelengths move faster than the longer. This would normally broaden a pulse temporally, but as mentioned above, the SPM effect will red shift the front part of a pulse and blue shift the trailing part of a pulse. Since the dispersion is a linear effect and the SPM is a nonlinear effect, there is a power level and pulse shape for which the two effects exactly cancel each other. The pulse shape for which this can be achieved is a hyperbolic-secant and the relation ship between its peak power, P_0 , its pulse length, T_0, and dispersion, β_2, is described by eq. 2.22 [23]:

$$N^2 = \frac{\gamma P_0 T_0^2}{|\beta_2|} \tag{2.22}$$

Such pulses are called solitons. The number N is the soliton number and is 1 for a fundamental soliton, which in theory can propagate infinitely without changing its spectral or temporal profile if absorbtion and the Raman effect is ignored. If the number N is larger than 1, the pulse will be a higher order soliton which will oscillate, periodically regaining its shape while shedding energy. Eventually a higher order soliton will break up into a number of fundamental solitons. The fundamental soliton shape is very stable and any pulse whose soliton number is between 0.5 and 1.5 will eventually evolve into a fundamental soliton [23]. During the adaptation the soliton will oscillate and shed energy, which either escapes the temporal confinement of the soliton while remaining at the soliton wavelength as non-solitonic radiation (NSR) or gets transferred to the dispersive wave of the soliton (see sec. 2.2.4 below). The soliton can thus also adapt to stay a fundamental soliton when its wavelength is changed by soliton red shift (see sec. 2.2.4 below), if its energy is changed by gain or absorption, or if the fiber parameters gradually change, as in a long fiber taper. Since solitons are temporally short and can have very high intensities, they play a fundamental role in many of the nonlinear processes which combine to generate a supercontinuum.

Dispersive wave generation

Solitons can be very short in time, in which case they become very broad spectrally. When their wavelength is close to a ZDW this may cause the solitons to spectrally overlap with wavelengths in the normal dispersion region, and if the phase matching condition from the FWM gain mentioned above is satisfied, the soliton will create a gain at these wavelengths. The spectral overlap from the soliton itself will serve as seed for this gain and energy will be transferred to the wavelength where the phase matching condition is satisfied. This transfer of energy is known as dispersive waves (DW) generation and is the main process responsible for transferring energy to the parts of a supercontinuum whose wavelengths are shorter than then pump. The efficiency of the dispersive wave generation is determined by the spectral overlap from and the gain created by the soliton. It is therefore heavily dependent on the wavelength shift between the soliton and the ZDW as well as the energy of the soliton. In order to generate a strong dispersive wave the soliton should be close to the ZDW, because this will minimize the wavelength shift between the soliton and the DW and thus give the best overlap between gain and soliton spectrum. The DW generation is also more efficient, the higher the energy of the soliton, because higher energy will mean

higher peak power and thus higher gain. Higher energy also means shorter soliton pulse length and thus broader spectrum and better spectral overlap between soliton and the gain wavelength where the DW is generated. Since the peak power is proportional to the soliton energy squared and the soliton pulse length is inversely proportional to the energy, the increase in dispersive wave generation is highly nonlinear with soliton power.

Soliton self frequency shift

The wide spectrum of a soliton shorter than $\approx 1ps$ allows Raman scattering to occur within the spectrum of soliton itself, so that there is a continuous transfer of energy from the shortest to the longest wavelengths within the soliton [23]. This causes a so-called soliton self frequency shift (SSFS), soliton red shift or intra pulse Raman scattering, which is a gradual shift of the soliton's central wavelength towards longer wavelengths. Considering the spectral width of the soliton, the Raman shift is rather large. It is therefore only the shortest wavelengths of its spectrum that have a large enough frequency shift to the longest wavelengths to transfer energy efficiently. Since solitons with a higher energy are also narrower in time, their spectrum is wider and more of their energy is therefore located in spectral parts which are far enough from each other to transfer energy efficiently through Raman scattering. This means that the more energy a soliton has the faster it will red-shift. The temporal length of a soliton is also depends on the local dispersion and nonlinearity of the fiber. These will vary with the wavelength. As the soliton red-shifts to longer wavelengths, it will eventually reach a point where the combination of reduced nonlinearity, energy loss due to material absorption, and energy leakage and increased dispersion will reduce its spectral width to less than the Raman shift. When this happens the soliton will gradually stop red-shifting. The red-shift rate of a pulse which is longer than 76 fs will be given by [23]:

$$\frac{\mathrm{d}\nu_0}{\mathrm{d}z} = -\frac{8|\beta_2|T_R}{2\pi 15 \mathrm{T}_0^4} = -\frac{T_R}{60\pi}\frac{\gamma^4}{|\beta_2|^3}E_s^4 = -\frac{4\pi^3 T_R n_2^4}{15}\frac{1}{\lambda^4 A_{eff}^4 |\beta_2|^3}E_s^4 \qquad T_0 \gg 76 \text{ fs} \tag{2.23}$$

where $\mathrm{T_R} \approx 3$ fs, β_2 is the group velocity dispersion, T_0 is the soliton length, E_s is the soliton energy, γ is the nonlinearity, $n_2 = 2.6 * 10^{-20}\mathrm{m}^2/\mathrm{W}$ is the nonlinear refractive index, A_{eff} is the effective area, and λ is the wavelength. The equation above is based on the assumption that the pulse is long compared to the oscillations of the silica, which has a period of 75 fs, and therefore it is only valid for pulse lengths much longer than this [57].

For shorter solitons the spectral width of the pulse is broad compared to the Raman gain and the pulse length will therefore have less effect on the

red shift velocity [57]:

$$\frac{\mathrm{d}\nu_0}{\mathrm{d}z} = -\frac{0.09|\beta_2|\Omega_R^2}{2\pi \mathrm{T}_0} = -\frac{0.09\Omega_R^2}{4\pi}\gamma E_s = -\frac{0.09\Omega_R^2 n_2}{2}\frac{E_s}{A_{eff}\lambda} \qquad T_0 < 76 \text{ fs} \tag{2.24}$$

where $\Omega_R = 2\pi 13.2$ THz is the Raman gain peak frequency. Thus in this regime the dispersion actually has no effect on the soliton red shift and is determined only by the soliton energy and nonlinearity, which in turn depend on the effective area (eq. 2.16) of the fundamental mode. For pulse lengths of approximately 76 fs there is no simple equation to predict the SSFS and more detailed computations will have to be made. This is unfortunate because many of the solitons involved in picosecond supercontinuum are in this regime and the soliton red shift is the main effect behind the long wavelength broadening of the supercontinuum.

Soliton recoil

When a soliton gives off a dispersive wave, it will slowly lose energy. To conserve the overall energy of photons, the center wavelength of the soliton will be shifted in the direction opposite to the emitted dispersive wave; this is known as soliton recoil [58]. When the dispersive wave is at a shorter wavelengths than the soliton, the shift will just add to the SSFS already shifting the soliton toward longer wavelengths. However, some fibers have two ZDWs which are both located in the silica transmission window. In these fibers, the SSFS may shift the wavelength of the solitons far enough that they start phase matching with part of their own spectrum in the normal dispersion region above the second ZDW. The soliton then generates a dispersive wave at longer wavelengths. The shift in the soliton central wavelength in the direction opposite to the radiation which accompanies the dispersive wave generation will then partially cancel out the red shift, as shown by Skyrabin et al. [59]. As the soliton approaches the ZDW, the dispersive wave generation will become stronger and eventually the shift induced by the SSFS balances the shift induced by the dispersive wave generation and the soliton wavelength will be locked. The soliton will then stay at a fixed wavelength while slowly radiating energy to the dispersive wave across the ZDW.

Soliton collisions

The initial modulation instability experienced by a high power wave propagating in anomalous dispersion breaks the pump pulse up in a large number of rather weak solitons with a random distribution of peak powers. Since the solitons have different peak powers, they will red-shift with different speeds

and therefore get different group velocities. This means that shortly after the breakup, solitons will start overtaking each other. As the solitons pass each other there will on average be a transfer of energy from the weaker to the stronger due to nonintegrability [60]. When part of the spectrum of the longer wavelength solitons is within the Raman gain interval of the spectrum of the shorter wavelength soliton, some energy will also be transferred from the short wavelength soliton to the long wavelength soliton through the Raman effect[61, 62]. The longer wavelength soliton, whose energy has now increased, will red-shift even faster, and thus, because of the anomalous dispersion, gain a lower group velocity. This process, which is called soliton collision, means that the initial pump pulse will not develop into a large number of solitons with almost identical pump powers. Instead the distribution of solitons will evolve into many weak solitons and a few much stronger ones which subsequently red-shift and break free from the initial pulse [61, 63]. Recently it has also been suggested that since the MI breakup is determined by noise and the MI generated soliton distribution thus varies considerably from pulse to pulse, this will combine with the effect of the collisions to create a strongly varying soliton distribution, with some pulses generating solitons with much higher energy than the average pulse. These very strong solitons have been called Rogue solitons and Rogue Waves in analogy with oceanic rogue waves [64]. The effect of these very high energy solitons in high power supercontinuum in short fibers will especially be seen in sec. 5.5.6.

The energy of the final solitons created from the soliton collisions will be determined by the initial peak power, the pulse length, the local dispersion profile and the nonlinearity of the fiber, and the noise or seed present in the MI gain band. However, an approximate relationship between these parameters and the soliton distribution generated has yet to be developed. When it was necessary to know the approximate energy of the solitons generating the supercontinua in this work, their energy was estimated by simulating the continuum numerically. The soliton energy was found by identifying the peak power of the most powerful solitons as the peak power of the supercontinuum between soliton collisions and using this to calculate the soliton energy assuming a fundamental soliton shape and using the dispersion and nonlinearity at the wavelength of the soliton peak.

Soliton pulse trapping

The strong gradients in intensity that a soliton creates in a fiber will not only affect the soliton itself but also light at other wavelengths which are temporally matched with the soliton. The soliton's front edge will thus red shift light at other wavelengths because of its strong positive intensity gradient

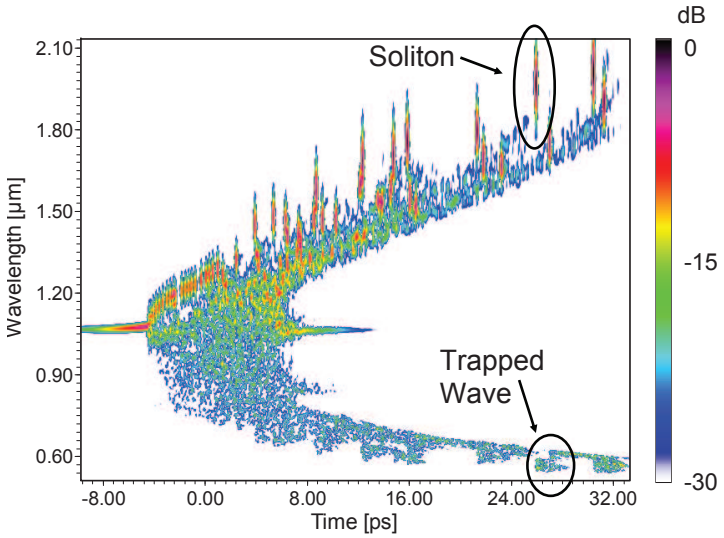

Figure 2.5: Spectrogram showing the temporal and spectral distribution of energy of a pulse which has broken up due to MI and the soliton trapping effect from red-shifted solitons is clear in the short wavelengths.

while the back edge will blue shift other wavelengths. The frequency shift will average to zero if the solitons pass the shifted light completely and the XPM will therefore only affect light which is propagating with almost the same group velocity as the soliton. For such light the effect can, however, be very pronounced because the light may have a very long interaction length with the soliton. Under the right conditions the soliton can actually trap waves from the normal dispersion region which are propagating at almost the same speed. This happens because the soliton overlaps with the radiation and blue shifts the radiation co-propagating with its back edge. Since the trapped wave is in the normal dispersion region, the blue shift will slow down the trapped pulse. The soliton will simultaneously red shift due to the Raman effect, and since the soliton is in the anomalous dispersion regime this will cause it to also slow down, so that its back edge is still overlapping with the trapped wave which is thus continuously blue-shifted. This trapping effect has been likened to how inertia can trap bodies at the bottom of an accelerating frame. It has been shown that the acceleration of the solitons thus traps the waves and partially confine them temporally despite the normal dispersion which would otherwise disperse them [65, 66]. The presence of solitons and trapped waves is visible in spectrograms obtained from the numerical simulation of supercontinuum generation as can be seen on fig. 2.5.

It should be noted that although the trapping of short wavelengths by a soliton is the normal process seen in SC generation, the opposite situation may also occur. It has been shown that the XPM effect can be utilized to stop soliton red-shift by balancing the red shift with a XPM induced blue shift [67]. It must therefore also be considered that if the short wavelength wave which is caught and blue-shifted at the back edge of the soliton contains significant power it will generate an XPM effect for the soliton and add to the red-shift of the soliton on the front edge of the trapped wave and thus accelerate their coupled frequency shifts away from the ZDW.

2.3 Damage threshold

Since all the nonlinear processes are dependent on the intensity of the light and become more pronounced the higher the intensity, it is important to consider how high an intensity the fibers can withstand. The maximum pulse power and the pulse repetition rate will decide the maximum average power that one can get from a system. In this project, part of the goal has been to achieve as high average power in the visible spectrum as possible and this has been done on the basis of a 1064 nm modelocked laser delivering pulses of about 10 ps. It has been reported that the bulk damage threshold fluence for fused silica at 1064 nm using 14 ps pulses is 25.4 J/cm^2 [68]. The pump power that has been used in this project goes up to 10 W, which translates to a fluence of approx. 1.25 J/cm^2. We should therefore be operating well below the damage threshold. However, it should be noted that the nonlinear processes involved in the SC generation process explained above lead to the generation of fundamental solitons of much higher peak power than the initial pulse and this may lead to damaging of the fiber. Thus one experiment with photo-thermo-refractive (PTR) glass showed that 783 nm 120 fs pulses did not cause a refractive index change until the point where continuum generation occurred a few mm into the glass and it was suggested that the nonlinear processes involved in SCG were required to cause the index change [69]. It should also be noted that when the pulse is only a few ps long the damage threshold changes from being due to thermal effects to being due to electron avalanche and ionization effects [68, 70, 71]. The ionization of silica requires the interaction of eight 1064 nm photons, and when pumping with a fluence close to the threshold of this process one has to consider the possibility of many other multiphoton processes which may alter the fiber characteristics over time. Especially since SCG process generates solitons with much higher peak power and a broader spectrum than the original pulse. Even though the original pulse and the individual soliton is far from damaging the fiber the combined train of solitons might

therefore generate changes in the material.

2.4 Picosecond supercontinuum generation

The effects described above all interact in the process of supercontinuum generation in a way which is highly dependent on pump pulse length and energy and the characteristics of the nonlinear fiber. The results described in this work were obtained by pumping PCFs in the anomalous dispersion region close to the ZDW using 1064 nm fiber lasers with full width half maximum (FWHM) pulse lengths of approximately 14 ps and peak powers of up to 10 kW. The explanation of the supercontinuum pulse will therefore focus on the interplay between the effects under these conditions.

When the pump pulse itself is not a fundamental soliton as is the case with ps pumping, the first step of the SC generation process is the pulse breakup. For very short pulses this breakup can occur through soliton fission where the resulting soliton energy distribution can be accurately predicted [72] and the resulting continuum can be coherent. However, when the soliton number becomes larger than $N \approx 16$, the soliton fission process becomes slower than MI and the MI induced breakup which is initiated by noise becomes the dominant process [9]. Since the MI process is based on amplification of noise and not on the pump itself, coherence is generally lost in spectra initiated by this process. The MI frequency determines the period of the breakup and the energy in each period will then contract into solitons while some energy is lost to dispersive waves. This will produce a distribution of soliton energies with peak powers considerably higher than the original pulse and the strongest solitons being created from the middle of the pulse.

Once created the solitons will start to red shift due to the Raman effect. This will shift them to longer wavelengths which have a slower group velocity than the pump, with the amount of frequency shift and slowdown proportional to the soliton energy. As the solitons are thus propagating at different velocities, they will start collide and this will on average transfer energy from the weaker solitons to the stronger ones. During the formation of the solitons and the subsequent collisions the solitons will generate dispersive waves below the ZDW and this dispersive wave generation will increase nonlinearly with the soliton power. As the dispersive waves feel the XPM from the red-shifting and decelerating solitons some of the dispersive waves will be gathered in trapped waves which are gradually blue-shifted. This combined blue and red shift will expand the continuum until the point where the solitons can no longer decelerate enough and the dispersive waves start to lag behind, no longer feeling the XPM from the solitons. This point

will determine the final bandwidth of the supercontinuum, so in order to extend it as far as possible it is necessary to keep the attenuation low so that the solitons do not lose energy. In addition it is necessary to ensure that the fiber group velocity profile allows the solitons to decelerate as much as possible while keeping the nonlinearity and dispersion from broadening the soliton temporally.

Chapter 3

Back seeding of supercontinuum

3.1 Introduction

It is well established that four-wave mixing (FWM) is one of the important processes initiating supercontinuum generation, and since FWM can be seeded it was suggested relatively early on that a better control of the generated spectrum might be gained by seeding the FWM gain wavelengths [73]. Since the FWM gain in unseeded SCG had to grow from noise fluctuation it was expected that seeding could enhance or accelerate spectral broadening and/or reduce the noise in the generated supercontinuum. A thorough investigation of the effect of seeding was therefore chosen as the first topic of this PhD and the results will be described in this chapter.

In sec. 3.2 we briefly summarize the prior literature relevant to back seeding. Then we go on to describe the measurement setup and fiber used in this investigation in sec. 3.3. In order to facilitate the understanding of the effect of seeding on the SCG process we first investigate SCG in the fiber without seeding in sec. 3.4. In sec. 3.5 we then demonstrate how the spectrum of a supercontinuum source can be modified by feeding part of the output light back into the PCF in which it was generated and time matching it with the pump pulses. We show that in this fashion strong amplification peaks can be created in the supercontinuum. We also investigate how seeding affects the pulse to pulse amplitude noise of the supercontinuum at different pump powers in sec. 3.6. The work of seeding in the higher order gain band gave inspiration to an investigation of seeding in the MI band of a fiber with a single ZDW in the silica transmission window. This fiber was more suited for wide band SCG generation and in sec. 3.7 we show the results of seeding MI gain band in this fiber through a simple all-fiber scheme based on allowing Raman gain in the pump system. The work described in

this chapter has been the subject of the publications [1, 3–6, 74, 75].

3.2 Previous studies relevant to back seeding

The concept of utilizing feedback in PCFs has been investigated earlier in several contexts. In the continuous-wave (CW) regime, several studies have been made in which an SC was produced by pumping a nonlinear fiber in a ring-cavity setup both with [76, 77] and without [77, 78] a gain medium in the ring. The effect of the feedback loop in these system was a broadening of the spectrum based on a more efficient growth of Raman peaks and a recycling of pump light. However, since all these systems were totally integrated fiber solutions, their maximum possible bandwidth was limited by the bandwidth of the fused fiber components. In a linear cavity scheme, a fiber Bragg grating (FBG) has also been utilized at the input and output of the nonlinear fiber to produce feedback and amplification of the Raman peak [79]. The result of this approach was that the center of the SC was shifted from the pump wavelength to the Raman gain wavelength. In the femtosecond regime feedback into an SC has been used in order to achieve broadband tuneable amplification [80]. Tuneable local peaks in a broad SC similar to the ones described in this chapter have previously been realized by Yeom et al. [81], who used a long period grating (LPG). However, in that case the generation of the peak was based on the transmission of solitons from a fs pump being modified by the grating, and not on amplification of light reflected back in the fiber, as is the case in the experiment presented here.

Altogether, though, the most interesting observations, and the ones most relevant to the work presented here are the ones which have been found in the context of "Rogue solitons" and "stimulated supercontinuum". In the simulations and experiments presented in that context, which were carried out approximately simultaneously with the ones presented here, it was found that major changes could be produced in the spectrum and noise of an SC by seeding the MI of the input pulse with a time matched pulse at the FWM gain wavelength.

3.3 Experimental setup for back seeding

3.3.1 Measurement setup

The supercontinuum discussed in this section is generated using a setup, a diagram of which can be seen in fig. 3.1. It is based on a custom built modelocked fiber laser based on Yb-doped polarization maintaining (PM) single mode fiber (SMF) and is passively modelocked using a semiconduc-

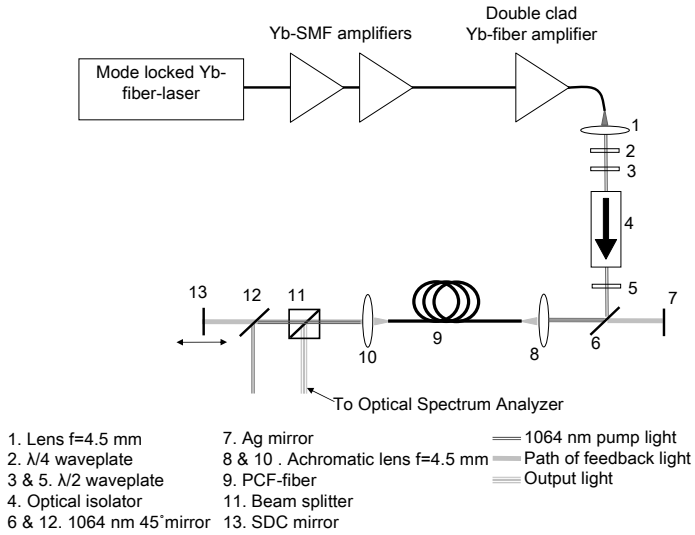

Figure 3.1: The setup used to produce the feedback and measure the spectrum. The "Spectral and Delay Control" (SDC) mirror could be replaced in order to produce different seed spectra. The round trip time of the seed was matched with pump pulse frequency by tuning the distance between the fiber output and the SDC mirror. Meanwhile the output light was monitored on an Optical Spectrum Analyzer. Mirror 7 was removed and substituted by a fiber going to the OSA or a power meter head when the seed light was measured. Mirror 12 is used to filter out residual pump power to avoid reflections back to the pump system.

tor saturable absorber mirror (SESAM). This laser generates a 70.2 MHz pulse-train which is subsequently amplified in two custom built fiber amplifiers based on Yb-doped non-polarization maintaining (PM) single mode fiber (SMF). This pump system was the third of three pump systems built during this project. The first was a modelocked solid state laser based on a Nd:$GdNO_4$ crystal and a SESAM with an output power of up to 250 mW. The second was a modelocked non-polarization maintaining fiber laser also based on Yb-doped fiber, a SESAM and pre-amplifier and amplifier made from non-PM fiber delivering about 200 mW power. But the third polarization maintaining system was by far the most stable in operation and was the solution used for the further work. After the initial amplification in the pre-amplifier and amplifier, the signal is finally amplified using a cladding

pumped Yb-doped non-PM double clad fiber amplifier (DCA). The pulse from the oscillator is not transform limited to begin with, and due to self phase modulation SPM and chromatic dispersion the pulse has broadened significantly at the output of the DCA. The spectrum of the light from the DCA corresponding to different supercontinuum power levels and the full width half maximum (FWHM) pulse length of the laser can be seen in fig. 3.7b.

The elliptical polarization of the output light from the pump system is converted to linear polarization using a $\lambda/4$ (2) and a $\lambda/2$ (3) waveplate, using a method described by Iizuka [82], before being passed through a free space isolator, OFR IO-5-1064-VHP (4). The transmission loss of the isolator is 1.5 dB. Beyond the isolator, the polarization with respect to the fiber axis is controlled using another $\lambda/2$ waveplate. Then the light is reflected off a 1064 nm mirror (6) and coupled into the PCF using an achromatic lens with a coupling efficiency of about 50%. The loss of the PCF is specified by the manufacturer to be 30 dB/km at 1000-1100 nm, and most of the pump power remains in this interval, so fiber losses are assumed to be of little importance. Using a 10% beam splitter, a fraction of the collimated output beam of the PCF is split off, coupled into a fiber, and guided to an ANDO 6315A OSA to be analyzed.

The main part of the collimated output is terminated in a beam dump when single pass measurements are made. For the feedback measurements, the main part of the output beam is reflected back into the PCF using the Spectral and Delay Control (SDC) mirror (13). The distance between the SDC mirror (13) and the PCF can be varied in order to match the round trip time of the feedback pulse to the period of the pump pulse-train. After the light has been fed back through the PCF, it is collimated by the achromatic lens at the fiber input (8) and passed through the 1064 nm mirror (6) to finally be reflected back by the silver mirror (7), which thus completes the feedback loop.

The feedback system had a loss of at least 8 dB for each round trip of the reflected wavelengths due to coupling and reflection losses and the 10% reflection of the beam splitter. Note that when the feedback light is being measured in the following, mirror 7 is replaced with a fiber to the OSA. The feedback spectra shown are thus the feedback when it is not interacting with the pump and not the feedback signal present when the entire loop is closed.

3.3.2 Characteristics of the nonlinear fiber

The fiber used in this work is 4 m of 1050-zero-2 fiber commercially available from NKT Photonics A/S, Birkerød, Denmark, which is characterized by having two ZDWs separated by a narrow wavelength interval in which

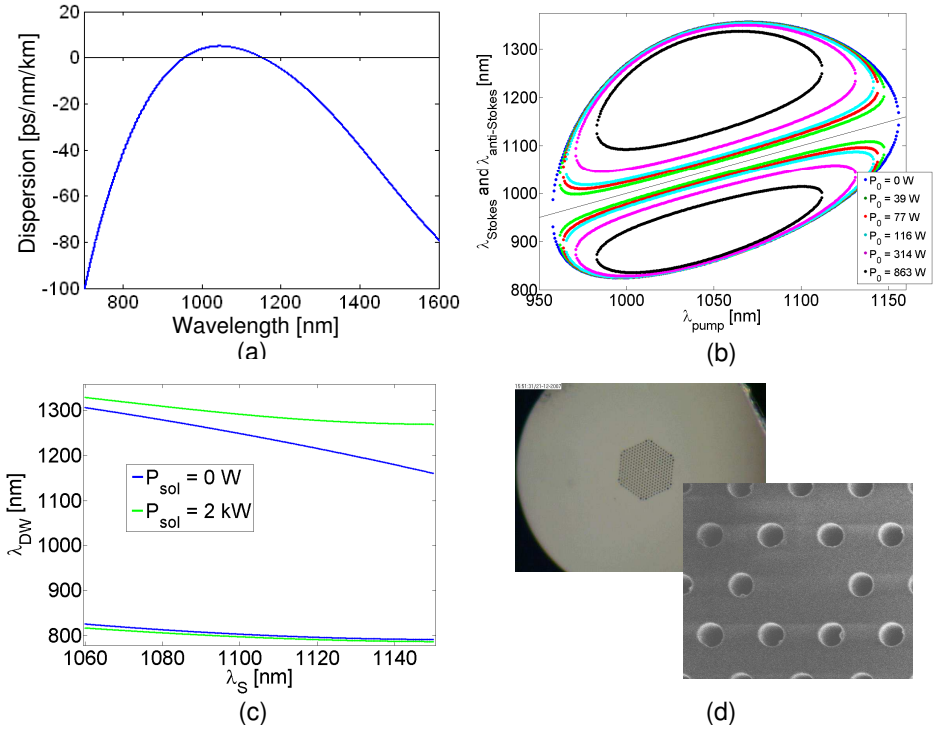

Figure 3.2: Characteristics of the 1050-zero-2 fiber. (a) Estimated dispersion profile with ZDWs at 954 nm and 1152 nm. (b) FWM phase matching gain bands as a function of power and pump wavelength. The FWM gain peaks for the 1064 nm pump at 116 W peak power are at 877 nm, 1039 nm, 1091 nm, and 1354 nm. (c) The phase matching wavelengths for dispersive wave generation from solitons as a function of the soliton's central wavelength (λ_S). This has been marked both without the contribution from the soliton power and for a soliton peak power of 2 kW. Simulations have indicated that the maximum soliton peak power should be around 1.5 kW. (d) Scanning Electron Microscope (SEM) image of a fiber cross-section; the core diameter is 2.2 μm. and the fiber diameter is 125 μm

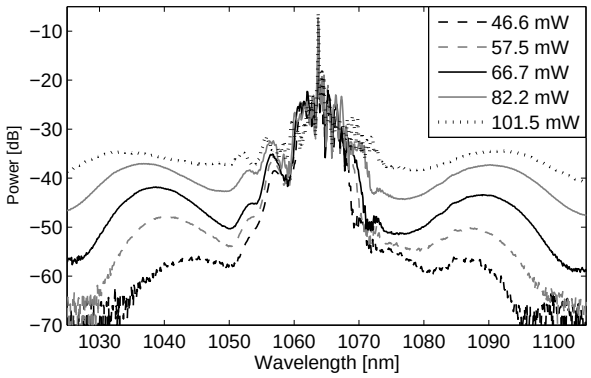

Figure 3.3: The measured pump transmission peak at low power levels, where the power dependence of the position of the modulation instability peaks at 1045-1035 nm and 1085-1095 nm is evident

the fiber has anomalous dispersion. This can be seen on fig. 3.2. Since the core diameter of this fiber is only 2.2 μm, it is very sensitive to variations in the hole size. In order to determine the dispersion profile of the fiber, its average pitch and hole size were determined from a scanning electron microscope (SEM) image and the dispersion profile calculated using fully-vectorial plane-wave expansions [28]. This method is highly sensitive to variations in the PCF hole size both across the slice inspected, which can be seen in Fig. 3.2(d), and along the fiber length. In order to find a more precise dispersion profile, the local dispersion at the pump was also determined experimentally. This was done using the relationship between the local dispersion and the frequency shift of the MI gain peaks given by eq. 2.17, when the nonlinearity parameter (γ) of the fiber is stated by the manufacturer to be 37 $(\mathrm{Wkm})^{-1}$.

The measured pump wavelength, the spectral position of the MI peaks, and the movement of the MI peaks as a function of power, all of which can be read off the spectra seen in fig. 3.3, were then used with eq. 2.17, which predicts the position of the MI bands, to find a local dispersion of 4.5 ps/nm/km. The dispersion curve was then shifted to fit this value. The dispersion curve calculated from the average structural parameters was then shifted to fit this value. A similar method of correcting a dispersion profile derived from a SEM image using local dispersion measurements was recently used by Cumberland et al. [83]. eq. 2.17 was used to estimate the dispersion although it is an approximation because it was shown in fig. 2.4 that the use of the full MI equation does not cause a major shift to the gain peak and the error arising from the simplification is small compared to the measurement

error on the pulse length, average power, and peak position. In the case of the 116 W pump peak power the MI peak estimated with eq. 2.17 was 1098 nm, whereas the MI peak calculated using the whole dispersion term derived from the shifted curve was at 1091 nm and the measured was 1093 nm. The adjustment of the dispersion curve was made because variations over the fiber length could not be determined from SEM images at a single spot, and the exact hole size was likely to vary [84]. By calculating the variation in the dispersion profile resulting from small perturbations of the fiber structure, it had been found that small variations in the hole size would mainly alter the position of the dispersion curve, while only modifying the shape slightly. Estimation of the local dispersion from the wavelength and power dependence of the MI peaks therefore made it possible to correct the calculated dispersion to fit the average dispersion experienced by the light.

The corrected dispersion profile of the fiber can be seen in Fig. 3.2(a). The two ZDWs mean that this fiber has two sets of close-lying FWM phase matching wavelengths. The position of these as a function of pump wavelength and power are shown in Fig. 3.2(b). Similar fibers with two closely-lying ZDWs have been investigated previously both numerically and experimentally using fs pulses, where the focus has been on low noise dual-spectrum generation [85], cross-phase modulation (XPM) SC generation [86], dual wavelength pumping [87], pumping close to the long wavelength ZDW [88], varying the long wavelength ZDW [89], tapering the fiber [90], varying the anomalous dispersion interval [91], the effect of spectral recoil [59, 92], the noise properties of a dispersion-flattened dispersion-decreasing fiber (DF-DDF) [93], and the use of the SC from such a fiber for low-noise optical coherence tomography (OCT) [10]. Several studies on the performance of these fibers with CW pumping have also recently been published. Herein the double ZDWs have been used to limit the spectral width of the SC through spectral recoil of solitons [83, 94–96]. However, in the CW investigations the contribution from a second pair of FWM gain bands, which is investigated in this thesis, was not discussed.

It must be mentioned that although the fiber has not been designed to be birefringent, it was found that the spectrum of the generated supercontinuum was highly dependent on the input orientation of the linearly polarized pump. The spectra which are shown throughout this paper were obtained with a constant pump polarization orientation, which was chosen because it transferred the most energy from the pump line to the SC. The relationship between the input polarization and the axis of the fiber structure has not been investigated.

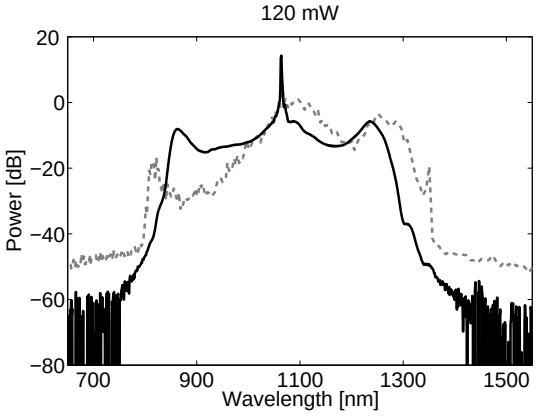

Figure 3.4: Comparison between simulated and measured spectra. Black: Measured spectrum. Grey dashed: Simulated spectrum.

3.4 Single pass SCG

3.4.1 Pumping at the SCG threshold

In order to be able to explain the interactions between the nonlinear processes generating the spectrum, a simulation was run of the experiment by Michael H. Frosz. The parameters and method of the generalized nonlinear Schrödinger equation (NLSE) based simulation performed is explained in greater detail elsewhere [1, 97].

The simulation of the unseeded spectrum was made using a sech-shaped pulse with 116 W peak power, 14.2 ps FWHM (corresponding to an average power of 131 mW for a repetition rate of 70.2 MHz), center wavelength of 1064 nm, and a fiber length of 4 m. The temporal resolution was 0.95 fs and 2^{17} points were used. This average power is very close to the SC generation threshold, and therefore illustrates a critical point where FWM processes and dispersive wave generation both are very important in the generation of light far from the pump.

The numerical simulations predict a spectrum which is similar to what has been found in experiments, as shown in Fig. 3.4. However, there are some significant differences, most notably that the simulations predict much less power in the short wavelengths than found through measurement. The differences are thought mainly to be due to errors in determination of the exact dispersion profile of the fiber. The dispersion of this fiber is very close to zero in a wide area around the pump and the simulations are therefore very sensitive to variations in the dispersion. It is difficult to determine the exact value of the dispersion and as the hole size of this fiber may vary up

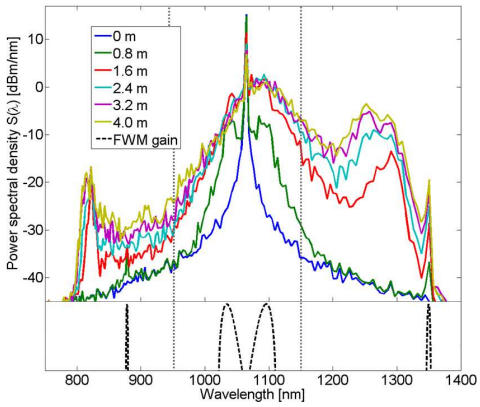

Figure 3.5: Development of the spectrum along the fiber according to numerical simulations. Vertical dotted black lines mark the ZDWs at 954 nm and 1152 nm. The FWM gain, shown in the lower part of the figure, is calculated for the pump power of 116 mW used in the simulation. The FWM gain peaks are at 877 nm, 1039 nm, 1091 nm, and 1354 nm.

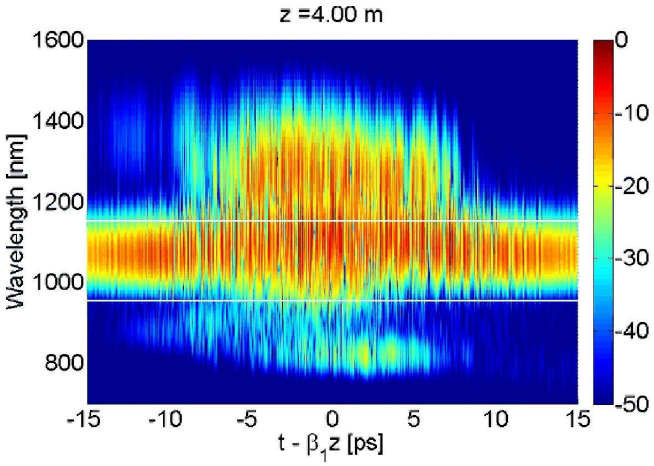

Figure 3.6: Spectrogram showing the calculated temporal distribution of the spectral energy at the output of the fiber. The white horizontal lines mark the position of the ZDWs.

to 2% along the fiber [84, 98] the dispersion will also vary. This means that the ZDWs can vary as much as +/- 50 nm along the length of the fiber. The differences between the simulated and measured output spectra of the fiber are therefore not larger than could be expected. Based on the differences between the simulated and measured spectrum it is expected that the actual ZDW wavelengths in the fiber of the experiment are located considerably closer to the pump wavelength than was simulated. This would explain why there appears to be little red-shifting of the solitons [95].

The processes behind the SC generation in the numerical simulations can be explained when one examines the development of the spectrum along the fiber as shown in Fig. 3.5 and Fig. 3.6 and compares this to the plots of the fiber dispersion, FWM phase matching wavelengths, and dispersive wave phase matching wavelengths in Fig. 3.2(a), 3.2(b), and 3.2(c), respectively. After 0.8 m four peaks start to grow at around 880, 1040, 1090, and 1355 nm. This FWM amplification of certain wavelengths is the spectral sign of the creation of temporal modulations on the pulse known as modulation instability (MI). The MI eventually leads to the breakup of the initial pulse into solitons. The solitons subsequently generate dispersive waves, which should grow at the phase matched wavelengths [90, 99] located around 820 nm and 1300 nm if one assumes the wavelength of the solitons to be around 1064 nm (see Fig. 3.2 (c). These can be seen in the spectrum (Fig. 3.5) from 1.6 m and beyond. Subsequently the solitons will start to red shift due to Raman scattering until they approach the ZDW at 1152. This will lead to a gradual shift in the dispersive waves toward the wavelengths 790 nm and 1160 nm as shown in Fig. 3.2 (c). As can be seen at 1.6-4.0 m the shift of the dispersive wave peaks stop at around 800 nm and 1230 nm. This may be due to the red shift of the solitons being limited by spectral recoil from their dispersive waves [59, 83, 88, 92, 94–96]. In addition to the dispersive waves and degenerate FWM there may also be some contribution to the spectral broadening from cascaded FWM processes.

3.4.2 SCG at higher pump powers

After using a simulation to investigate the evolution of the spectrum along the fiber at a single power level, an experiment is used to investigate the the evolution of the output spectrum of the fiber at different power levels. This combination gives the insight into the generation process possible while minimizing simulation time and avoiding cutting up the fiber in experimental propagation length tests.

The development of the spectrum with increasing power which can be seen in fig. 3.3 and 3.7 is similar to the development along the fiber. However, the FWM gain peaks around 1045 nm and 1085 nm shift outwards to 1035 nm and 1095 nm respectively as the power is increased from 46 to 101

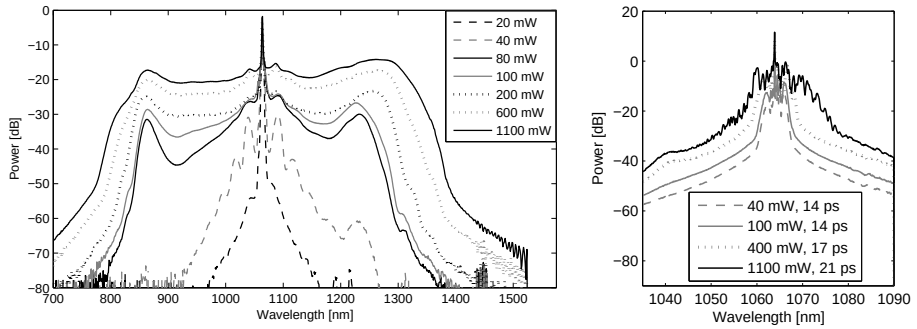

(a) **(b)**

Figure 3.7: The supercontinuum generated in 4 m of 1050-zero-2 at different pump average power levels (a). Spectrum of the pump at various pump powers, measured before the PCF (b)

mW. The frequency shift of these peaks is approximately proportional to the square root of the pump power. This corresponds to the normal behavior of peaks generated by MI as given by equation 2.17. The outer FWM gain peaks around 860 nm and 1235 nm remain almost stationary as they should according to the peak power curves in fig. 3.2 (b). As the average power increase above 100 mW the MI has progressed enough that powerful solitons are created and they generate dispersive waves which fill the valleys in the spectrum and extend it to wavelengths further away from the pump than the FWM gain bands. This corresponds to the typical development in an SC pumped by ps pulses in the anomalous dispersion region, where MI causes the pulse to break up temporally and creates a large number of solitons which collide [63] and create dispersive waves in the normal dispersion region [9].

3.5 Back seeding

3.5.1 Feeding back the SC spectrum in the experiment

It has been shown in the previous section that the 1050-zero-2 fiber allowed the generation of light in a spectrum of over 400 nm. The light is generated by a combination of dispersive wave generation and FWM. It was therefore natural to continue the investigation of this fiber by exploring the effect

of providing a seed for FWM gain by recycling part of the light generated near the FWM phase matching wavelengths and time matching it with the input pump pulses. In order for the FWM processes to be efficient this investigation was focussed at an average power of 100 mW, which was one of the highest power levels where the FWM was still clearly an important process in the spectral evolution. The NL-1050-zero-2 fiber was particularly good for investigating the effect of seeding because it had an outer FWM gain band which was nearly stationary with increasing power far removed from the pump. This meant that the same wavelength interval would experience gain no matter the pump power and that it was it was simpler to find mirrors which could feed back the seed without reflecting pump power back into the pump system.

In the measurements a Fabry-Perot cavity design was chosen for the feedback cavity. The first step was therefore to send part of the output light back through the PCF. The spectrum of this feedback light was determined mainly by the reflectance spectrum of the SDC mirror, but also in part by the collimation optics and the transmission of the 1064 nm 45 ° mirrors which separate the path of the pump from the feedback light. The spectrum which was sent back through the PCF can be seen in fig. 3.8. The gray line

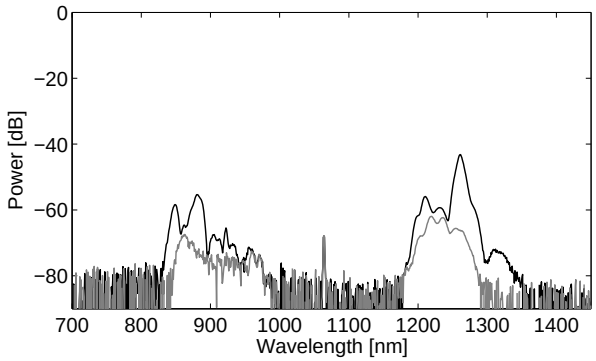

Figure 3.8: Spectrum of the light traveling back to mirror 7 with (black) and without (gray) the SDC mirror aligned. The SDC mirror used in this case is a 1200-1700 nm mirror. The multi peaked nature of the spectrum is caused by ripples in the transmission spectrum of the 1064 nm 45 ° mirrors, which filter out the pump light. The short wavelength peak is caused by unwanted reflection from the 1200-1700 nm mirror because it lacks a broadband anti-reflex coating.

shows the light which is reflected back by the fiber facets, even though these have been cleaved at an angle. The black line shows the increased feedback when a mirror is used. When the total output power was 110 mW, the transmission of the 1064 nm 45° mirror, which removed the pump at the output to avoid reflecting it back into the pump system, was 5.22 mW. Of this, 250 μW was coupled back through the fiber to mirror 7, and it is estimated that 50% of this was then coupled back into the fiber to be time matched with the pump pulse so that their interaction would alter the output spectrum. With a pump power of 110 mW, the power of the seed is thus approximately 0.12 mW.

3.5.2 Effect of feedback

The spectrum of the feedback was first sampled using a fiber at the position of mirror 7. However, in order to close the feedback loop, mirror 7 was then repositioned and aligned so that the feedback light could be seen to slightly increase the relevant sections of output spectrum with its linear contribution. After the spatial alignment was thus completed the temporal matching had to be found by altering the delay distance between the PCF output and the SDC mirror. The delay distance was first roughly tuned using a fast photodiode (Thorlabs D400C) and oscilloscope (Tektronix TDS5052B) in order to match the arrival of the feedback pulse at the output with the arrival of the pump pulse after one round trip. Subsequently, the delay distance was fine-tuned using a micrometer screw to find the strongest amplification of the feedback light.

The spectrum generated in the fiber changes significantly when there is time-matched feedback, as can be seen in fig. 3.9. The most important

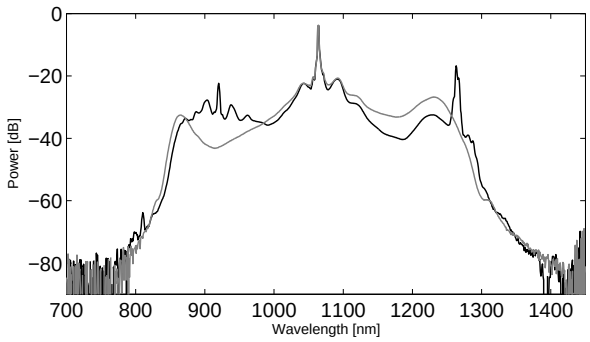

Figure 3.9: The effect of feedback light in the fiber. Gray: spectrum without feedback. Black: spectrum with feedback

features are the growth of a 20 dB peak at the long wavelength end of the spectrum and gains of up to 18 dB in a wide section of the short wavelength side. At the same time, the pump peak and MI shoulders appear to be dampened slightly, while the long wavelength dispersive wave at 1150-1250 nm is reduced by 5-10 dB. It is important to note that the strongest gain peaks occur at 923 nm and 1271 nm and that the sum of the energy of photons corresponding to these two wavelengths is just 0.5 % less than the energy of two photons of the pump wavelength. This is a strong indication that the gain is caused by FWM with the pump. The FWM process removes energy from the pump, which reduces the efficiency of normal SC generation processes, and this may explain the reduction of power at 1150-1250 nm. The FWM, which creates the sharp long wavelength peak, also causes the broad region of peaks in the shorter wavelength end of the spectrum. As can be seen, the short wavelength gain is a broad region with a central peak and two main side peaks. This closely corresponds with what one would expect if a single strong peak in the long wavelength region had a parametric gain derived from the broad region of the pump and its side peaks. When only inspecting the measurements it is difficult to identify whether other effects than FWM are required in its generation. However, when comparing with the FWM gain bands, shown in Fig. 3.5, it appears that the gain in the region at 890-955 nm is too wide for simple degenerate FWM.

3.5.3 Varying the feedback delay

In order to investigate the length of the temporal overlap between the pump pulse and feedback pulse which resulted in an amplification, the length of the delay arm was altered slightly while the spectrum was monitored. In this fashion the spectrum as a function of temporal delay between the pump pulse and the feedback pulse could be measured, and this has been plotted in fig. 3.10. The spectrum at a few sample delays can be seen in fig. 3.11.

The most noticeable characteristic of the temporal gain interval is that the strongest effect occurs around 0 ps delay. The 0 ps delay point was set to be the delay distance at which the fast diode measurements showed that the feedback pulse and the pump pulse were exactly overlapping at the beam splitter at the output of the PCF. One would expect that the greatest effect of the feedback would occur when the feedback pulse was temporally matched with the pump at the input of the PCF. The fact that the strongest effect of feedback coincides with the temporal overlap at the output indicates that the temporal overlap at the output occurs with the same delay as the temporal overlap at the input and thus that the group velocity of the feedback pulse must closely match the velocity of the pump pulse. A close matching of group velocities is a requirement for efficient FWM in a pulsed setup, and as the gain occurs at the point when the pulses

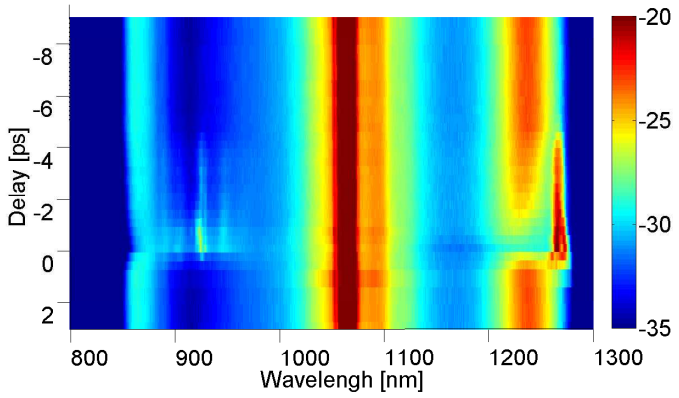

Figure 3.10: Spectral intensity of the output light with feedback as a function of the delay of the feedback light. The intensity in dB is indicated by the scale on the right. The Y-axis shows the delay, relative to the delay at which the pump pulse was matched with the output pulse at the output beam splitter (component 11 on fig. 3.1)

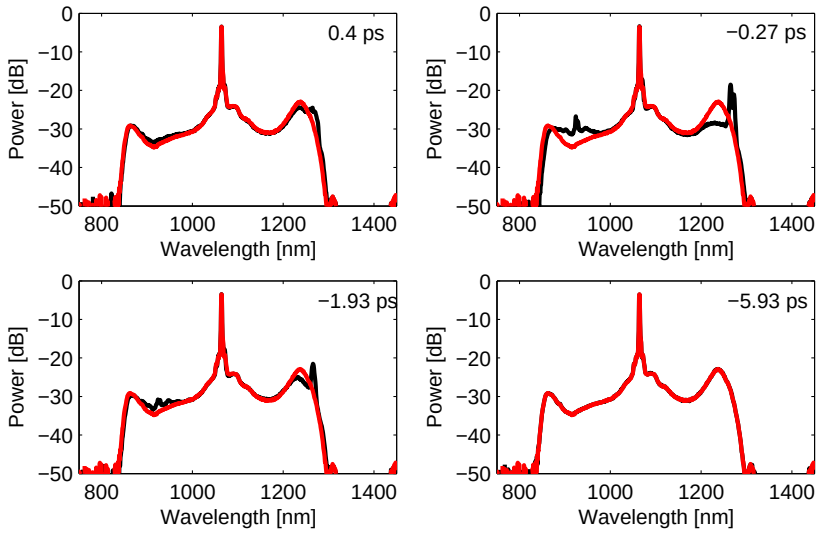

Figure 3.11: Spectra measured with different feedback delays corresponding to slices in the plot on fig. 3.10 with (black) and without (red) feedback. The lower right plot shows the effect of feedback without time matching.

overlap at the output the gain could be caused by a FWM process. It is also evident that the interval of -1.8 ps to 0.2 ps in which a strong gain is produced is very narrow, when considering that the pump pulse has a FWHM of 14.2 ps. Compared to this the roundtrip of the feedback pulses is 42.7 ns, while the period of the spectral modulations induced by the MI is approximately 135 fs. The short peak generation interval could indicate that many round trips are necessary to build up the gain, so that the length of the roundtrip time must be very close to a multiple of the pump pulse separation period in order for the seed to overlap with the pump pulse through many roundtrips.

It may be noted that the effect of seeding and delay dependence presented here is somewhat similar to effects seen in the noise seeding of "Rogue solitons" by Solli et al. [64]. They found that the generation of powerful "Rogue solitons" was connected to noise present in the MI/FWM band in a 0.5 ps time interval just at the leading edge of a 3 ps pump pulse. The spectra generated in the later experimental implementation of the seeding of rogue solitons [56, 100, 101] is qualitatively very similar to the one generated here with a seeding in the FWM band in a 1.2 ps time interval at what appears to be the leading edge of the 14 ps pump pulse. It is very probable that the effect of seeding here is in fact the same effect as the seeding of Rogue solitons, but the movement of the solitons in this fiber is limited by the second dispersion wavelength. The creation of more powerful solitons as a result of seeding would therefore not result in the generation of a more red-shifted spectrum but only in added dispersive wave creation and added dispersive wave red shift. It must also be noted that the spectral effect of seeding presented here closely resembles the one later presented by Solli et al. in connection with the experimental verification of the possibility of seeding Rogue solitons [56].

3.5.4 Varying the feedback spectrum

In order to better understand which wavelengths played a dominant role in the FWM processes, the feedback system was tested using three different mirrors for the feedback, as can be seen in fig. 3.12. The mirrors were: the 1200-1700 nm mirror, which has been used for all other measurements and which mainly fed back the long wavelength peak of the SC (fig. 3.12 left and fig. 3.8), a silver mirror which fed back both sides of the SC (fig. 3.12 center) and finally a broad mirror with reflection centered around 780 nm which mainly fed back the short wavelength peak of the SC (fig. 3.12 right). The measurements show that as the size of the long wavelength peak is decreased, the amplified long wavelength peak in the output also decreases, although the decrease is not linear with the decrease in the feedback peak. However, the short wavelength peak in the output does not scale with the feedback

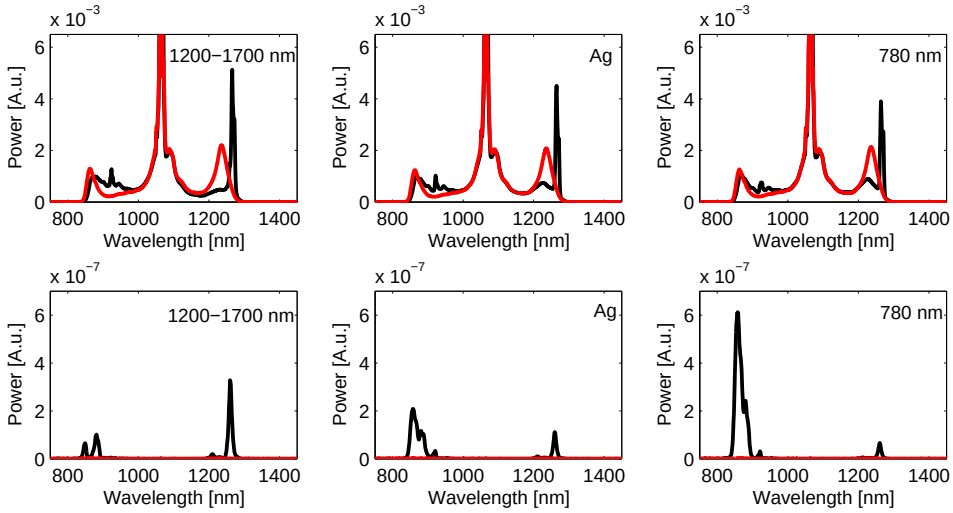

Figure 3.12: SC spectra generated using various feedback spectra. The three columns correspond to the spectra produced using a 1200-1700 nm mirror (left), an Ag mirror (center), and a broad spectrum mirror centered at 780 nm (right) as the SDC mirror. The top row shows the output spectrum from the PCF with (black) and without (red) feedback, while the bottom row shows the spectrum which is fed back through the system, measured at mirror 7 in the setup. Only the light being fed back with the SDC mirror is shown, because the reflection from the fiber facets alone is too small to be seen on a linear scale. Note that all these spectra are plotted on a linear scale.

power at short wavelengths. Instead, the short wavelength increases with the long wavelength amplification peak. This indicates that it is created by the FWM of the long wavelength peak and the pump, instead of being a direct amplification of the feedback at the short wavelengths. Interestingly it also indicates that seeding the long wavelength FWM gain band is more efficient than seeding the short wavelength band. Since the the created peak decreases nonlinearly with the seed, the amplification must be highly nonlinear. This corresponds to what was found by Solli et al. for the seeding of rogue waves were a seed of 0.01 % was shown to increase the power in sections of the spectrum by 30 dB [56, 100].

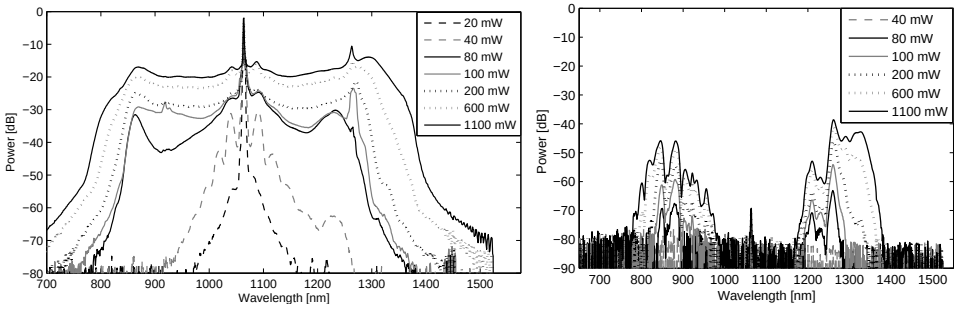

Figure 3.13: Left: The spectrum of the supercontinuum with feedback at a selection of power levels. Average transmission power is noted in the legend and the spectral power is plotted in dB. Right: The feedback spectra generating the amplification peaks.

3.5.5 Feedback at higher pump powers

All measurements on the effect of feedback in the above were made with a constant average pump power of about 100 mW, because seeding produced the greatest modifications in the spectrum at this pump level. In order to get a better understanding of the dynamics of the seeding process, the signal with feedback was measured at a number of pump powers between 20 mW and 1100 mW average power, and the resulting spectra can be seen on fig. 3.13.

At very low power level there is no effect of the feedback, but this is because the pump does not undergo sufficient broadening for there to be any significant light at the wavelengths which are fed back. As the power increases above 80 mW, the pump broadens enough to create a significant feedback spectrum, and amplified peaks around 860 nm and 1270 nm starts to become visible in the output spectrum. In the interval between 80 and 200 mW the increase in power due to feedback is most evident, as the feedback is now sufficiently powerful to be amplified effectively, but other spectral broadening processes, which are unaffected by feedback, are still weak. After this, the long wavelength feedback peak continues to be present and the power of the peak is also rising, but the spectrum around the peak is rising faster than the peak because the normal spectral broadening processes are becoming more and more efficient with increasing pump power. The amplification at the short wavelengths only give rise to defined peaks just around 100 mW pump and thereafter the short wavelength amplification results in an increase in power over the entire region between the pump peak and the short wavelength end of the spectrum. This means that the sharp 1270 nm peak must be the product of FWM from a very wide region,

because otherwise it should be accompanied by a correspondingly narrow low wavelength peak for the sum of the photon energies to add up. Otherwise the 1270 nm peak must be created by some other process. For example it could represent the dispersive wave of solitons in the anomalous dispersion region if the seeding of the FWM/MI band had created especially many solitons generating dispersive waves at this wavelength.

3.5.6 Numerical implementation of feedback

In order to numerically simulate the feedback, the output from the first simulation (termed 'unseeded') was numerically filtered through two super-Gaussian transmission filters to simulate that the Ag mirror reflects light in a broad spectrum while the light around the pump is removed by the 1064 nm mirrors. One transmission filter had a center wavelength of 1300 nm and a bandwidth of 200 nm; the other filter had a center wavelength of 900 nm and a bandwidth of 160 nm. The power of the filtered pulse was then scaled down to 40 % to represent coupling losses of 60 % ($\sim$ 4 dB). The filtered pulse was propagated in 4 m of fiber to simulate the back propagation. It was assumed that there was no interactions with the counter propagating pump pulses on the way back though the fiber since the interaction length with these was extremely short. Finally, the output of this simulation is scaled to 40%, again to represent a coupling loss of 60%, added to a new pump pulse, whose noise was identical to the first one, and propagated in 4 m of fiber to simulate the first back-seeded pulse. This procedure was repeated for simulating multiple back-seeds.

3.5.7 Effect of feedback in simulations

When the pump pulses were propagated through the fiber together with a time matched seed from the output light it was found in the simulation that the seeded output spectrum grew significantly different from the unseeded one, as can be seen in Fig. 3.14. The regions in which the unseeded spectral power is increased by seeding are similar to those found in experiments. However, the increase in power in the numerical simulations is much smaller than in the experiment. This is thought to have two causes. First, only a few round trips of the seed are simulated, whereas the gain in the experiment may build up as the steady-state produced by the contribution from many round trips. Second, as has been shown in sec. 3.5.3, the gain was highly dependent on the delay between the seed and the pump pulse. The spectra shown for the experiment were measured when the delay between the seed pulse and the pump had been optimized to produce the largest gain. In contrast it has not been possible to find the optimal delay point in the simulations as the number of simulations have been limited by long

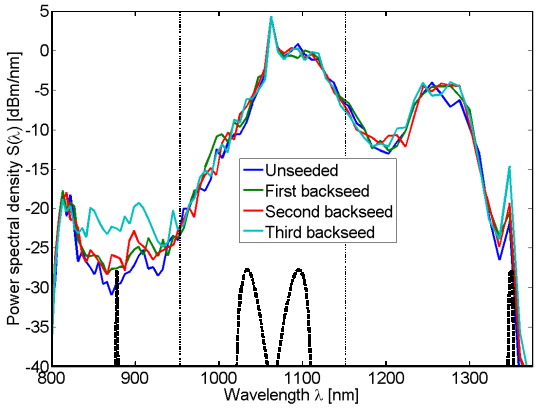

Figure 3.14: Numerical simulation result of a seeding with one, two and three roundtrips in the cavity. Dashed black lines mark the FWM gain areas. Vertical black dotted lines mark the outer ZDWs.

computation times. The gain observed in the simulations is therefore much smaller.

It appears that the gain is created mainly by seeding the FWM gain. The seeding of the outer FWM gain band leads to a significantly stronger peaks at these wavelengths. This leads to a depletion of the pump, which may hamper the soliton creation through modulation instability and thereby the dispersive wave generation. On the other hand the increased transfer of energy from the pump to the FWM gain band should increase the modulation imposed on the pump pulse and could in that way increase modulation instability. In order to find which process is dominant one may inspect the changes in spectrum when seeding seen in fig. 3.14. It appears that the two areas where the energy is increased are centered around the outer FWM gain bands. Meanwhile the long wavelength dispersive wave is red-shifted as can be seen when the seeded spectrum fills the "valley" in the unseeded spectrum at 1275 nm on Fig. 3.14. This would occur if the solitons produced by the seeded MI/FWM had a lower intensity and their red-shift therefore does not bring them as close to the 1152 nm ZDW as in the unseeded case (see Fig. 3.2 (c)). A reduced intensity of the solitons would also make the short wavelength dispersive wave generation less efficient and give a reduction of the 820 nm peak, where a slight reduction is observed. It would thus appear that the seeding of the FWM band in this case primarily leads to a depletion of the pump without significantly increasing the modulation instability. In this fiber, and with this pump, and this time delay the effect of seeding the FWM bands is thus different from what was recently found with noise

seeding of the FWM band in a fiber with a single ZDW [54, 64]. There the seeding of the modulation instability band lead to an increase in the frequency of solitons with very high peak power and thereby an increase in the maximum soliton red-shift. The difference in results may arise because the FWM region seeded here is in a normal dispersion region, or it may also be an effect of the soliton dynamics here being modified by soliton recoil.

3.5.8 Numerical investigation of the feedback delay

The variation of the delay, which was investigated experimentally in sec. 3.5.3, was also tested numerically. This was done by temporally shifting the seed -2 or -4 ps before it was added to the pump pulse and otherwise running the simulation as described in sec. 5.2. The result can be seen in Fig 3.15. As can be seen, both the peak at 1354 nm and the short wavelength interval at 830-950 nm grows significantly stronger when the seed is delayed. The optimal delay has not been found, but the plots shown here indicate that the strong dependence on delay, which was found in the experiment, is also present in the numerical simulations. It is possible that the strong dependence on delay is due to the FWM gain being much stronger when the seed is temporally exactly matched with the peak of the pump pulse.

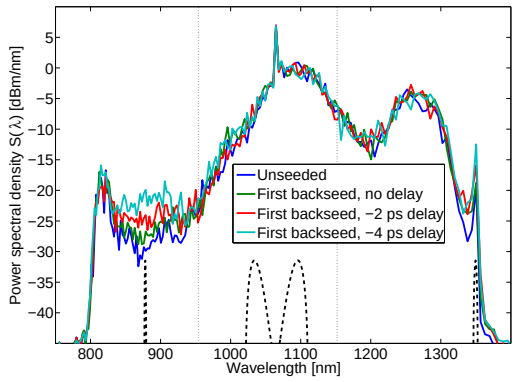

Figure 3.15: Numerically simulated effect of varying the feedback delay. Dashed black lines mark the FWM gain areas. Black dotted lines mark the outer ZDWs.

3.6 Noise investigation

In many applications where supercontinua light sources are currently being applied the amplitude noise of the continua is a severely limiting factor. With picosecond pumping, noise is inherent in the SC generation process, because the generation is initiated by modulation instability, which amplifies random fluctuations in the pump pulse as explained in sec. 2.4. The origins and spectral distribution of the noise will also be discussed further in sec. 4.2. Recently it has been shown that by seeding the FWM gain wavelengths in fibers with a single ZDW, SC generation close to the threshold can be accelerated and the noise can be greatly reduced [1, 56]. The noise is reduced because the seed initiates the MI in a controlled manner, thereby removing a great deal of the randomness in the SC generation process [56]. However, when ps pumping is used one has to use a high peak power in order to generate the wide high power supercontinua which are used in most applications. In this case the pump power is significantly higher than the SC generation threshold and the effect on the noise by seeding has not been investigated at these pump powers.

Experimentally the seeding of the MI band close to the pump is challenging because the wavelength of the MI band moves with the pump power and one must therefore be able to shift the seeding wavelength as one increases power. At the same time one has to ensure temporal matching between the pump pulse and the seed pulse. As shown above we found that a seed only produced a significant effect in a 2 ps interval compared to the 14.2 ps length of the pump pulse and the 14 ns between the pulses. The required shift in wavelength of the seed with increasing pump power means that the seed will experience a different group velocity. One therefore also have to adjust the delay of the seed when increasing the pump power to maintain time matching. The correct delay adjustment can be difficult to find because, as we will show, the effect of the seeding is only very clear at near the threshold, and thus it is difficult to identify when time matching has been achieved at higher powers.

The system that we have used in our studies of back seeding used a higher order gain band for seeding. As was shown in fig. 3.2(b), the spectral position of this band is almost stationary with increasing pump power and this made it much simpler to test the power dependence of seeding in this fiber versus seeding in a PCF with a single ZDW. The SC was filtered through a 1250 nm long pass filter and a pulse train was measured on a diode with and without seed and the signal was recorded on a digital oscilloscope. The pulse train was then analyzed by speciality software at NKT Photonics, which basically integrated the radio frequency (RF) noise over the interval of 7.5 kHz-10MHz and deducted the background noise from the same interval to yield a noise percentage. The integration was chosen to only include the frequency interval well above mechanical noise and well below the pump

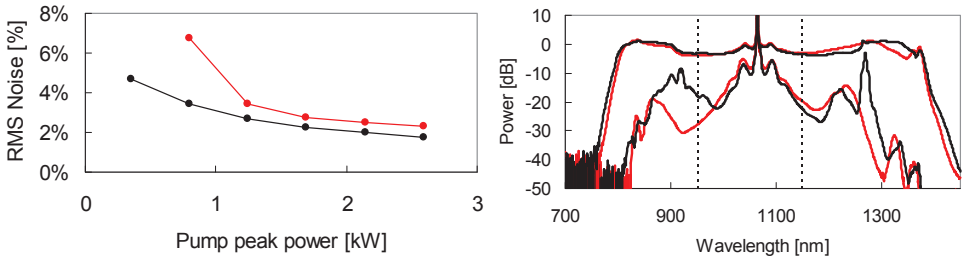

(a) **(b)**

Figure 3.16: (a) The RF amplitude noise integrated over 7.5 kHz-10MHz of the power above 1250 nm as a function of average pump power with (black) and without (red) back seeding. (b) The SC generated with (black) and without (red) back seeding just above the threshold 0.2 W average power ($P_0 = 0.35$kW) and at 1.5 W ($P_0 = 2.6$kW).

repetition rate as it is normally in this regime that sampling noise would be important for applications. The result can be seen in fig. 3.16a. The spectra relating to the highest and lowest pump powers can be seen in 3.16b. It should be noted that at 2.6 kW the effect of the seed on the spectrum is no longer seen in the FWM gain peak at 1270 nm but rather as the growth of a strong shoulder at 1300-1360 nm. This increase is over 4 dB or more than 150% and the only gain process in the fiber acting at these wavelengths is the dispersive wave generation from the solitons in the anomalous dispersion region. The change in the dispersive wave region is thus a sign that the distribution of solitons produced in the MI breakup has been altered by the seeding.

When inspecting the noise curve it is clear that the seeding gives a huge reduction of the noise at pump powers close to the threshold as has been found in earlier investigations on seeding in the MI band [54–56], but as the power is increased, the noise in the seeded spectrum approaches that of the seeded. Although the seeded spectrum still has only 3/4 of the noise of the unseeded even at the highest levels where the noise difference seems to be saturating, this is hardly enough to merit the considerably more complicated setup which is necessary to incorporate the seed in commercial systems. We therefore developed a simpler seeding scheme which was more compatible with the fibers commonly used for picosecond supercontinuum generation and this will be described in the next section.

3.7 Seeding through Raman scattering

3.7.1 Introduction

The investigations of seeded SCG that we have described so far have focussed on SCG in a fiber with two ZDWs in the silica transmission window, but this type of fiber will only generate a supercontinuum of rather limited bandwidth while most applications require high power supercontinua in the visible spectrum preferably extending deep into the blue and violet wavelengths. As will be explained in chapter 4, it is now well understood that in order to extend the spectrum well below 500 nm, the nonlinear fibers must have a group velocity of light at the shortest wavelengths of the SC which matches that of solitons at the longest. It has been shown how the spectra can be extended into the blue by optimizing the fiber structure [102], doping the material [2], or tapering the fiber [103].

In order to reduce the noise, particulary apparent in the longest and shortest wavelengths of the spectrum, it has, as mentioned previously, been proposed to provide a seed within the MI gain spectrum in order to ensure that the pulse breakup is dominated by a deterministic process instead of noise [55, 56].

In particular, Genty et al. [55] numerically investigated seeding at different frequency shifts in a fiber in which the MI gain peak had a frequency shift of 8 THz from the pump. They showed that a seed with a shift of 0-8THz accelerated the pump broadening and that shifts of 0-5 THz increased the coherence of the SC while 5 THz gave the greatest broadening of the SC. Thus the optimal seeding frequency was in this case 63% of the MI gain peak frequency. A frequency shift of 8-15 THz, i.e. outside the MI gain, but inside the Raman gain, gave a pronounced red shift of the SC with little soliton and dispersive wave generation while at 15-20 THz the seeding appeared to have little effect. The pump power of 75 W was split between the pump and seed wavelength and a significant effect of seeding was found when the pump modulation generated by the seed became more than 50% [55]. However, these results have yet to be verified experimentally.

While it has thus been shown that seeding can reduce the noise of supercontinua at low pump powers close to the MI threshold, visible supercontinua are normally pumped using 5-20 ps pump pulses with peak powers of approx 10 kW and we therefore investigate the effect of seeding at this power level.

Initially we have numerically analyzed some typical PCF designs optimized for broad visible generation presented by Stone et al. [102]. The endlessly single mode (ESM) design presented in [102] is typical of fibers previously used for the generation of high power visible continua, whereas designs with larger relative hole sizes and thus higher index contrast between core and cladding, called high-Δ fibers [104], have been shown to expand the

SC to significantly shorter wavelengths [102]. We used a mode solver based on the finite element method to calculate the dispersion profiles for three of the fibers presented in [102], as well as for Fiber A, which will be tested here. We then calculated the MI gain spectra at 10 kW taking into account the Raman response function by using eq. 2.18 as shown in sec. 2.2.3. [53]. The calculations showed that the MI gain band for all these fibers (see fig. 3.17) overlaps with the Raman gain band. In particular it should be noted that the MI gain peaks of the high-Δ fibers are at about 21 THz compared to the 13.2 THz peak of the Raman gain. The Raman peak is thus located at about 63% of the MI gain peak frequency, which was shown to give the widest SC by Genty et al. [55].

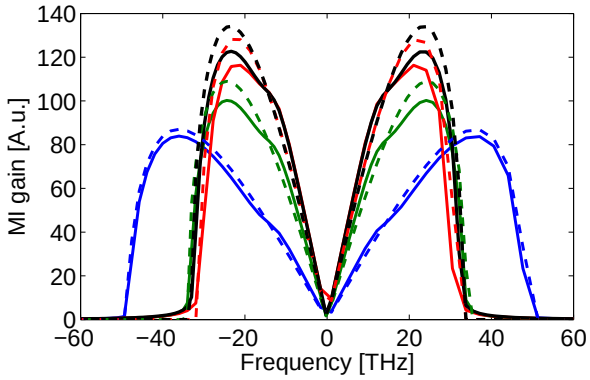

Figure 3.17: The calculated modulation instability gain spectra with (solid) and without (dashed) the Raman contribution for an ESM-fiber (blue) and two high-Δ fibers with $\Lambda = 3.7\ \mu m$ (green) and $\Lambda = 3.38(red)\ \mu m$ described by Stone et al. [102] and Fiber A (black), which is tested here.

This result indicates the possibility of generating a seed in the MI band simply by ensuring that amplified spontaneous emission (ASE) in the amplifier is amplified by the Raman effect and allowed to build up before the nonlinear fiber. This is much simpler than previous experimentally proven seeding methods. They have relied on generating the seed by splitting off part of the pump [56] or SC [1], in both cases controlling the seed spectrally and injecting it with temporal overlap with the pump pulse. The exact time matching of an injected seed is very difficult to control in a completely fiber integrated solution and a non fiber solution is difficult to make robust enough for many applications. A seed based on the Raman effect would, if it worked, be all-fiber, simple to make and inherently time matched. However, while the numerical investigation at low powers in [55] indicated that a Raman seed may accelerate and stabilize the pulse breakup, the calculation of the MI gain at 10 kW showed that the inclusion of the Raman

response in the equations reduced the MI gain in all four fibers. The reduction of MI gain when it overlaps with the Raman gain band has been seen in previous numerical investigations of the interaction of Raman and MI gain [53, 105, 106], but it has also been shown that the Raman gain may be considerably increased by matching with the MI gain [107]. A seed in the Raman gain band will deplete the pump power, which will reduce the power available for other nonlinear processes, but on the other hand the seeding may also seed the MI and stabilize the pulse breakup process. It is thus not easily predicted how the SC will be affected by seeding in the Raman gain band and to the best of our knowledge it has not been investigated previously. In order to test the Raman seeding method, Fiber A was fabricated by NKT Photonics A/S so that it would have an MI gain spectrum matching those of the high-Δ fibers optimized for broad visible SC generation in [102] and we have used this to experimentally investigate the effect of Raman seeding in high power SC generation.

3.7.2 Experimental investigation of Raman seeding

An all-fiber integrated custom made system was used in which a 1064 nm mode-locked Yb-doped fiber laser was amplified in several stages and spliced to an intermediate fiber before being spliced to Fiber A in which the spectrum was generated. The length of the intermediate fiber was varied in order to vary the Raman gain and thereby control the strength of the seed. This setup differed from the one used previously and was based on a 80 MHz pump laser and all fibers were spliced together to avoid the free-space isolator and coupling used above. The SC spectra generated as a function of the length of the intermediate fiber can be seen in fig. 3.18 and the fraction of pump depletion and Raman peak conversion can be seen in fig. 3.19. Almost 20% of the pump power can be shifted 13.2 THz to the Raman peak at 1114 nm by varying the length of an intermediate fiber from 0.9 to 2.75 m. The pump peak was thus reduced and the Raman seed strengthened while the total pump power was kept constant. This is similar to the principle used in the seed power test by Genty et al. in [55]. As can be seen in the insert on fig. 3.18 the seeding reduced the power in the 460–490 nm peak in the output SC. The power at 460–490 nm as a function of intermediate fiber length has been plotted in fig. 3.19 together with the pump depletion and Raman seed growth.

As the intermediate fiber was added the 460–490 nm peak was reduced by up to 35% while the power in the infrared wavelengths was increased. The reduction in power in the short wavelength peak at 2.4 m is nearly equivalent to the reduction in power obtained by reducing the power 20% while maintaining an intermediate fiber length of 0.9 m. The reduction in power in the blue can thus be explained simply by the reduction in pump

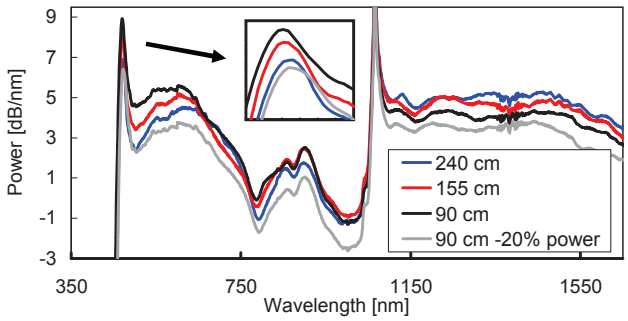

Figure 3.18: Output spectrum from Fiber A for different lengths of the intermediate fiber. The spectrum generated with a short intermediate fiber but 20% lower power has been included so that the effect of pump depletion can be estimated.

peak power if one assumes that the Raman peak does not add to the SC generation. However, since the power in the infrared wavelengths is significantly increased it is evident that energy in the Raman peak still contributes to the spectrum. The modified spectral power distribution in the output could be explained by the Raman seeding reducing the number of very high power solitons which red shift furthest. The high power solitons are responsible for shifting power to the shortest wavelengths and when there are fewer high power solitons there will be less power in the peak at 460–490 nm. It should also be noted that the MI breakup may to some degree be seeded by the pump itself because the spectral width of the 1064 nm pump pulses as it enters the PCF is approx. 18 nm or 5 THz and thus the pump line has a significant overlap with the MI gain band. This could also influence the effect seen from the Raman seeding because it may actually be the effect of two competing seeds and not a comparison between unseeded and seeded.

3.7.3 Noise in the Raman seeded supercontinuum

The pulse to pulse amplitude noise of the generated visible light was measured by passing the light through a 560 nm band pass filter with a FWHM width of 12 nm and measuring the transmission with a fast diode and analyzed using the same method as described above (sec. 3.6). There was a slight increase in noise from 11.5 to 12.6% as the intermediate fiber length was increased from 90 cm to 275 cm. However, this increase was close to the uncertainty limit of the measurement. The seeding was thus shown to have no significant effect on the noise in the signal. The noise at other wavelengths in the visible spectrum was also measured, but the general trend was the same.

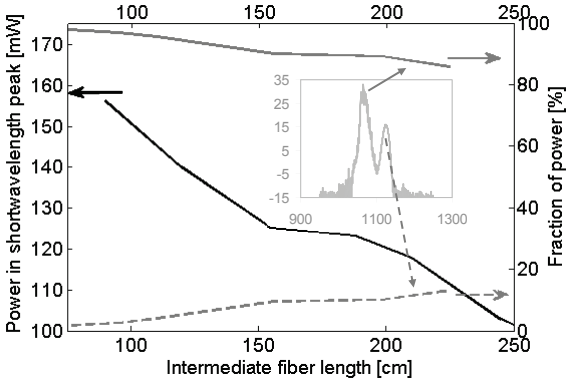

Figure 3.19: Power transferred to the 460–490 nm peak in the output with intermediate fiber length (solid black, left scale) compared to the fraction of power remaining in the 1046–1094 nm peak (solid gray, right scale) and converted to the 1102–1160 nm Raman peak in the input (dashed gray, right scale). The insert shows the input spectrum with 1 m intermediate fiber on a dB scale.

3.7.4 Conclusion on Raman seeding

We have shown numerically that the Raman effect reduces the MI gain in PCFs optimized for high power visual SC generation and we have shown experimentally that seeding the overlapping Raman and MI gain band with Raman generated light reduces the efficiency of power transfer to the shortest wavelengths of the SC. We have also shown that the seeding does not improve the noise properties of the SC. Thus this investigation shows that the simple approach of seeding in the MI/Raman gain band cannot be used to reduce the noise in high power visible supercontinua. However, seeding may still have a positive effect in other MI gain wavelengths with higher powers or with narrower spectra. The conclusions presented here are important to keep in mind when designing a fiber integrated SC generation system because it shows the importance of keeping the fiber length of the amplifier and any intermediate fibers to a minimum as power transfer to the Raman peak can significantly reduce the efficiency of the final system.

3.8 Conclusion on seeding

In this work it has been demonstrated both numerically and experimentally how a SC spectrum is generated when one pumps with picosecond pulses in the anomalous dispersion region between two closely spaced ZDWs. As has been shown earlier with CW pumping [83, 94–96], the long wavelength ZDW limited the SC by stopping the Raman shift of the solitons. However, the dispersive wave generation above the ZDW was more prominent than for CW pumping, as one should expect from the higher peak power. It has also been shown that a double pair of FWM gain bands contributed very significantly to the SC generation in this case. To the best of our knowledge this is the first time that pumping of the second pair of FWM gain bands has been experimentally verified with picosecond pulses. Since these pulses are in the quasi-CW regime it is expected that these effects may also be found with nanosecond and CW pumping.

We have also investigated the effect of feeding part of the SC output back into the PCF and time matching it with the pump pulses so that it could act as seed in the FWM gain band. Using this method it has been shown that strong local amplification peaks can be created. In an experiment it has been shown that the local increase in the spectrum can reach over 27 dB and it is thus a promising spectral modification technique. For some pump powers the creation of the local peak is accompanied by a strong increase in power over more than 100 nm of the short wavelength side of the continuum.

The generation of a peak in the SC could be useful for a number of pump-probe applications, such as Coherent Anti-Stokes Raman Scattering (CARS), where a strong pump peak is needed for excitation with a weaker continuum for probe wavelengths [108].

It is important to be aware of the possible effect of a feedback loop, which is demonstrated here, even if one does not wish to use it to modify the SC spectrum, because it can appear accidentally. This may occur if the facets of the PCF are not angle cleaved and its length accidentally gives it a round trip time which is close to a whole number of pump repetition periods. The effect will also be important if one uses long ns pulses with short PCFs or CW light, where the pulse is longer than the round-trip time for the light in the fiber, and the pulse thus can overlap temporally with its own reflections.

The noise in the feed back has also been investigated and it was found that close to the SCG threshold a great decrease in noise could be achieved by adding a seed, as has also been found in recent studies on seeding of Rogue solitons by seeding the inner MI gain band [56]. However, the effect of the seeding rapidly decreased as pump power was increased. Even at high powers the seeding did reduce the amplitude noise, but the reduction was too small to merit the considerably more complicated SCG setup which it required. Finally it was shown that a simple Raman based scheme of seeding the MI band of a fiber typical of those used for high power wide band SCG

with a Raman peak did not have any effect on the noise and in fact reduced the generation of blue light in the continuum. These results indicate that the improvement of the noise characteristics and spectral broadening of high power supercontinua which can be achieved through seeding is limited, and as we have simultaneously achieved more promising results through the use of fiber structure optimization and tapered PCFs the rest of this thesis will be devoted to these subjects.

3.8.1 Outlook for seeding

While the presented experimental results indicate that seeding has relatively little effect at high pump powers it has also been shown that it has great effect at low powers. It is therefore deemed that the greatest potential for the use of seeding will be in supercontinuum systems based on CW pumping where the peak pump power is much lower and the significant problem of time matching the seed is removed. In CW SCG it is difficult to generate light at wavelengths shorter than the pump with good efficiency because the solitons generated contain too little energy to generate strong dispersive waves. If seeding could stimulate the creation of stronger solitons it could therefore be an important tool in increasing the short wavelength power content in CW SCG. Generally CW SCG also require very long PCFs and the acceleration of the SCG which have been observed with seeding could allow one to significantly reduce the fiber length.

One could also use the feed back seeding to generate new laser wavelengths from a standard pump laser. The seeding of a higher order gain band that we have demonstrated could thus be used to shift the wavelength of a laser to wavelengths rather far removed from the original laser wavelength by choosing the right design of the fiber. It has also been suggested by Solli et al. [56] that the 30 dB switch in power which may be created at the seeding wavelength could be used as a switch or gain mechanism in e.g. telecommunication and the fact that this may also be done in a higher order gain band as demonstrated here should extend the wavelength flexibility of this application significantly and may also affect the noise of the operation of the seed-switch. However, this application is very similar to existing parametric amplifiers, and it is unclear if the performance the PCF based method is superior.

Chapter 4

Optimizing the dispersion profile of a fiber

The effect of seeding four-wave mixing in supercontinuum generation has been investigated in the previous chapter and it was found that this can considerably modify the spectrum and reduce noise in the supercontinuum when the pump power is near the MI threshold. However, it has also been shown that the effect of the seeding, especially on the noise, is much less pronounced at higher pump powers. The main focus of this PhD has been improved control of ultra broadband picosecond supercontinuum generation and this type of SCG operates with powers far above the MI threshold. This has been combined with a focus on approaches which could realistically be incorporated in mass produced supercontinuum sources so that improvements provided could benefit a wide range of supercontinuum applications. Technologies which could be built into all fiber systems were therefore much preferable because all-fiber systems are generally simple to produce and can be very durable in the field. It was deemed that seeding the continuum had too little effect at the relevant high power levels to merit the considerably more complicated system it called for and the main effort was shifted to what improvements could be gained from optimizing the fiber. In sec. 4.1 the data and the theoretical model which describes the short wavelength limit of the supercontinuum is described together with the guidelines that this gives for the design. It should be noted that while this development work was going on at NKT Photonics and DTU Fotonik, very similar work was carried out independently by Stone et al. [102], which resulted in very similar fiber designs. Section 4.2 discusses the processes that generate noise in the supercontinuum and presents some data on how the noise may be reduced with optimization of the design. The conclusion in sec. 4.3 sums up the results before the future prospects of the dispersion optimization will be presented in sec. 4.3.1. When evaluating the connection between the PCF structure and the generated spectra it may be interesting for the

reader to consult appendix A where the dispersion, group velocity, group velocity matching,effective area, MI spectrum, and leakage loss curves for a wide range PCF design have been plotted. Section 4.1 is based partly on a fiber optimization program already ongoing at NKT Photonics before the author joined the investigation, partly on a theoretical understanding and presentation of the results developed by Michael H. Frosz and partly on data gathered by the author. The rest of the chapter is fully the work of the author.

4.1 Maximizing blue shift by fiber design

As was explained in chapter 2, picosecond supercontinuum evolves because the pump pulse breaks up due to modulation instability and soliton collisions then lead to a concentration of energy in some of the solitons, which become much more powerful than the rest. During the breakup and collisions of the solitons, they emit dispersive waves in the normal dispersion region below the ZDW. Subsequently part of the dispersive waves will be blue-shifted due to soliton trapping as the solitons start to red shift. Traces of these mechanisms can be seen from the extent of the spectra of the supercontinua generated in different fibers. This was shown experimentally in the spectra generated by a series of fibers fabricated at NKT Photonics A/S. The group velocity profiles of the fibers, whose structural parameters can bee seen in table 4.1, can be seen in fig. 4.1. The dashed vertical lines mark the wavelength of the shortest wavelength peak in the continuum and the horizontal dashed lines mark the group velocity matching speed of these visible wavelengths to solitons in the infrared.

Table 4.1: Structural parameters of 5 different tested PCFs

Fiber pull	Pitch Λ [μm]	Relative hole size [d/Λ]
1	2.42	0.46
2	2.18	0.45
3	2.01	0.45
4	1.81	0.45
5	2.63	0.48

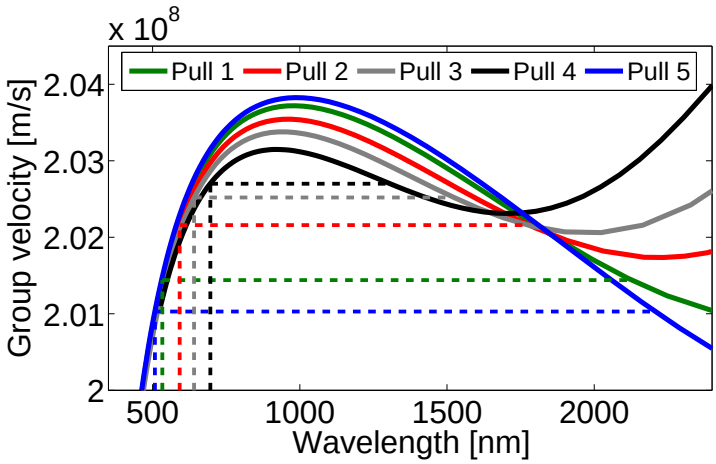

Figure 4.1: Group velocity curves of the five fibers from table 4.1. The vertical dashed lines mark the position of the short wavelength end of the continuum and the horizontal dashed lines trace the connection to the wavelengths of the solitons which match these wavelengths and where the infrared edge of the continuum is expected to be.

It is clear from fig. 4.1 that the group velocity (GV) of the shortest wavelengths all match wavelengths a bit below the local infrared minimum of the GV curves. This local minimum is caused by a second ZDW in the fiber dispersion profile. The red-shift of solitons generated from the pump will stop at wavelengths a little below reaching the ZDW due to soliton recoil from the dispersive waves that are generated above the ZDW as explained in sec. 2.2.4. Based on the knowledge gained from these five fiber pulls, a new fiber with $\Lambda = 3.55$ and $d/\Lambda = 0.522$ was designed by Kent E. Mattson at NKT Photonics. This fiber was designed so that its second ZDW would be considerably above the silica transmission window, which would ensure that the red-shift of the solitons would never be arrested by soliton recoil. The GV curve of this fiber along with dashed lines marking the extent of the continuum generated can be seen in fig. 4.2a. As can be seen, this fiber surprisingly did not generate a spectrum reaching far down into the visible wavelengths. This is mainly because its the spectrum also did not reach very far into the infrared. This show that even though the second ZDW is outside the transmission window the solitons may still stop red-shifting. Initially it was thought that the absorption of silica stopped the red shift in this fiber, but since the spectrum only extends to 2200 nm, the attenuation is only 0.1-0.2 dB/m and this is not enough to have a major effect on the

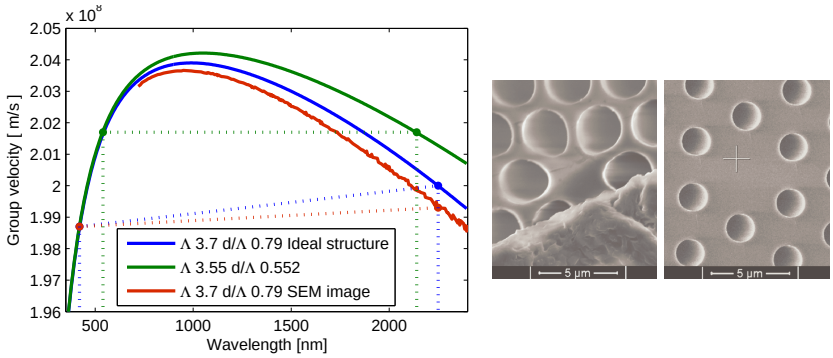

(a) **(b)** **(c)**

Figure 4.2: (a) The group velocity curves of the two new fibers with the second ZDW outside the silica transmission. The vertical dashed lines mark the wavelengths of the short wavelength and IR edges of the continua. The approximately horizontal dashed lines trace the approximate group velocity matching of the edges. The blue curve marks the group velocity curve calculated for a idealized structure with $\Lambda = 3.7$ and $d/\Lambda = 0.79$ where all holes are assumed to be exactly the same size and perfectly circular. The red curve marks the group velocity calculated from a SEM picture of the $d/\Lambda = 0.79$ fiber. (b) SEM of core area of the $\Lambda = 3.7$ fiber. A particle is blocking the lower half of the picture. (c) SEM of core area of the $\Lambda = 3.55$. fiber

supercontinuum generation. The fiber has rings of holes enough to ensure that the spectrum is not cut off by confinement losses. The only possible explanation for the limited red-shift is thus that the solitons created in the pulse breakup have too little energy and that the combination of dispersion and nonlinearity lets the solitons broaden too much temporally for the red-shift to continue.

In order to solve this problem another fiber with $\Lambda = 3.7$ and $d/\Lambda = 0.79$ was designed. It has a smaller core area and in a group velocity profile with greater deceleration at the long wavelengths in order to obtain GV matching with even shorter wavelengths. Because the area of this fiber is smaller, its nonlinearity is higher. According to eq. 2.22 this ensures that the pump pulses only have half as high a soliton number in this fiber compared to in the fiber with $\Lambda = 3.55$. With a rough estimate this should mean that the pulse breakup should generate half as many solitons with on average twice as much

energy in the fiber with $\Lambda = 3.7$ compared to in the fiber with $\Lambda = 3.55$. The effective area in the $\Lambda = 3.7$ fiber also increases less at longer wavelengths, because its larger air holes confines the light better. This ensures that the solitons continue to red shift until about 2375 nm and the blue edge of the continuum is pushed down to 420 nm. Even though the GV curve of this fiber is pushed further down at the long wavelengths, the curve calculated based on the idealized fiber structure (fig. 4.2a blue) does not explain how the spectrum could extend as far as observed into the blue wavelengths. Therefore the GV curve was re-calculated based on a SEM picture of the curve and this reduces the difference in the calculated group velocities at the two edges. This is because the air holes in the innermost ring of holes are slightly elongated toward the core (see fig. 4.2b) giving a core area which is in effect smaller than expected from the idealized structure. The elongation of the central holes is caused by the combination of temperature, strain and pressure on the holes during fiber production and is found in many fibers with large relative hole sizes. In the $d/\Lambda = 0.522$ fiber the holes are much more circular as seen in fig. 4.2c and the idealized model is therefore a good approximation.

There is some difference between the GVs calculated at the two edges of the SC even when using the SEM picture of the fiber for dispersion calculation partly because it is difficult to determine the exact hole size from the pictures (for more on this see sec. 5.3) but also partly because there is some uncertainty involved in determining the wavelength of the end of the SC. It should also be noted that the shortest wavelength of the SC should actually have a slightly smaller group velocity than the longest wavelength soliton because the trapping effect dictates that XPM from the trailing edge of the soliton will blue-shift the dispersive waves as long as they are time matched with the solitons trailing edge. This time matching will only stop when the soliton has stopped red-shifting and the dispersive wave is then blue-shifted to a wavelength which has a lower GV than the soliton. Thus the blue edge of the SC should have a slightly slower GV than the red.

It was found that as one altered the structure of the PCF fibers in order to get velocity matching deep in the visible, one loses efficiency in the conversion of pump light to visible light. This is because the ZDW is shifted away from the pump wavelength, which in turn makes the dispersive wave generation less efficient by reducing the spectral overlap between solitons and their phase matched wavelength. This effect is demonstrated experimentally in the study made by Stone et al. [102]. So the cost of the shorter wavelengths is less efficiency in their generation. In addition the core of the fibers must also be very small and it therefore becomes more difficult to couple light into the fiber or splice them to normal fibers.

Earlier the PCFs for supercontinuum generation were made with relative hole sizes below 0.45 because it was thought that it was necessary to keep them close to endlessly single mode (ESM) in order to create a single mode

continuum and they have therefore been named ESM-fibers [102]. However, it has been found that even when operating quite far from the ESM regime one can selectively pump the fundamental mode of the fiber and keep the supercontinuum in this mode. The fiber with larger air-holes which could thus be used to give group velocity matching deeper in the visible spectrum have been called high-Δ fibers [104] because the large air holes give a larger index difference between the core and the photonic crystal cladding.

4.2 Pulse to pulse noise with dispersion optimization

In most of the applications that high power supercontinuum is used for at the moment, the continuum it is basically treated as a CW source and measurements are only performed on long timescales where averaging is made over hundreds or thousands of pulses and the pulse to pulse noise is of little importance. This is acceptable for many applications. However, many new applications are appearing where the tolerance for pulse to pulse amplitude fluctuations is small because the measurements are made at much shorter time scales or the absolute amount of light emitted is critical. In order to generate a visible continuum efficiently from the commonly available picosecond lasers at 1060nm it is necessary to pump in the anomalous dispersion region close to the ZDW and it is well known that the pulse to pulse amplitude noise in a supercontinuum generated using these conditions is considerable [9].

The spectral broadening under these pump conditions is initiated by MI seeded by noise which converts the pump pulse into a train of solitons which subsequently collide and transfer energy to the strongest solitons. Since both the MI process and the collision stage amplify the effect of many small random fluctuations, the result is a large number of solitons with a very random distribution of powers. This was recently quantified by Solli et al. [64] who used a new measurement method to show that the distribution of the soliton energies at the long wavelength edge of a supercontinuum was described by an L-shaped probability distribution where extremely powerful solitons were much more common than predicted by a Gaussian distribution [56]. The energy of the solitons determines how far the solitons red-shift due to the Raman effect and the energy distribution therefore determines the spectral power distribution in the IR part of the supercontinuum. Since the visible part of the supercontinuum is mainly produced by the soliton trapping effect discussed in sec. 2.2.4, the infrared power distribution, and thus the soliton energy distribution, determines the visible energy distribution. The strong variations in the distribution of soliton energies from pulse

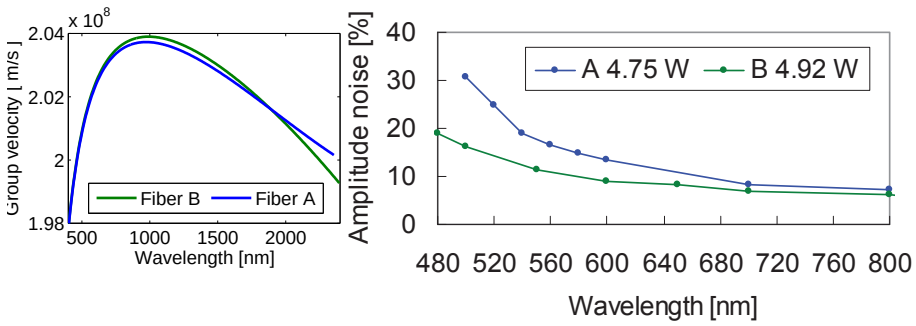

Figure 4.3: Group velocity curve (left) and amplitude noise curve (right) of a fiber with smaller air holes (fiber A) and a high-Δ fiber (Fiber B).

to pulse thus translates into large fluctuations in the spectral power available in any spectral slice. By controlling the final spectral position of the solitons, the energy distribution also determines their temporal position in the pulse and this means that there is also a large fluctuation in the temporal position of the sub pulses of the output supercontinuum pulse. There will therefore be very little coherence between pulses of the supercontinuum.

Due to the L-shaped probability distribution of the solitons, few solitons have the highest energies and above some threshold there will not even be a soliton of that energy level in every pump pulse but it will still be there once in every ten, hundred or thousand pulses on average. When combined with the energy-dependent red-shift this means that as one moves toward longer wavelengths from the pump there will be fewer and fewer solitons whose power can be averaged in every pulse and this means that the pulse to pulse amplitude noise in spectral slices should increase toward longer wavelengths. Since the visible light is generated by the IR light by the soliton trapping effect the visible power should fluctuate with the IR power so the noise will also increase the further down in wavelength one goes from the pump.

It has been shown that proper engineering of the dispersion profile can be used to group velocity match shorter wavelengths to the same infrared wavelengths and this has been used to expand the spectral width of the supercontinuum. However, so far it has not been considered how this affects the pulse to pulse amplitude noise of the supercontinuum. We made an initial investigation of this by comparing the noise from a fiber with smaller air holes (fiber A) and a high-Δ fiber (Fiber B) and the result can be seen in fig. 4.3. The noise measurement method was the same as the one described above in sec. 3.6. It is clear from the noise plot that the fiber B with the matching to the shortest wavelengths has a lower noise and one possible

explanation was that this is because the noise in the visible spectrum is determined by the noise of the infrared spectrum, which increases with increasing wavelength. The group velocity matching of shorter wavelengths to the same infrared wavelength therefore means that one can push the spectral noise in the spectrum down to shorter wavelengths by modifying the group velocity curve.

To test this conclusion the noise curves from the visible spectrum were plotted with their noise levels mirrored by their group velocity matched IR wavelengths. If the difference in noise level between the two fibers were only due to the visible wavelengths being matched differently to the same noise distribution in the infrared, the group velocity matching of the noise should approach to the same curve. Fig. 4.4 shows that the group velocity matching shift of the curves do not approach the same curve but rather indicate that the noise in fiber B is also considerably lower in the IR. This means that there is something inherently less noisy in the supercontinuum generation process in fiber B. The soliton number of the pump pulse, calculated from the data of the idealized structures, is 827 in fiber B and 816 in fiber A so the degree of chaos in the pulse breakup should be the same in the two fibers. One explanations could be that the larger air holes in fiber B means that there is a smaller increase in effective area with increasing wavelength and this means that the Raman shift does not slow down as quickly. However, the effective area in fiber B is larger than in fiber A, which means that its Raman shift per meter is lower. This could in turn mean the there are more soliton collisions before the solitons shift too far away from the main pulse

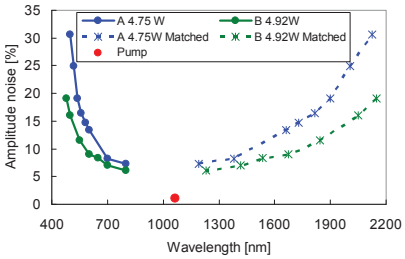

Figure 4.4: The noise curves measured in the visible spectrum for fiber A and B transferred to the wavelengths which have the same group velocity. This indicates the approximate noise spectrum for the infrared wavelengths. It is evident that this is different for the two fibers. The total output power in the fibers is noted in the legend. The noise and wavelength of the pump has been marked by a red dot.

to receive energy and this could mean that the solitons acquire more energy in fiber B. The conclusion at this point must be that there is no obvious reason why the spectrum from one fiber is considerably less noisy than from the other and the subject is in need of further study for clarification.

4.3 Conclusion on dispersion optimization

In this chapter we have shown how the PCF structure can be optimized to generate a wider bandwidth supercontinuum. It has been shown how the spectral limit in the blue is linked to the group velocity profile of the fiber the spectral limit in the IR. This limit can be set either by soliton repulsion from a second ZDW, by the soliton red shift due to low soliton energies and large core area, or by the IR absorption of silica. The first two limits can be removed by optimal fiber design, but the silica absorbtion sets the final IR limit of the supercontinuum. The group velocity of the shortest wavelength components in a supercontinuum will match the velocity of the longest and the fiber therefore has to be designed so that the IR red light will have a low group velocity. This is achieved by increasing the size of the air holes and reducing the core size but it has the side effect of shifting the ZDW away from the pump and reducing the conversion efficiency to the visible. It has been noted that when the air holes become large the shape of some air holes in the cladding easily become deformed and it is necessary to model the dispersion based on SEM pictures of the fiber to get a good fit to measurements. Finally it has been observed that the fiber structure also has a significant effect on the pulse to pulse amplitude noise of the fiber. Too little data is available to draw any conclusions as to the nature of the relationship between fiber structure and amplitude noise but it is a promising topic for further research.

4.3.1 Outlook on dispersion optimization

The quest for the fiber which generates the widest supercontinuum with the highest possible conversion efficiency will continue. It is still necessary to find the largest possible air fill fraction which can still keep the fiber single moded and to combine this with the right pitch to produce GV matching deep into the visible. The main problem is now that the efficiency of the light conversion to the short wavelengths falls as the size of the air holes is increased and the ZDW moves away from the pump. It is possible that this could to some degree be avoided by using a more advanced fiber structure. The work so far has focussed on fibers with a fixed pitch and relative hole size over the whole structure, but perhaps some of the radial hole size

variation techniques from dispersion flattened PCFs [109] could be used to optimize the dispersion profile even further. The modification of the material dispersion by doping has also been suggested as an interesting option [2] although the effects of the dopants on the silica nonlinearity and attenuation would still have to be considered further. Doping the core or cladding to produce a refractive index profile in the material might also be used to increase the single mode regime of the large air hole fibers in order to be able to achieve GV matching even deeper into the visible. As we have shown here, the fiber structure affects the pulse to pulse amplitude noise considerably, and although this dependence was expectable since the pulse breakup is heavily dependent on the dispersion profile, the connection between fiber structure and continuum noise has never been investigated in the high power picosecond regime. Therefore there remains considerable work to be done in characterizing how the noise is affected by the fiber structure and relating this to the physical processes involved in supercontinuum generation.

Chapter 5

Tapering photonic crystal fibers

5.1 Introduction to Tapering

The previous section described how optimization of the air hole structure of PCF fibers has been used to increase the spectral bandwidth of supercontinua. However, in the investigation of the fibers it was also found that one would need a very high air fill fraction and a small core in a fiber with a uniform cross-section to obtain group velocity matching of infrared wavelengths within the silica transmission window to wavelengths deep in the blue [102]. A Small core is, however, difficult to couple light into efficiently. In addition, a small core combined with a large relative hole size will shift the zero dispersion wavelength far below 1064 nm, which is the wavelength of many affordable and efficient pump lasers. This makes the dispersive wave generation inefficient [102], reducing the amount of power transferred from the pump to the short wavelengths.

To efficiently generate a very broad continuum one would therefore prefer a fiber that at the input has a large core and a dispersion profile with a ZDW just below the pump wavelength and further along the fiber beyond the point where the dispersive waves have been generated, has a dispersion profile which allows group velocity matching between the infrared part of the continuum and very short wavelengths in the violet region. This can be obtained by combining two fibers [73, 110], but since it is difficult to splice two fibers with very different core sizes without significant losses, it would be better change the fiber profile gradually. Using this approach very good results have been obtained with very long tapers [103, 110], but the fabrication of these tapers required the tapering to be done on a fiber drawing tower. This manufacturing method would make large scale production of these tapered fibers rather costly and keep the technology from having

an impact on most supercontinuum applications. In order to simplify the production method greatly so that tapers may be manufactured at a price which allows their use in a wide range of applications it is necessary to develop a tapering method which is based on the post-processing of standard PCFs on commercially available equipment. To this end we investigated the post processing of off-the-shelf PCFs on a Vytran tapering station. The size of the tapering station limited the total length of tapers to 10-15 cm. This is much shorter than the 5-20 m of fiber that are used in the ns and ps pulse-based commercial supercontinuum sources available today [18]. The taper profile therefore has to be carefully optimized in order to generate a wide supercontinuum in a fiber this short.

5.1.1 Nanosecond and picosecond pulses in tapers

When ps or ns pump pulses are used for supercontinuum generation in PCFs the pump pulses normally quickly break up into a train of solitons and in the process generate dispersive waves at the phase matched wavelengths in the beginning of the fiber. However, most of the supercontinuum width is only generated when the solitons red shift due to the Raman effect and a fraction of the dispersive waves is simultaneously blue shifted because of soliton trapping. The solitons red shift and decelerate so that their group velocity matches the group velocity at the short wavelength edge of the supercontinuum. This pushes energy down into the shortest wavelengths because the trapped short wavelength waves are caught behind the infrared solitons where they experience a blue shift from the cross phase modulation with the soliton [65]. However, unless the soliton energy is very high the soliton red shift is a relatively slow process which requires many meters for the soliton to reach its maximum wavelength, therefore the dispersive wave blue shift is also rather slow.

In a tapered fiber the deceleration of the solitons is mainly achieved by the changing of the fiber structure and only to a small degree by the continued red shift of the solitons. The soliton trapping process can therefore be greatly accelerated [111] and much shorter fibers can be used. If the relative hole size of the fiber is large the taper will also ensure that the $|\beta_2|/\gamma$ value, which determines the length of a soliton of any given energy, is considerably smaller at long wavelengths than for an untapered fiber. This will keep the intensity of the solitons high and increase their Raman shift and the resulting trapped wave blue shift.

5.1.2 Previous work on supercontinuum generation in tapers

Short PCF tapers have previously been studied by Lu and Knox, who showed that tapers can be used to create a highly coherent supercontinuum with 100

fs pulses at optimized wavelengths, while Mazhirina et al. [112] have shown numerically that spectral broadening can be enhanced by slightly modulating the core width. However both these studies relied on fs pumping where relatively short fiber lengths are the norm. In the ns regime Leon-Saval et al. have produced a wide visible spectrum using short PCF tapers with 532 nm nanosecond pump pulses in the anomalous dispersion region [113]. This required the waist to be less than 1 μm in diameter which made it very susceptible to damage from high pulse powers and therefore impractical for high power systems. Later Xiong et al. have made an impressive demonstration of how FWM in an untapered fiber with small air holes can be combined with a taper with inflated holes to produce a highly efficient supercontinuum reaching from 400-1400 nm using a 0.6 ns 1064 nm microchip laser [114]. Here we experimentally investigate short tapers with a constant high air fraction pumped with ps pulses. We thoroughly investigate the connection between the taper dimensions, the generated supercontinuum and the pulse to pulse amplitude noise in the spectrum. We also explore the generation process numerically and show how the temporal distribution of the spectrum of the output supercontinuum can be radically different from that of a supercontinuum generated using long fibers with a uniform cross section. Some of the results discussed in this chapter will be submitted in a journal paper shortly after the completion of this thesis. The numerical simulation of the supercontinuum generation described in sec. 5.2 were performed by Michael H. Frosz, but all other work including experiments, the calculation of fiber data, the tapering of fibers and the analysis of the all results is the work of the author.

In the following, a shorthand notation of L1-L2-L3 will be used to describe tapers with a input transition region of the length L1, a waist length of L2, and an output transition length of L3 see fig. 5.1. All the taper profile lengths are noted in mm, all waist diameters will be measured as the outer diameter of the fiber at the waist in microns and all untapered fiber lengths in centimeters. It will be assumed that the relative reduction in core size at the taper waist is equal to the relative reduction in outer waist diameter. The diameter of the untapered fiber is 125 μm

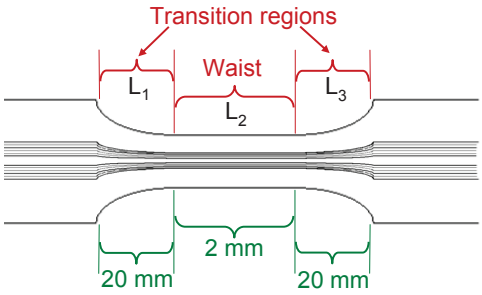

Figure 5.1: Diagram of the tapers produced. Normally about 20 cm of untapered fiber will be left before and after the taper. In this thesis a short form of 20-2-20 will be used to describe the profile of a taper such as this which has 20 mm long transition regions and a 2 mm long waist.

5.2 Numerical results

In order to estimate the feasibility of producing ps supercontinua using short tapers the design was first explored numerically. For the overall design we chose the PCF from chapter 4 with pitch $\Lambda = 3.7\ \mu m$ and a large relative hole size (d/Λ) of 0.79 because fiber with high air fractions had previously been used by Kudlinski et al to generate SCs reaching deep into the blue using long tapered fibers [103]. It was decided to have 20 cm of untapered fiber before the taper in order to ensure that the pulse breakup and soliton creation began before the taper, this also made it easier to handle the taper in the subsequent experimental testing. The taper profile was chosen to have a 20 mm transition region going down to a waist of 2 mm and a 20 mm transition region back to the original diameter of 125 μm. The taper was then followed by another 20 cm of untapered fiber to facilitate handling. A mode solver based on the finite element method was used to calculate the dispersion profile of the fiber assuming an ideal structure where all air holes were perfectly circular and their diameter (d) and pitch (Λ) constant across the entire PCF structure. This calculation was made for the untapered fiber and the structure reduced to 90%, 80%, 70%, 60%, 50%, 40%, and 30% of original pitch assuming constant (d/Λ). The dispersion curves (fig. 5.2a), group velocity curves (fig. 5.2b), group velocity matching curves (fig. 5.2c), and β_2/γ curves (fig. 5.2d) for these profiles have been plotted in fig. 5.2. The value of β_2/γ is important because this value determines the length of a soliton with a fixed energy (see sec. 2.2.4). Note that the use of the assumption of the idealized fiber structure for this fiber is not completely valid and that e.g. the group velocity curve is altered if one instead bases

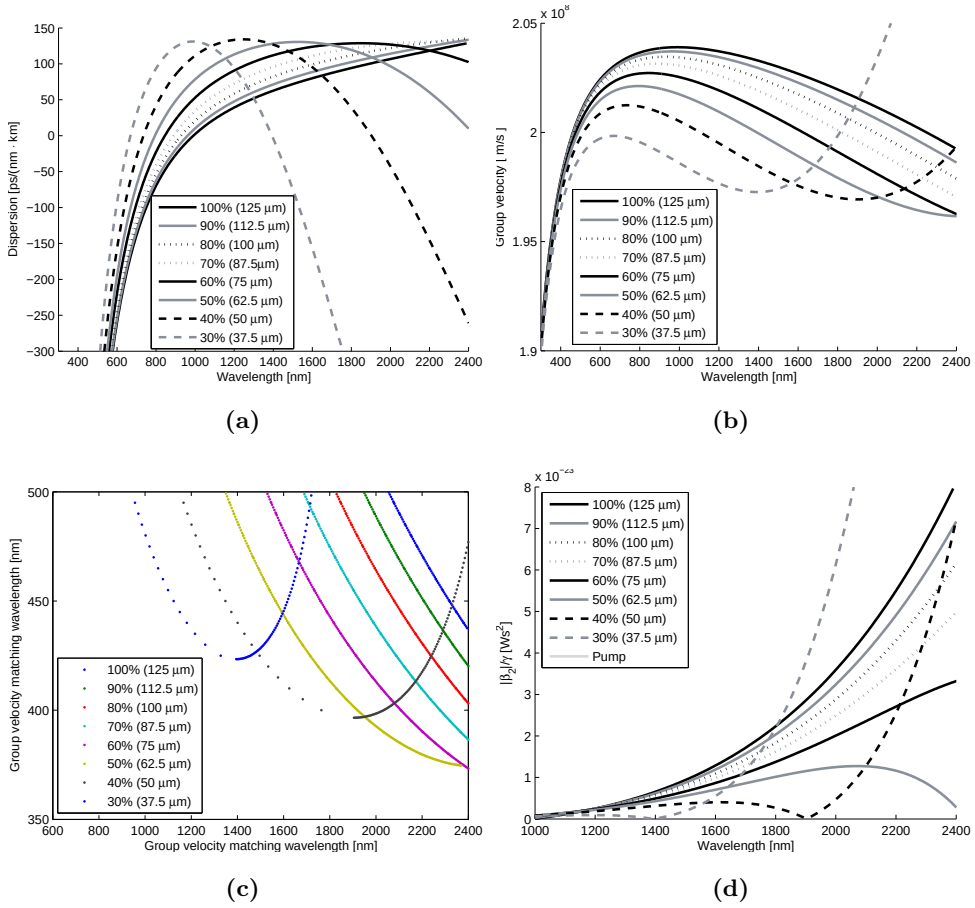

Figure 5.2: Fiber parameters as a function of fiber diameter calculated using a fully-vectorial plane-wave expansions method. 5.2a Dispersion profiles. 5.2b Group velocity profiles. 5.2c Group velocity matching wavelengths. 5.2d β_2/γ which determines the pulse length and thereby the Raman red shift of solitons relative to their energy.

the calculation on a SEM picture of the fiber as shown in fig. 4.2a. However, calculations based on the SEM images were slow and was therefore not used for estimates for the tapered fiber.

Among the most important parameters for generating SC that reaches into the short wavelengths using ps or ns pulses is the group velocity curve (fig. 5.2b) and the group velocity matching curve (fig. 5.2c) which is derived from it. As can be seen, the tapering of the fiber reduces the wavelength

which is matched to the maximum infrared wavelength of 2400 nm from approx 440 nm to approx 375 nm as the fiber diameter is reduced to 50% of the original diameter. If the fiber is tapered further, the second zero dispersion wavelength (see fig. 5.2a) moves down to wavelengths below 2400 nm where it will limit the red shift due to soliton recoil from the dispersive waves generated above the ZDW [59](see sec. 2.2.4). Thus the minimum wavelength with matching to the infrared increases with smaller waist diameters from this point. The β_2/γ relationship (fig. 5.2d) combined with the soliton energy decides the temporal length of the solitons and thus determines the rate of their Raman induced red shift. As the taper waist is reduced from 100% to 50% of the original diameter, β_2/γ is decreased, which assuming a constant energy means that the soliton pulse length is decreased, and thus the Raman shift will increase. This is an advantage for the SC generation because the soliton deceleration caused by the red shift will add to the deceleration caused by the taper and allow group velocity matching of even shorter wavelengths.

Based on these curves it was decided that the fiber should be tapered to 50% since this allowed group velocity match to the shortest wavelengths and the fastest Raman shift of the solitons while still keeping the long wavelength zero dispersion wavelength out of the silica transmission window.

The β_m values were then determined from each of the dispersion profiles for the 50%-100% diameters by a polynomial fit and m polynomial fits describing how each β_m value varied with taper width were then calculated as demonstrated by Falk et al. [90].

The propagation of the pulses was modeled using the NLSE [9, 23]

$$\begin{aligned}\frac{\partial \tilde{A}}{\partial z} =& i\sum_{m\geq 2}\frac{\beta_m}{m!}\left[\omega-\omega_0\right]^m\tilde{A}-\frac{\alpha(\omega)}{2}\tilde{A} \\ &+ i\gamma(\omega)\left[1+\frac{\omega-\omega_0}{\omega_0}\right]\mathcal{F}\left\{A(z,T)\int_{-\infty}^{\infty}R(T')\left|A(z,T-T')\right|^2\mathrm{d}T'\right\},\end{aligned} \tag{5.1}$$

where $A(z,T)$ is the field envelope in a retarded time frame $T = t - \beta_1 z$ moving with the group velocity $1/\beta_1$ of the pump along the fiber axis z. $\mathcal{F}\{A\} = \tilde{A}$ denotes the Fourier transform. ω_0 is the center angular frequency of the computational frequency window. In this eq. 5.2 was used to implement the nonlinearity because this has been shown to give good results in simulations. [2, 115]

$$\gamma(\omega) = \frac{n_2 n_{\text{eff}}(\omega_0)\omega_0}{c n_{\text{eff}}(\omega)\sqrt{A_{\text{eff}}(\omega)A_{\text{eff}}(\omega_0)}} \tag{5.2}$$

where $n_2 = 2.6\times10^{-20}$ m^2/W is the nonlinear-index coefficient for silica, c is the speed of light in vacuum,$n_{\text{eff}}(\omega)$ is the effective refractive index, and $A_{\text{eff}}(\omega)$ is the effective core area.

The transverse field distribution $E(x, y, \omega)$ of the fundamental mode was calculated using a mode solver based on the finite element method. From this $A_{\text{eff}}(\omega)$ was calculated using the definition suitable for fibers where some of the field energy may reside in the air-holes [116]. $R(t)$ is the Raman response function [23, 117]

$$R(t) = (1-f_{\text{R}})\delta(t)+f_{\text{R}}h(t) = (1-f_{\text{R}})\delta(t)+f_{\text{R}}\frac{\tau_1^2+\tau_2^2}{\tau_1\tau_2^2}\exp(-t/\tau_2)\sin(t/\tau_1)\Theta(t) \tag{5.3}$$

where $f_{\text{R}} = 0.18$ is the fractional contribution of the delayed Raman response, $\tau_1 = 12.2$ fs, and $\tau_2 = 32$ fs. $\Theta(t)$ is the Heaviside step function.

The propagation equation, eq. (5.1), is solved using the split-step Fourier method [23], with an implementation of the adaptive step-size method [118] using a local goal error of 10^{-6}.

To realistically model the finite linewidth of the pump laser, we used the same phase noise model as in Ref. [63], since the underlying phase-diffusion model is physically well-founded [119, 120]. The linewidth in the simulations was set to 530 GHz ($\sim$ 2 nm). The average power was set to 7.9 W because most tapers were only pumped with up to 11.3 W in order to avoid melting the waist and the coupling from the pump to the fiber was approx. 70%. The pump repetition rate was 80 MHz and the FWHM pulse length length of 14.6 ps which had been measured on the system was used in the simulation.

The supercontinuum spectra derived by the numerical simulation can be seen in fig. 5.3. The pump pulse has already broken up in solitons before the taper and the SC generation in this regime is dominated by solitons collisions, dispersive wave generation, and soliton red-shifting while the soliton trapping is just beginning to take effect. This can also be seen in the spectrogram of the pulse seen in fig. 5.4a. As the fiber is tapered down the spectrum grows considerably toward the shorter wavelengths because the solitons are decelerated by the taper and trap waves in the visible which are blue-shifted to slower wavelengths (see fig. 5.3 and fig. 5.4b). In the taper waist the waves become slightly more blue-shifted as the solitons red shift slightly, but this effect is minor because the taper is only 2 mm long. As the fiber diameter starts to increase in the output transition region, the solitons accelerate and the blue waves which they had trapped fall behind and do not interact further with the solitons and there is little further change in the visible part of the spectrum. Meanwhile the solitons will continue to red shift, which is seen in the continued growth of the spectrum towards the infrared wavelengths.

The temporal shape of the spectrogram on fig. 5.4b showing the pulse at the waist is radically different from those of conventional supercontinuum output pulses based on ps pumping of long fiber with uniform cross section (see e.g figure 5.4c). The spectrum at the taper waist goes all the way

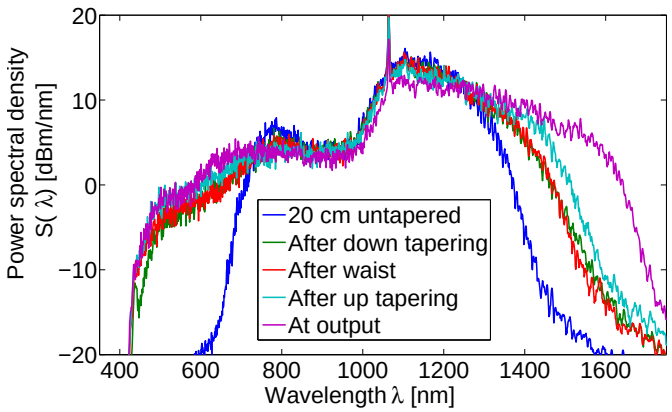

Figure 5.3: The Supercontinua derived from the numerical investigation of a 20-2-20 mm taper with a waist of 62.5 μm. The spectra were averaged over 5 simulations with different noise seeds and smoothed using Savitzky-Golay filtrering.

down to 400 nm, but all the energy is still contained roughly within the original temporal pulse envelope with a FWHM length of about 14.6 ps. In a conventional supercontinuum the light at the shortest wavelengths is only generated after the solitons have had a long fiber in which to be red-shifted and delayed and the result is that the pulse gets a U-shaped spectral-temporal profile in which the leading part is centered around the original pump wavelength and ZDW and the short and long wavelength wings trail far behind. In a conventional ps supercontinuum pulse the light in the bluest wavelengths may thus lag hundreds of ps behind the remains of the original pump pulse as seen in fig. 5.4c. This huge intra pulse chromatic dispersion can naturally greatly complicate the design of systems in which timing of the signal is critical. The spectra generated in these short tapers is on the other hand temporally very well confined because the fiber is so short that its chromatic dispersion does not have considerable impact on the pulse shape. It should, however, be noted that the short supercontinuum pulse generated in the waist will quickly be elongated if the output fiber is long because the light at the ZDW and at 400 nm will separate with 150 ps/m due to the difference in group velocity.

The numerical study has thus confirmed that it may be possible to generate a wide SC in a PCF taper of only a few centimeters' length and that the output continuum pulses could have a very interesting temporal shape. We therefore moved on to fabricating the tapers.

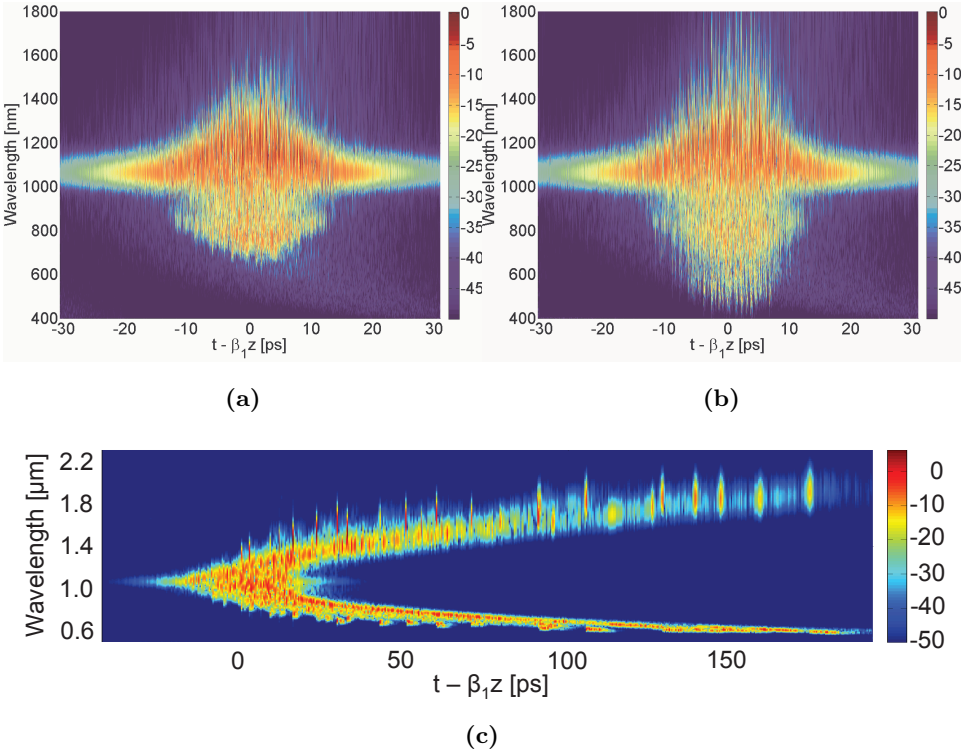

Figure 5.4: Spectrogram of the supercontinuum at the input of the taper (a), at the waist of the taper (b). The spectrogram of a SC pulse generated in 5 m untapered PCF with $\Lambda = 3.55$ and $d/\Lambda = 0.522$ (d) has been included for comparison as an example of a conventional picosecond generated SC. Note that the time scale of fig. d is compressed relative to fig a and b in order to fit on the page. The bars on the right of each figure show the relative energies in the spectrograms.

5.3 Taper Fabrication

The raw fiber chosen for the fabrication was a PCF with a pitch (Λ) of 3.7 and relative hole size (d/Λ) of 0.79. Sections of the fiber was tapered using a Vytran LDS-1250 tapering machine. This machine uses a small furnace based on a resistor heated by electrical current. The fiber is passed through the furnace which has a width of a few millimeters and is fixed at both ends to two translation stages. Fiber tapering is performed by gradually moving the fiber through the furnace while the speed difference between the mount

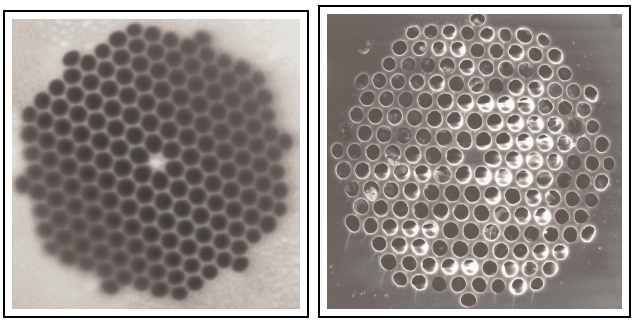

Figure 5.5: Left: Optical microscope photograph of the waist cross section of a fiber tapered to 60 μm waist width recorded with x100 magnification. Right: SEM picture of the waist cross section of a fiber tapered to 62.5 μm. The color differences across the fiber facet on the SEM picture are caused by surface damage from the imaging electron beam, contamination and astigmatism in the lens effect created by the electric field.

pulling on the fiber and the one feeding the fiber into the furnace controls the the local reduction of the fiber width. Thus the machine in effect functions as a miniature drawing tower. The tapers were drawn without pressure control on the holes in the PCF structure, instead relying on a cold and fast drawing technique [113] to avoid hole collapse. The loss at 1550 nm was measured while the tapers were drawn and was approx 0.2 dB $\pm$ 0.1 dB when the process had been optimized.

When using the fast and cold tapering technique without pressure control finding the right temperature for the taper drawing is critical. If the temperature is too high, the viscosity of the glass will become too low and surface tension will cause the holes of the PCF structure to contract. If the temperature is too low, the strain on the glass will rise too high and the fiber will break at the waist. If the temperature is just right, the relative hole size will be maintained while still minimizing the risk of breakage. The correct temperature depends on the velocity of the fiber through the furnace and on the waist diameter. Considerable research was therefore required to determine the correct process parameters. Even after optimization it is important to ensure that there is no contamination of the fiber and no vibrations during the drawing, otherwise the loss of the tapers becomes too high. Nevertheless when the correct parameters have been found, tapering the fiber should in principle be superior to directly drawing a fiber of the same dimensions [113].

In order to determine the correct temperature for tapering it was im-

portant to be able to monitor the structure of the PCF. This was done by cleaving the tapers at the waist and inspecting the PCF structure using optical microscopy and/or scanning electron microscopy (SEM). The resolution of the optical microscope is intrinsically limited by the optical wavelength of light and diffraction limits the smallest visible details to about 0.2 μm. The diffraction blurs the fine details of the fiber structure and the decision of where to set the boundary of the holes relies heavily on the discrimination and experience of the of the operator. When measuring the pitch this is not a serious problem because one can measure the pitch over many periods and divide by the number of periods. Thereby the blur affect 0.2 μm over a distance of e.g. 26 μm when measuring 7 periods. However, the hole diameter has to be measured on individual holes and the blur therefore affects 0.2 μm on a diameter of e.g. 1.5 μm in the case of a hole in the fiber tapered to 50 %. As the cross section of the fiber is reduced this problem becomes more and more pronounced.

SEM imaging of an isolator material such as silica has the intrinsic problem that as one bombards the surface with electrons it becomes charged, producing an electric field that acts as a lens which blurs the image. This can be avoided by covering the fiber facets with a conducting metal like gold, but this is an additional time consuming and expensive process and was therefore bypassed here. Instead we used an advanced FEI NovaSEM 600 in which images could be recorded with low voltage and low vacuum to reduce surface charging. Using this approach SEM images can show the structure in much greater detail but the process is relatively time consuming. In general we used the optical microscopy as an online fabrication analysis while SEM microscopy was only used for examination of details in the structure. The typical difference in image qualities between optical microscopy and SEM can be seen in fig. 5.5.

Using either method the relative hole size measured had by far the highest error margin since it was difficult to pinpoint the exact boundary between air and glass on optical microscope and SEM pictures. It was found that when the tapering fraction was confirmed by measuring the outer diameter of the fiber, the pitch of the fiber structure gave a good indication of the absolute hole size. If the pitch had been reduced with a greater factor than the fiber diameter it was a sign that the temperature was too high and the viscosity of the glass had been so low that surface tension had caused the holes to contract. The combined contraction of all the holes in the PCF structure then contracted the size of the entire PCF structure relative to the fiber diameter, reducing the pitch of the structure compared to the fiber diameter.

5.4 Single and Multimode transmission

From the early days of PCFs it has been known that one of their unique characteristics is that they can be endlessly single mode (ESM) [41], as was described in sec. 2.1.4, but it has been found that a PCF only will be strictly endlessly single mode if its relative hole size is smaller than 0.43 [121]. If the holes are bigger, the fiber can support higher order modes. However, the higher order modes will have higher leakage losses and with careful alignment at the input it is still possible to pump selectively so that nearly all light propagates in the fundamental mode. This is because the effective refractive index difference between the fundamental mode and the higher order modes is large and the coupling between the modes is therefore weak [104]. It is important that the pump is in the fundamental mode, not only because we want a single mode output, but mainly because the dispersion between the modes (see sec. 2.1.4) means that the temporal confinement necessary for efficient SCG will be ruined if the pump is distributed between several modes.

It is well known that the tapering of a fiber has to be gradual in order to avoid losses due to mode mixing in the taper. In order to avoid this the taper should be adiabatic and which can be calculated with eq. 5.4.

$$|\frac{dr}{dz}| \leq \frac{r(\beta_{Core} - \beta_{FSM})}{2\pi} \tag{5.4}$$

Where dr/dz is the taper gradient, r is the radius of the fiber, β_{Core} is the β value for the core mode and β_{FSM} is the β value for the fundamental space filling mode of the cladding structure in the absence of defects. We experimentally tested that this criterion was fulfilled by coupling a wide supercontinuum through one of the narrowest tapers and verifying that there was no significant losses anywhere in the spectrum: If coupling to cladding modes had been a problem a significant losses at the longer wavelengths should have been visible. It was also calculated by Peter John Roberts, formerly at DTU Fotonik, that the taper structures we consider here should not have any problems with mode coupling to higher order modes from the fundamental mode. The coupling to higher order modes should be more efficient than coupling to cladding modes and thus there should also be no coupling to cladding modes. If there were significant coupling to higher order modes it would not be possible to efficiently couple the light into another singlemode fiber or focus it to a diffraction limited spot on a target and this would severely limit the applications of the taper generated supercontinuum. Since the calculations relied on an ideal taper with no longitudinal fluctuation it was decided also to test experimentally that the output light was in the fundamental mode. It was enough to test that the shortest wavelengths were in the fundamental mode since it has been shown by e.g. Folkenberg et al. [121] that if a PCF or conventional fiber guides only the fundamental

mode at one wavelength it also guides only the fundamental mode at longer wavelengths, if it guides the light at the longer wavelengths at all.

In order to verify that the shortest wavelengths were in the fundamental mode, the output light from a 20-20-20 mm taper with a waist of 60 μm was coupled into a fiber which was single mode in the visible spectrum. This type of coupling can only be done efficiently with light in the fundamental mode. The coupling and transmission efficiency through this fiber is shown in fig. 5.6 and is approx. 50–70 % from 425 nm to 650 nm, which is good considering the fiber attenuation, the spectral sensitivity of the achromatic lenses used and the bandwidth of the spectrum. Far field inspection of the spot shape did not show any trace of higher order modes either. Since the short wavelengths of the supercontinuum could be coupled efficiently into a single mode fiber, the whole supercontinuum must be expected to be primarily in the fundamental mode.

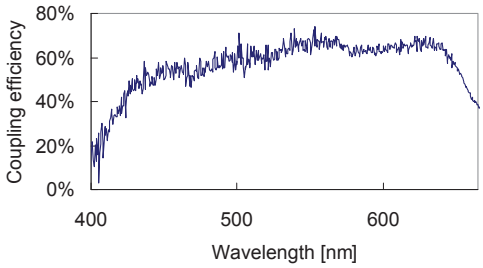

Figure 5.6: Broadband visual light coupling efficiency from the output of a tapered fiber through a conventional step index single mode fiber.

As mentioned in sec. 2.1.3, a PCF fiber may also exhibit confinement losses from core light leaking through the cladding structure. These confinement losses have a step-like shape, suddenly increasing rapidly above a certain wavelength. This wavelength is known as the cut-off wavelength of a mode. This cut-off wavelength will move to shorter wavelengths as the fiber is tapered down. For the tapers described here, the cut-off was estimated from the imaginary part of the effective refractive index as discussed in sec. 2.1.3. Due to the large air fraction of the tapers, the light is strongly confined to the core of the fiber and significant leakage (>0.1 dB/m) was only found above 2400 nm when the fiber was tapered to $\Lambda = 1.11\mu$m (30 %). This corresponds to $\lambda/\Lambda = 2.16$ for a taper with $d/\Lambda = 0.79$. This is similar to the results found by Nguyen et. al. [122] who measured a fundamental mode cutoff of $\lambda/\Lambda = 1.68$ for $d/\Lambda = 0.56$ and $\lambda/\Lambda = 1.91$ for $d/\Lambda = 0.70$. The findings also correspond well to the value of λ/Λ just over 2 predicted by Kuhlmey [123]. However, if fibers with smaller air holes are tapered, the fundamental mode cut-off will be an important limit on the minimum waist

diameter that can be made as can be seen from fig. A.6 in appendix A.

The cut-off wavelength of confinement losses is shorter for the higher order modes than for the fundamental mode. This could be seen as the transmission of the PCF was measured during tapering using multimode light from a mercury lamp. When the loss was measured after a section of the PCF had been tapered, it was noted that there was a loss in the long wavelength transmission whose cut-on wavelength moved downwards when the waist of the fiber was narrowed. This loss did not appear when transmission was measured using a singlemode source. A series of tapers with decreasing waist diameter was made in order to investigate this loss and it was found that the short wavelength edge of the loss was proportional to the pitch of the waist section with the approximate relation of $\lambda_{loss} = 0.84\Lambda_{waist}$. This is somewhat less than the value of derived by the equation for the multimode cut-off derived by Kuhlmey [124]:

$$\lambda/\Lambda \simeq \alpha(d/\Lambda - 0.406)^{\gamma} \tag{5.5}$$

where $\alpha = 2.80 \pm 0.12$ and $\gamma = 0.89 \pm 0.02$, which for this fiber with $d/\Lambda = 0.79$ would give $\lambda/\Lambda = 1.19 \pm 0.07$. This difference is explained by several factors. It is difficult to set the exact cut-off wavelength for the loss, the taper may not be adiabatic for higher order modes leading to mode mixing, the holes of the structure may have contracted during tapering if the tapering temperature was too high, which would give a shorter cut-off wavelength, and finally Kuhlmey's equation deals with a fiber structure with ideal circular holes whereas this structure has visibly elongated holes around the core leading to a core which is in effect smaller than the in the idealized case and thus with a shorter multimode cut-off wavelength.

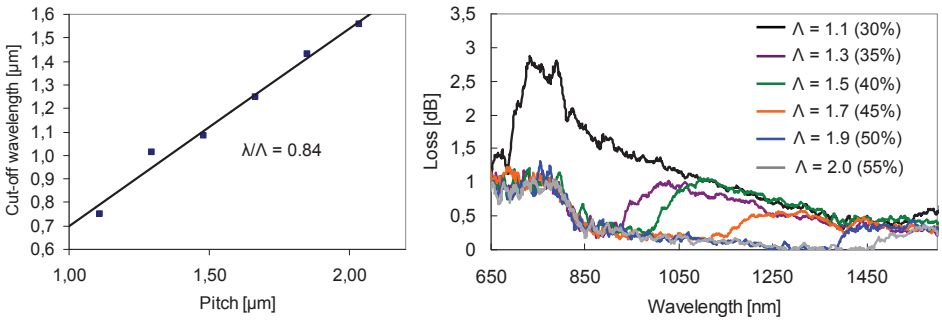

Figure 5.7: Measured multimode cut-off wavelength plotted as a function of pitch of the taper waist (left). Spectra of the loss produced by the multimode cut-off for different waist diameters. All tapers had a 20-2-20 mm profile.

5.5 Experimental setup and results

The tapered PCFs were tested on a measurement setup which was based on a modelocked ytterbium PM fiber laser amplified in several stages to an average power of up to 14 W at 1064 nm with a repetition rate of 80 MHz. The pulse Full Width Half Maximum (FWHM) length was measured to be about 14.6 ps using an autocorrelator. The pump light is coupled into the tapered PCF with a coupling efficiency of about 70% and spectra were recorded through an integrating sphere using an Ando Optical Spectrum Analyzer (OSA) AQ6315A. The power was measured using a thermal power meter and the spectra were then normalized to the power readings.

Since the amplitude noise in supercontinuum is important for many applications, it was measured for many of the tapers presented. The pulse to pulse amplitude noise was measured by the same method described in sec. 3.6, filtering the supercontinuum through bandpass filters with a width of 12 nm and various center wavelengths in the 480 nm to 800 nm interval. The transmission of the filters was measured using a fast diode (Thorlabs DET210) connected to a fast oscilloscope. The sample rate was 2 ns per point and the sample length 4 ms. The sample train containing 320.000 pulses was analyzed, using a custom program at NKT Photonics, which basically performed a Fourier transformation, and integrated the noise over the interval 7.5 kHz-10Mhz and deducted the background noise. This quantified the noise of a trace as a percentage which could be used for comparison. The noise frequency interval was chosen well below the pump repetition rate but above the effect of mechanical noise sources. The visible wavelength interval was chosen for noise investigation since it covers the overlapping intervals of the wavelengths generated by current commercial supercontinuum sources and the wavelengths used in important applications such as microscopy.

5.5.1 Taper compared to uniform fiber

The first step of the experimental investigation was to produce the tapers, measure the output supercontinuum they generated, and compare the output to spectra from the untapered fiber. This comparison is shown in fig. 5.8. The fiber with 20 cm long untapered delivery fibers and a 20-2-20 mm taper in the middle is actually able to deliver a spectrum which goes just as far down in wavelength as the 10 m long fiber and which goes 90 nm further down in wavelength than a 50 cm untapered fiber. However, the broad spectrum comes at the price of lower power in the visible wavelengths. Compared to the untapered fibers, the taper has much lower power in the short wavelengths, while the infrared spectrum above 800 nm contains considerably more power. The conversion efficiency from the long wavelengths is thus considerably lowered. In the spectrum of the taper one can see a

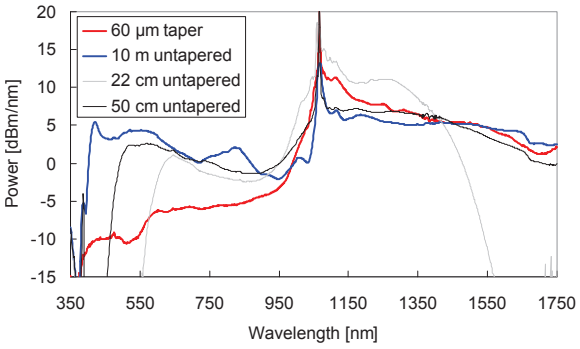

Figure 5.8: The spectrum generated in a taper with a 60 μm waist compared to a 10 m long untapered fiber (solid gray). The taper has 20 cm untapered fiber before and after the taper and it has 20-2-20 mm profile. The spectrum from 22 cm untapered fiber (gray dotted) is similar to the spectrum entering the taper while the 50 cm long untapered fiber (black dotted) has the same length as the fiber on which the taper is made.

significant increase in power at wavelengths over 550 nm; this is the point which marks the end of the spectrum generated by the 20 cm untapered section before the taper and the light below this wavelength is generated by the taper.

The amplitude noise in the 480-800 nm interval measured for the taper and untapered fibers can be seen in fig. 5.9. As can be seen, the noise of the 10 m untapered fiber is steadily increasing toward the shorter wavelengths in an approximately exponential fashion. This shape of noise curve is very general for uniform fiber pumped in the anomalous dispersion region and the ps regime, at least when the second Zero Dispersion Wavelength (ZDW) is at a much longer wavelength than the maximum extent of the SC. It is natural that the noise increases exponentially toward the short wavelengths since the light here is coupled to the light at the longest wavelengths. The soliton self frequency shift determines that the light at the longest wavelengths represents the most powerful solitons and the literature on Rogue waves by Solli et al. [64] and others has thoroughly described how the most powerful solitons are also the ones most rarely generated from a pulse. The shortest wavelengths generated are connected to these rare and very powerful solitons and thus will also be the ones with the greatest variation in amplitude from pulse to pulse. In the noise analysis this results in the noise rising exponentially towards shorter wavelengths.

As seen in fig. 5.8, the 22 cm untapered fiber, has the same exponential

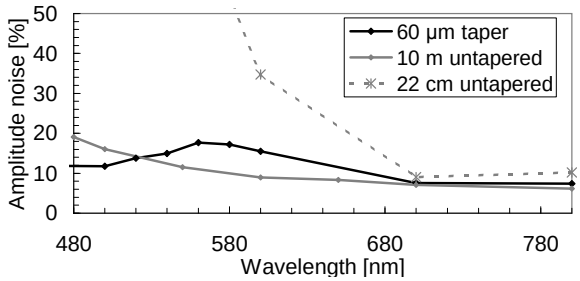

Figure 5.9: Noise curves for a taper with a 60 μm waist compared to a 10 m long untapered fiber (solid gray). This is compared to a 22 cm untapered fiber (dotted gray) which represents the spectrum entering the taper.

increase in noise as the 10 m fiber but the noise rises to a much higher level as it approaches the edge of the generated spectrum at 550 nm. The short fiber is much more noisy because at 22 cm the modulation instability induced breakup is just beginning. This means that there is a significant amount of noise arising from the variation in the exact fiber length at which the breakup occurs for the different pulses. The breakup point varies significantly because of small variations in the input pulse and in the amount of light present in the modulation instability gain band. After the pulse breakup there is a large number of soliton collisions which create the most powerful solitons [63]; the collision process has only just begun at 22 cm and this will also affect the noise in the spectrum. The noise from 22 cm untapered fiber shows the approximate amount of noise in the spectrum when it enters the taper.

The noise of the tapered fiber differs remarkably from the untapered fiber in that from 800 nm it increases down to 560 nm, which is approximately where the spectrum from the 20 cm fiber before the taper ends, then the noise decreases down to 480 nm where the light is half as noisy as that from a 10 m long untapered fiber. The fact that the short wavelength light is much less noisy with the taper may be explained by looking at the spectrogram in fig. 5.4b where it is evident that the light between 600nm and 400nm is created all along the pulse. This is in sharp contrast to a uniform fiber (see fig. 5.4c) where the short wavelengths are generally delivered as a few trapped waves matched to a few very powerful infrared solitons. The blue light in the taper might therefore be less sensitive to the exact power of the individual solitons created in the breakup and therefore less noisy. It is difficult to identify why the taper generated continuum noise differs from that of uniform fibers because the exact mechanisms leading to differences in noise level between SCs from ps pumped uniform PCFs have still not been

thoroughly investigated. Such an investigation is beyond the scope of this thesis, but the measurements presented here may help to shed some light on the area.

Some insight can be gained into the possible origin of the peak in the noise profile of the taper by comparing it with the spectrum as has been done in fig. 5.10 (a) and (b). There it is clear that the noise peak at 560 nm corresponds to the edge of the continuum generated before the taper. This region is very noisy because the extent of the supercontinuum fluctuates from pulse to pulse due to the fluctuations in the soliton distribution. The high noise in these wavelengths is the short wavelength correspondent to the fluctuations in the wavelength of the IR supercontinuum edge which has been investigated in connection with Rogue solitons [54–56, 64]. In fig. 5.10 (c)-(f) are also shown samples of the diode traces from which the noise percentages have been calculated. These should convince any sceptics that the differences in noise level measured are due to actual fluctuations in the signal and not artifacts created by the different amounts of light and thus different signal-to-noise ratios at different spots in the spectrum.

5.5.2 Comparison between experiment and simulation

When the numerical data are to be used to interpret the experimental results it is important to be sure that the results are comparable. The measured and simulated spectra after the 20 cm untapered fiber and after the taper and second 20 cm untapered fiber section can be seen in fig. 5.11. It is clear that there is good correspondence in the general shape of the spectra and the alteration caused by the inclusion of the taper. However, it is also clear that the measured spectra (fig. 5.11a) are considerably broader but weaker than the simulated spectra (fig. 5.11b). The residual energy in the pump is also considerably higher in the measured spectra.

The increased broadening of the measured spectrum after 22 cm compared to the simulated after 20 cm is explained by two factors: the measured fiber is slightly longer and the central air holes of the fiber are slightly elongated as shown in fig. 4.2b. The elongation means that the fiber core is slightly smaller, which increases the nonlinearity, the soliton red shift, and thereby the blue shift. In addition the smaller core pushes the GV curve downward at long wavelengths (see fig. 4.2a) and when comparing with the data plotted in fig. 5.2 one will find that this corresponds to a movement of the ZDW towards shorter wavelengths and away from the pump. This will mean that the dispersive waves are generated with lower efficiency, but at shorter wavelengths, and this is seen as a broader, weaker spectrum in the measurement.

As stated the measured output spectrum after the taper again is broader and weaker than the simulated one. It is weaker mainly because the spec-

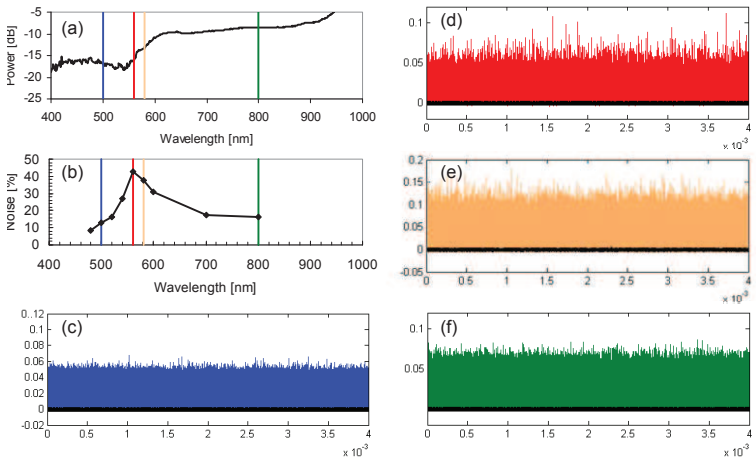

Figure 5.10: Noise measurement on a taper with a 5-50-5 mm profile and a 60 μm waist. This profile was chosen for this example because as shown in sec. 5.5.5 it has a particularly large variation in noise across the spectrum. (a) 400-1000 nm output spectrum with the wavelengths of the shown noise traces marked by vertical lines. (b) The noise spectrum measured on this taper with the wavelengths of the shown traces marked with their respective colors. (c) Diode trace at 500 nm; the noise sum was calculated to 13 % (d) Diode trace at 560 nm; the noise sum was calculated to 43 %. (e) Diode trace at 580 nm; the noise sum was calculated to 38 %. (f) Diode trace at 800 nm; the noise sum was calculated to 16 %. The black line marks the background noise, measured when the light from the supercontinuum was blocked. For these measurements an effort was made to keep the diode signal power the same for all wavelengths, but the amount of power received on the diode has little influence on the measured noise percentages as long as the signal was well above the background noise and well below the diode saturation.

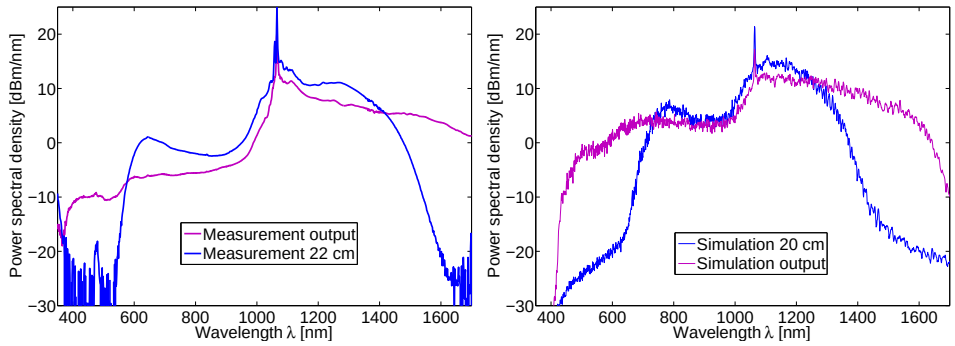

(a) (b)

Figure 5.11: Comparison of measured spectra and simulated spectra. 5.11a Measured spectra from 20-2-20 mm taper with 60 μm waist. 5.11b simulated spectra of 20-2-20 mm taper with 60 μm waist.

trum generated in the first 20 cm is weaker and the energy is distributed over a wider spectrum, but there must also be some increased losses from the taper even though these should be small, and these are not included in the simulation. The increased bandwidth is partly observed because the spectrum from the first 20 cm was wider than in the simulation, but SEM pictures have also shown that the elongation of the central holes is maintained after tapering (see fig. 5.5) which should push the actual GV curve for the taper waist downward at the long wavelengths compared to the idealized curve, thus providing GV matching to shorter wavelengths. The movement of the ZDW will also increase the dispersion at the pump wavelength, delaying the MI breakup and partly explaining the greater residual energy in the pump in the measurement. In addition the actual pulse is spectrally wider than the simulated pulse and has a chirp, which may both add to the delay of the breakup.

It is our conclusion that the differences between measurements and simulations are tolerable and they can be accounted for as the result of simplifications made in the simulations. The simulations should therefore be reliable as a tool to understand the measurements

5.5.3 Taper waist diameter

Naturally the output spectrum of the tapered fibers is heavily affected by how strongly the taper is tapered. In order to quantify this dependence we measured the spectrum from a series of tapers with different waist diame-

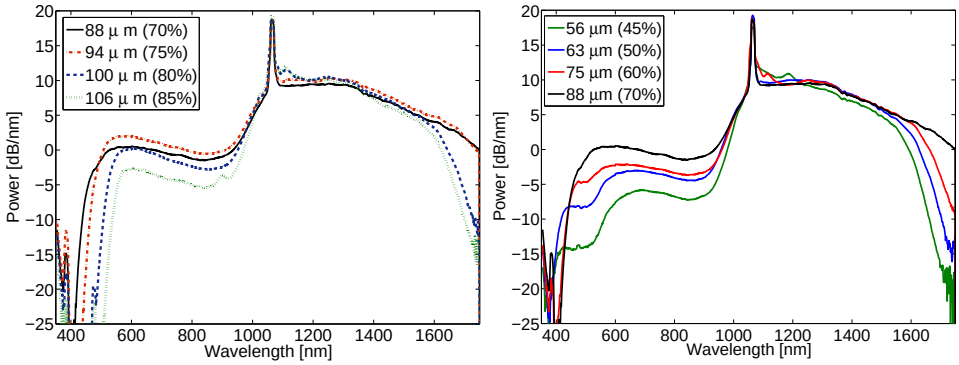

(a) **(b)**

Figure 5.12: Change in output spectrum as a function of taper waist width variation. 5.12a weak tapering to 106-88 μm or 85-70% of original diameter. 5.12b strong tapering to 88-56 μm or 70-45% of original diameter. The spectrum from the taper with a width of 88 μm or 70% of original diameter has been included in both plots to ease comparison of the spectra. All these tapers had a 20-2-20 mm profile and 20 cm of untapered fiber before and after the taper.

ters. As can be seen in fig. 5.12a, the spectra initially widen as the taper waist diameter is reduced from 85% to 75% of the original diameter. The transfer of energy from the pump wavelength to the continuum gradually becomes more and more efficient and the continuum expands to both longer and shorter wavelengths. This must mainly be due to the altered group velocity matching characteristics of the taper but the increase in nonlinearity, which adds to the red shift will also increase the spectral broadening. As the taper waist is reduced further from 75% to 70% the conversion efficiency drops, however, and although the continuum still expands to shorter wavelengths, the drop-off in energy at the long wavelength edge starts to sharpen. This development can be seen to continue as the taper waist is reduced further (fig. 5.12b): The conversion efficiency continues to drop and the long wavelength extent of the continuum decreases. There continues to be a small increase in broadening to shorter wavelengths, but an increasing dip in spectral energy appears below 600 nm marking the edge of the spectrum generated before the taper.

It should be noted that a dip in the spectrum similar to what we see in fig. 5.12b at 550 nm has earlier been reported in a supercontinuum generated

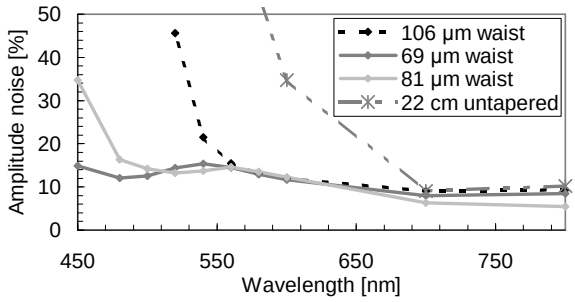

Figure 5.13: Pulse to pulse amplitude noise measured on tapers with various waist widths. All these tapers had 20-2-20 mm profiles, 20 cm input fiber, and 20 cm output fiber. The data for the 22 cm untapered fiber has been included for comparison and illustrates the noise at the input of the taper.

in a sort PCF taper by Xiong et al. [114]. They explained their dip as the result of FWM from a spectrum over the ZDW to a spectrum below the ZDW, because the ZDW of their taper waist was located just above the dip. However, in our case the dip is located far below the ZDW and as will be shown later the power below the dip does not increase with increased waist length as should be expected from a build up of FWM. The light below 550 nm therefore cannot be the product of FWM in our case.

The noise curves of the taper spectra were also found to vary significantly with the taper waist width. As can be seen in fig. 5.13 the widest tapers have a noise curve which approaches that of its input spectrum. As the taper is narrowed, the noise curve flattens while the peak in the noise around 550 nm becomes more and more apparent as the dip in the spectra in fig 5.12b become more and more pronounced.

5.5.4 Taper waist length

The length of the waist section of the taper was found to have little effect on the output spectra the curves in fig. 5.14a illustrates this for tapers with a waist diameter of 88 μm (70% of original diameter); similar results were found for tapers with 60 μm waist diameter (48% of original). In the insert it can be seen that when the waist length is increased there is a slight growth in the shortest wavelengths and a small decrease in the interval from 500 nm to 850 nm, but the spectrum is largely unaffected. This indicates that very little spectral broadening occurs in the waist and thus confirms the result of the simulation (fig. 5.3). Like the spectra, the noise profiles of the output shows very little dependence on the waist length, as seen on fig. 5.14b.

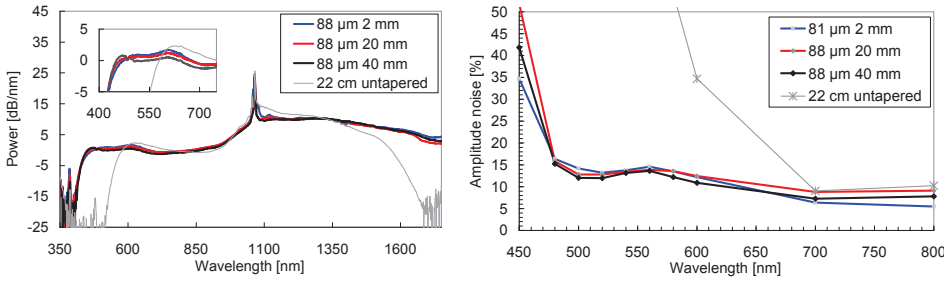

(a) **(b)**

Figure 5.14: (a) Output spectrum from tapers with different waist lengths. The insert shows a magnification of the change in the shortest wavelengths. (b) Noise from tapers with various waist lengths. The taper widths are noted in the legend. All the tapers had 20 cm of input and output fiber and 20 mm transition length. For this measurement there was very little signal at 450 nm so this measurement point has a high degree of uncertainty. The curves for the 22 cm untapered fiber illustrates the spectrum at the input of the taper.

5.5.5 Taper transition region length

The length of the transition region between the untapered fiber and the taper waist was the last parameter to be investigated. The results for a 60 μm diameter (48% of original diameter) taper has been shown in fig. 5.15. Similar results were obtained with tapers with 50 μm diameter (40% of original diameter). The length of the transition region had a very significant impact on the generated spectrum. Within the lengths treated here the efficiency of the energy transfer to the short wavelength side of the continuum became more efficient when the transition length was increased. There was an especially strong growth in the interval from 400 nm to 550 nm, which is the part of the spectrum generated only in the taper. From noise curve in fig. 5.15b it can be seen that the longer transition lengths also reduce the noise in the spectrum and especially reduce the peak in the noise at 550 nm.

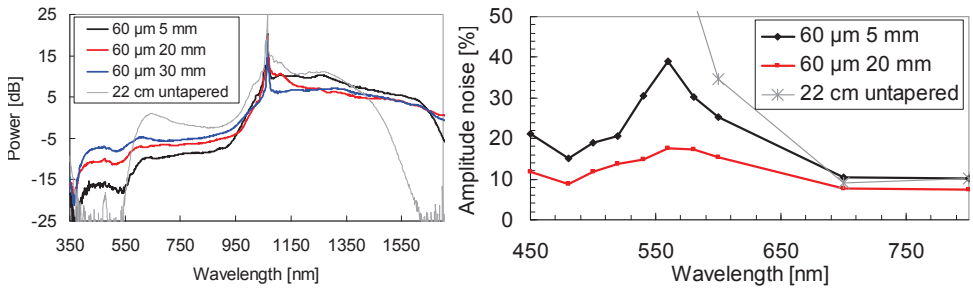

(a) **(b)**

Figure 5.15: (a) Output spectrum from tapers with different transition lengths. (b) Noise from tapers with different transition lengths. The width of the waists and length of the transition regions is noted in the legend. The tapers had 20 cm of input fiber and 20 cm output fiber. The curves for the 22 cm untapered fiber illustrates the spectrum at the input of the taper.

5.5.6 Rogue events before the taper

Rogue events, rogue solitons or rogue waves and control of these by seeding have recently been the subject of much discussion and research in the supercontinuum community [54–56, 64] as described in some detail in chapter 3. The conclusion from the experiments presented in chapter 3 was that seeding had little effect at high pump powers, which could lead to the conclusion that the extreme soliton energy fluctuations from pulse to pulse disappeared as the power was increased. However, when we measured the noise of the 22 cm input fiber for the tapers we noted that below the edge of the supercontinuum, which had been measured using a spectrum analyzer, the diode still detected light from some pulses in the pulse train. The average power at these wavelengths was too small to allow a proper noise analysis at these wavelengths, but a few signal traces have been shown in fig. 5.16. The traces cover 4 ms or 320,000 pulses with a 2 ns resolution and at 500 nm (blue trace) only around 32 peaks are visible as the result of pulses that deliver energy significantly above the noise floor. The edge of the SC measured on the spectrum analyzer was around 560 nm and, light at these wavelengths is shifted here by the soliton trapping effect, so they must be matched by solitons which according to the group velocity curves should have wavelengths of about 1800 nm. The light which is detected at 500 nm should accordingly match solitons around 2050 nm. Thus, from these measurements it appears that in approximately 1 in 10,000 pulses the most powerful soliton has red-shifted 250 nm further after 22 cm than in the

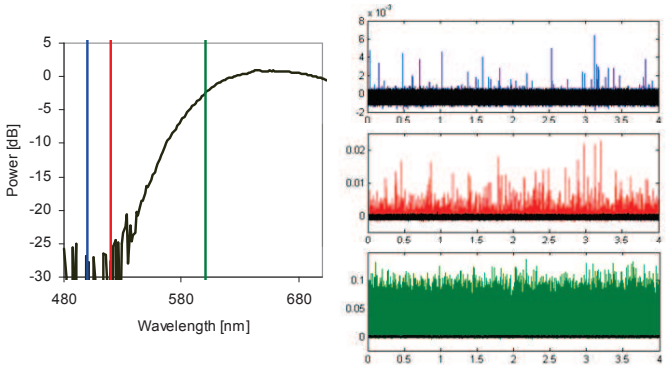

Figure 5.16: Pulse intensity measurements around the spectral edge of the supercontinuum measured just before a taper. The spectrum on the left shows the spectral edge of the continuum and the wavelengths at which it has been filtered. On the right are the diode measured intensity traces of the filtered output light during 4 ms. Blue at 500 nm, red at 520 nm and green at 600 nm. The black line mark the background signal in all three traces.

average pulse, and thus must have had a considerably higher energy than the average soliton. This shows that there are also extreme fluctuations in the power of the solitons generated when pumping at high powers and these fluctuations has to be considered when one seeks to explain the spectral behavior of the continuum.

5.5.7 Noise dependence on pump power

As explained above, it seems likely that the pulse to pulse fluctuations derive from variations in the pulse break-up, and as the pulse break-up is heavily dependent on pulse power, the noise spectrum of a continuum is also dependent on pulse power. As an example, fig. 5.17 shows the spectra generated by a taper and the way the noise a different wavelengths changes with increasing output power. As can be seen, the noise decreases exponentially with increasing output power, as in long fibers with uniform cross section, but here the decrease in noise is significantly faster at the shortest wavelengths than at the longest and the noise around 600 nm decreases the slowest. This results in the noise around 560 nm being the highest in the spectrum investigated here at the highest pump power.

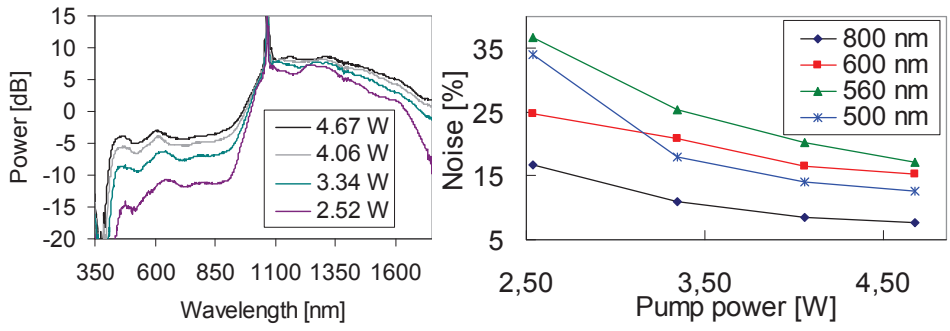

(a) (b)

Figure 5.17: (a) Spectrum of a 10-40-10 mm taper with a waist of 75 μm measured at different output powers. (b) Pulse to pulse amplitude noise as a function of output power measured at 4 wavelengths.

5.6 Discussion

5.6.1 Discussion of noise data

Based on the noise data presented above it appears that the noise curves of the tapers can be interpreted as the combination of two noise curves. One curve, which derives from the light generated before the taper, has high noise, dominates the noise down to 550 nm, and has a strong increase in noise near 550 nm but drops off below 550 nm where the energy corresponding to this curve decreases going to zero at wavelengths near 500 nm. The second curve, which derives from the light generated in the taper, has low noise with an increase in noise toward the shorter wavelengths. The size of this increase is dependent on taper waist core size and is lower the smaller the core. The energy corresponding to this second curve continues to the end of the measured spectrum at 400 nm. The relative contribution from the two noise curves to the total noise curve appears proportional to the relative contribution to the total spectrum from the spectrum generated before the taper and in the taper respectively.

For the strongly tapered fibers, this relationship is visible from the relative difference in power between the wavelengths below the dip at 550 nm and the ones above. The changes in taper waist length which do not change the spectra also do not change the noise curve, while the increase in transition length which gave an increase in the power below 550 nm also increases the contribution from the low noise curve and thus lowers the total noise curve. The variation in waist diameter width with fixed waist length and

transition length described in sec. 5.5.3 gave a constant noise curve down to 550 nm but decreasing noise with decreasing waist diameter below this wavelength as the amount of noise generated in the taper was altered. Overall it is clear that the lowest noise spectrum is generated by the tapers with the narrowest waists and the longest transitions regions but further investigations will be needed to find how long the transition region has to be to generate the minimum noise.

5.6.2 Discussion of the spectral effect of tapering

From the presented data it is clear that short tapers can be used to extend the spectrum generated in a short PCF. In the numerical simulation it was seen that nearly all the added spectral width was produced during the down-tapering, with the waist, output transition region and output fiber adding only a little power at the short wavelengths and some additional red shift of the solitons at long wavelengths. It was subsequently shown experimentally that the length of the taper waist has little effect on the spectrum but that increased transmission length can considerably increase the efficiency of the light conversion to the short wavelengths. Finally it was shown that as the taper is tapered down to 70 % of the original width the generated spectrum grows with narrowing waist, with further reduction the total spectrum shrinks even though the minimum wavelength continues to shift toward shorter wavelengths. Also, as the waist is reduced below 70% of the original width, a dip appears in the spectrum around 550 nm, marking the transition previously mentioned between the spectrum generated before the taper from the one generated in the taper. The emergence of the dip indicates that there is a transition in the effects governing the spectral broadening as the fiber is tapered strongly. The interpretation of the results is made difficult by the complexity of the pulse, however. When the taper is located 20 cm into the fiber, the pulse that enters the taper is still relatively well confined in time, the pulse breakup has started and the pulse is a collection of hundreds of solitons which are colliding, red-shifting and emitting dispersive waves. Many effects may therefore contribute to the spectra broadening.

There are two main ways in which the light in the 400-560 nm interval could be produced as the fiber is tapered down. Either it is directly generated at the short wavelengths as dispersive waves or the light is shifted there through an accelerated soliton wave trapping process. For the consideration of either of the two processes it is useful to have a rough idea of the length and energy of the solitons involved and how much the solitons should adapt their shape as they propagate through the taper.

From the simulations described in sec. 5.2, the peak power of the most powerful soliton in an average pulse can be estimated as the peak power of

the pulse between soliton collisions at the end of the 20 cm untapered fiber. This power was on average 55 kW. The length and the energy of the most powerful soliton can then be found by assuming that it is a fundamental soliton with N=1 and rewriting eq. 2.22 for the soliton number:

$$T_0 = \sqrt{\frac{\gamma P_0}{|\beta_2|}} \quad \text{(a)} \qquad E_s = \sqrt{\frac{4|\beta_2|P_0}{\gamma}} \quad \text{(b)} \tag{5.6}$$

where P_0 is the peak power, T_0 is the soliton length, $E_s = 2P_0T_0$ is the soliton energy, β_2 is the group velocity dispersion and γ is the nonlinearity. The most powerful solitons in the simulations were located at a wavelength of approx. 1400 nm, at which $\gamma = 9.96$ km^{-1}W^{-1} and $\beta_2 = -6.5 \times 10^{-26}$ ps/m were calculated from the idealized untapered fiber structure (see curves in fig. 5.2 and and in appendix A). The pulse length was thus found to be $T_0 = 10.9$ fs and the energy $E_s = 1.2nJ$. This should be the approximate energy of the most powerful soliton in the pulse; there should be hundreds of solitons with lower power. It should be noted, however, that it was seen in sec. 5.5.6 that some of the pulses entering the taper have solitons which are considerably more red-shifted that the average and thus must have higher power. Their contribution to the average spectrum must also be considered.

Next, to estimate how much the solitons should adapt their shape we assume for a moment that the soliton does not adapt its length and power as the fiber is tapered down to 50%. Its soliton number would then increase to just above 1.5 as γ grows to 31 km^{-1}W^{-1} and β_2 becomes -1.3×10^{-25} ps/m. A soliton whose soliton number exceeds 1.5 would start to oscillate, leak energy and break up. In order to avoid this and ensure a relatively low energy leakage from the soliton, the taper should be long enough that the soliton has time to adapt its shape to the local fiber parameters, which means that the change should be slow compared to the oscillation of the soliton field envelope of $2\pi/\mathrm{k_{sol}}$ with $\mathrm{k_{sol}} = -\beta_2/(2\mathrm{T}_0^2)$ [23]. For the 10.9 fs soliton at the beginning of the fiber, this length is 2.3 cm, which is not short compared to the length of the taper and it must therefore be assumed that the soliton does not have time to adapt slowly. This is especially likely considering that the above calculation is based on the most powerful soliton in the pulse and all the lower power solitons will be temporally longer and therefore have longer oscillation periods.

It could be thought that since the length scale of the taper is so short compared to the soliton, the soliton would not feel the change in parameters at all, but only feel the average of the fiber parameters over longer fiber lengths. However, the experimental results show that long waist lengths, where the parameters of the waist would have an effect even with averaging, did not alter the spectrum significantly. On the other hand changing the

transition region, from 5 to 30 mm, which would have smaller effect on the average fiber parameters had a strong effect on the spectrum.

The results and calculations therefore indicate that the taper lengths that we work with are too short to allow solitons to adapt slowly to the fiber parameters at the waist but long enough for the solitons to actually feel the local parameters. Thus knowing the approximate energy of the solitons involved and how much they may adapt to the taper, the two explanations for the spectral growth in the visible region can be considered.

First we investigate whether the solitons at 1400 nm could generate dispersive waves close to 400 nm. The group velocity profile is very steep at the short visible wavelengths, so the phase matching equation is strongly dominated by the group velocity (GV) and we will therefore assume that the phase matching criteria is fulfilled if there is GV matching. If one inspects the GV matching diagram in fig. 5.2c it is found that for the 50% curve, 1400 nm should match to about 480 nm. If the actual shape of the air holes were included it would reach an even shorter wavelength, and in any case this is well below the wavelengths generated before the taper. The phase matching criteria is thus fulfilled for at least some of the wavelength where the short wavelength light is generated. However, if a dispersive wave were to be generated from the soliton there must also be a spectral overlap, which can be calculated from a Fourier transform of the temporal shape of the pulse. The energy from the soliton which overlaps with the 480 nm turns out to be well below -100 dBm/nm. With such a poor spectral overlap there cannot be any considerable dispersive wave generation. It could be argued that as the fiber parameters are changing, the soliton will be oscillating and may simultaneously collide with other solitons, leading to a considerably higher peak power and shorter temporal length than the soliton had before the taper, but its temporal length should be reduced to one third of the calculated value to generate a spectral overlap of more than -100 dBm/nm. We do not find this realistic, especially since this consideration again is based on the single most powerful soliton in the pulse, whereas the spectrogram in fig. 5.4b clearly showed that the energy in the interval of 400-560 nm is generated all along the pulse and not only from a few very powerful solitons. In addition, a spectrum generated by dispersive waves should grow when the waist length is increased and the dispersive wave gain has a chance to build up, but as seen in fig. 5.14a that was not the case. Altogether we do therefore not find it likely that the light could be generated directly at the short wavelengths by dispersive wave generation. The light must therefore have been shifted to the short wavelengths by dispersive wave trapping.

When considering whether the short wavelength energy could be generated by dispersive wave trapping it is important to note that the shortest wavelength that we generate decreases as the taper is tapered more (seed fig. 5.12a), but if the taper is tapered to less than 70% the generation of the short wavelengths becomes inefficient and the long wavelength extent of

the supercontinuum is reduced (seed fig. 5.12b). It is also noteworthy that increasing the taper transition length increases the efficiency of the short wavelength generation (see fig. 5.15b). These two observations show that the dispersive wave generation depends on the steepness of the taper as their generation is reduced both if the waist is narrowed or the transition region region is shortened. In addition it was found in the argument above that the tapers are long enough to affect the solitons but too short to allow them to adapt slowly to the fiber parameters at the waist. As the solitons are starting to adapt they will be oscillating and leaking energy. If the solitons lose energy in the taper they will red-shift more slowly after the taper. It must be expected that the solitons oscillate more and lose more energy when adapting to the steeper changes in fiber parameters in the narrower waists compared to in the wider waists. If the solitons leak more energy the narrower the waist, it would explain why the infrared extent of the SC decreases with narrower waist in fig. 5.12b.

It has not been investigated what effect oscillations of the soliton would have on the trapping mechanism which should generate the short wavelengths, but it must be expected that it would be detrimental, since the blue shift relies on the dispersive waves continuously being temporally matched with the blueshift from the XPM from the soliton. If the soliton shape is oscillating, the temporal position and the strength of the blue shift caused by the XPM will also be oscillating and it is expected that more energy from the dispersive wave will escape the confinement caused by the trapping effect and thereby escape the blue shift. In addition, the heavily oscillating soliton will have lost more energy and be weaker and thus be able to trap less energy. If the waist of the taper is wider or the length of the transition region is longer, the change in fiber parameters is more gradual and it must be expected that the oscillations in the solitons as they adapt to the local parameters will be weaker. This would explain why both the short wavelength generation efficiency and the infrared extent of the continuum increases with longer transition region or wider waist. In total the dispersive wave trapping and blue shift mechanism can explain the observed results if it combined with the theory that the solitons leak energy when propagating through steep tapers. We therefore find the explanation that the 400-560 nm light is generated through blue-shifting of dispersive waves to be the most likely.

No matter what physical effect is causing it, it is clear that taper performance can be greatly improved by increasing the length of the taper, and considering that the power in the shortest wavelengths increases 3 dB when the length of the taper transition region is changed just from 2 to 3 cm it seems likely that efficient tapers can be relatively short. In addition significant improvement can be made by optimizing the fiber lengths before and after the taper and varying the relative hole size along the length of the taper. The short tapers should like the long PCF tapers described by

Kudlinski et al. [103] be able to generate significantly shorter wavelengths than long uniform PCFs. In addition the short fiber length will reduce the effect of the absorption of silica and this should make it possible to expand the supercontinuum spectra even further. Finally tapering could be combined with modifying the glass material [2] to give an even wider spectrum.

5.6.3 Tapering and the damage threshold

During the tapering process, the core of the fiber is narrowed considerably and the peak intensity of the pulses is thereby increased considerably. This has the benefit that many of the nonlinear processes are accelerated greatly, but it also means that the intensity of the light approaches the tolerance limits of the glass material. The pump pulses have an energy of up to 125 nJ and the effective area of the untapered fiber is about 10 μm^2 at 1064 nm, so the fluence in the fiber core is 1.25 J/cm^2 per pulse. The bulk damage threshold fluence for fused silica at 1064 nm using 14 ps pulses is 25.4 J/cm^2 [68]. In theory the fiber can thus be tapered to 22% of the original diameter before the glass breaks down. During the pulse fission, however, solitons are generated with much higher intensity, and since the breakup is caused by a combination of peak power and intensity, this may reduce the breakdown threshold. During measurements on narrow tapers, melting of the fiber occurred frequently and it was found that no fiber which was tapered to less than 56 μm could be pumped at full power without melting. This is thought to be mainly a cooling problem. The fibers were air cooled with fans, which helped significantly, but a more effective cooling system should be developed in the long term.

5.7 Conclusion on tapering

We have demonstrated how commercially available equipment can be used to taper of-the-shelf fiber in order to modify its characteristics for supercontinuum generation significantly. We have shown how a taper can be used to extend the short wavelength end of a spectrum generated in a 0.5 m fiber from 500 nm to 400 nm. However, the extension so far comes at the cost of lowering the efficiency of the energy transfer to the continuum compared to the same transfer in long uniform fibers pumped with the same pump powers and pulse lengths. A detailed experimental analysis has shown that the efficiency of the spectral generation is considerably increased if the length of the transition region of the taper is increased just a few cm. It is therefore expectable that with increased development the efficiency of short taper supercontinua can be increased to the level of long uniform fibers. It

was explained that spectral broadening was limited by the taper being too short for solitons to adapt their shape but more simulations on the behavior of single solitons in tapers could be used to improve the understanding of this process greatly. Numerical simulations presented here showed that the supercontinuum pulse produced from a tapered fiber is much more temporally confined than those delivered from a system based on long uniform fibers. This may simplify many application systems, which rely on timing or interference, and open up possibilities for new applications. Finally we thoroughly investigated the noise properties of the short wavelength part of the taper generated supercontinuum and showed that it differed considerably from that of supercontinua developed in a long uniform fiber and that in the short wavelengths the noise in the taper generated supercontinuum was considerably smaller. It is the opinion of the author that if the efficiency of the short taper generated supercontinuum is increased to the level of that of the continua generated in long uniform fibers, it is likely that this will become the preferred method for long pulse supercontinuum generation because it delivers a shorter pulse in which all colors overlap temporally, which has lower amplitude noise in the spectrum and it should be able to produce a spectrum which reaches deeper into the violet regime.

5.8 Outlook on tapers

It is clear from the results presented here that the work on optimizing the tapered fiber profile is not yet complete. The length of the transition region of the tapers still has to be increased in order to make visible light generation efficient. In addition, the length of untapered fiber which precedes the taper has not yet been investigated, but it expected that a longer fiber before the taper would benefit the growth of dispersive waves and let the solitons red shift further. This would both increase the efficiency of the visible generation and increase the bandwidth which can be generated. It is the firm belief of the author that the efficiency problem can easily be solved and that it will then be possible to use table top equipment like a Vytran tapering machine to tailor off-the-shelf fiber for efficient deep blue supercontinuum generation.

The freedom in local fiber parameter control offered by tapers leads to some new considerations. As has been shown above the soliton trapping mechanism is very strong so the tapers can blue shift dispersive waves to shorter wavelengths very quickly when the group velocity of infrared solitons is reduced by tapering. It is therefore no longer important that the fiber before the taper supports a wide GV matching range. The untapered fiber section should instead be designed to first let the solitons generate strong dispersive waves by having a ZDW very close to the pump wavelength and subsequently the fiber should ensure that solitons red shift quickly so that

a large part of the silica transmission window may be used. The taper must then be long enough to ensure that the solitons can adapt gradually and have a large relative hole size in order to give the widest possible group velocity matching region. The optimal pitch of the structure can be found by calculating the GV profiles and finding the ones that provide GV matching to the shortest wavelengths. This was done by Travers for long tapers and the optimal pitch found was 2 μm [110] but it was unclear exactly which criteria had been used to arrive at this value.

As the maximum deceleration of the solitons produced in the taper sets the limit on how short wavelengths can be generated, it may become relevant to expand the matching region by doping the material in order to modify the material dispersion which dominates the short wavelengths [2]. The minimum wavelength which have been produced so far in tapered fibers is at approximately 350 nm [110] and below 280-300 nm the UV two photon absorption will become too strong to allow propagation (see sec. 2.1.3. It is the view of the author that with sufficient optimization of all parameters in tapered PCFs the final limit of supercontinua should be close to 300 nm. It remains to be seen whether applications will emerge to drive supercontinuum development to this limit. Since the tapered fibers are quite short, an interesting approach to finding the perfect PCF taper structure could be to use computer design generation methods such as genetic algorithms based on repeated propagation simulations. This would require a lot of computer power but as the capabilities of computers continue to increase this may soon be a minor problem.

Chapter 6

Conclusion

In this thesis we have explored the use of seeding and modification of fiber dispersion to control supercontinuum generation. It has been shown that seeding can be used to create local peaks in the supercontinuum while the dispersion of the fiber can be tailored to extend the spectrum of the supercontinuum. Both methods can be used to lower the amplitude noise of the spectrum.

In chapter 3 we investigated the use of a seed in the outer of two sets of four-wave mixing gain bands in a fiber with two zero dispersion wavelengths surrounding the pump wavelength. We showed how seeding at pump powers near the modulation instability threshold can be used to create a local peak in the outer long wavelength FWM gain band with over 27 dB more power than in the unseeded spectrum. In order to do this, however, the seed has to be in the long wavelength FWM gain band and be temporally matched with the pump pulse within 1 ps. At higher powers the sharp peak created by the seeding almost disappears in the surrounding continuum, but the seeded continuum then generates more power in a broad long wavelength band which was interpreted as the result of stronger dispersive wave generation. The increase in the dispersive wave gain is a sign that the seeding modifies the soliton distribution generated during the pulse breakup at high pump powers. We found that seeding of the higher order gain band is considerably simpler than seeding the inner gain band because the higher order band does not move significantly with increasing power. We also investigated the amplitude noise of the edges of the continuum with and without seeding and found that in agreement with investigations of seeding in a simple MI gain band in the literature, the noise reduction at pump powers corresponding to the supercontinuum generation threshold was very large, but that as the pump power was increased the reduction in noise became much smaller. Since the focus of this work was high power supercontinuum generation and the seeding here appeared to have rather little effect at high power compared to the complexity of the system required to implement it, it was decided to

focus on simpler techniques for spectral control. To this end we investigated a simple solution based on seeding the MI gain band with a Raman peak from the pump system, but this unfortunately only transferred power from the visible to the infrared wavelengths and failed to reduce the noise in the continuum.

In chapter 4 we went on to investigate how the optimization of the dispersion profile of the PCF affects the supercontinuum. It was shown that the visible bandwidth is limited by the infrared bandwidth which in turn is limited by either a second ZDW, a slow-down of the soliton red-shift, or silica absorption. In order to extend the spectrum as much as possible it is necessary to ensure that only the silica absorption limits the infrared edge and the group velocity at the red edge is a slow as possible. This can be done by increasing the relative hole size but such an increase has the disadvantage of reducing the conversion efficiency from the pump to the visible wavelengths because it shifts the ZDW too far away from the pump. We also found that the fiber structure can be used to reduce the amplitude noise of the continuum, but too few data have been gathered on this to explain the the connection between fiber structure and noise.

This thesis has also explored the use of short tapered fibers to produce supercontinua that reach far into the blue spectrum with little noise. The results on this have been collected in chapter 5. In the literature very long tapered PCFs have been suggested as a way to expand supercontinua to even shorter wavelengths than those reached with uniform fibers without loosing efficiency in the power conversion to the visible. However, the tapers previously applied in picosecond supercontinuum generation relied on tapering performed on a drawing tower, which makes it a very costly process unlikely to be applied in greater scale. Here we experimentally investigated how this technology could be transferred to short tapers made with off-the-shelf PCF fiber using commercially available equipment. We thoroughly investigated the dependence of the output spectrum and amplitude noise on the tapers waist diameter, waist length and transition region length. We show that a 8 cm taper in the middle of a 50 cm PCF fiber can generate light down to 400 nm but that the efficiency of the generation at short wavelengths is limited by the length of the taper transition regions. The waist diameter has an optimal value, which for the fiber treated here is 50-60 % of the original fiber diameter; if the fiber is tapered beyond this, the second ZDW starts to limit the infrared spectrum and therefore also limits the extension to short wavelengths. We also show that the amplitude noise in the supercontinuum generated in the tapers is considerably lower than for a conventional picosecond supercontinuum generated in a long uniform fiber with similar pump power and pulse length and that the increase in transition length which increases the generation efficiency also reduces the noise in the continuum. Finally we predicted through numerical simulations that the output pulse from the taper generated supercontinuum can be much shorter and have a

much better temporal overlap among spectral parts than the output pulse of a supercontinuum source based on long fibers. Our results indicate that the efficiency of the short wavelength generation can easily be increased by increasing the length of the taper transition regions. In addition the optimization of fiber lengths before the taper and the variation of hole sizes along the taper is expected to improve the taper generated spectra even further. If the efficiency of the short taper generated supercontinuum is increased, the simplicity of the fabrication equipment required for these tapers combined with the low noise, wide spectrum, and good temporal confinement that they offer will make this a very promising supercontinuum generation technology for the future.

6.1 Outlook

Among the technologies investigated in this thesis, dispersion optimization of both uniform and tapered fiber is expected to have the greatest impact whereas seeding required a setup too complicated to merit the results it could achieve for high power picosecond supercontinua. However, seeding may have a future within continuous wave supercontinuum generation where the problem of time matching is removed.

The dispersion optimization which we have demonstrated only represents the first steps toward solutions in which the dispersion of the fibers is optimized at every point throughout the system. This would include compressing the pulses temporally before they enter the nonlinear fiber, as the self-phase modulation in the current high power pump systems generates a wide bandwidth which could be utilized to greatly shorten the pulses temporally, which should in turn extend the spectral bandwidth of the possible supercontinua. In an even more advanced system, one could imagine the high power amplifier being designed as an adiabatic taper which gradually compresses the pump pulse as it is amplified and gains bandwidth.

Supercontinua generated in PCFs have now been extended to cover almost the full spectral bandwidth of the silica transmission window and the next stage will be to go even further using other materials. The first steps in this direction have already been taken with the use of soft glasses to generate supercontinua that reach far into the infrared. These far infrared supercontinua could unlock a wide range of new applications in a wavelength interval where the main broadband light sources at the moment are weak thermal sources.

In this study it has been shown how significant spectral broadening can be produced in just a few centimeters of PCF taper instead of many meters of uniform PCF. When this is idea is combined with the idea of using other materials, which may have nonlinearity many times the nonlinearity of silica,

the possibility of producing supercontinua in completely novel ways quickly springs to mind. Is it e.g. possible that we at some point will see wide band supercontinuum generation performed on chips based on tapered photonic crystals made from highly nonlinear glasses directly integrated with diode lasers? If this could be achieved, supercontinuum might not simply be used in a small niche of optics for special analysis application but could become an everyday light source for homes and offices.

Appendix A

Data curves for various PCF structures

The tapering of a PCF fiber as described in chapter 5.1 allows a huge flexibility for controlling different parameters along the fiber. In order to give the reader some basis for evaluating the appropriateness of the structures chosen in this thesis, we will here present some additional data curves for the tapered fiber as well as a comparison with PCFs with different relative hole sizes and three different pitches.

A serie of fibers with constant relative holesize but varying pitch represents the $\Lambda = 3.7$ μm and $d/\Lambda = 0.79$ PCF which was used for tapering in sec. 5. This series has $d/\Lambda = 0.79$ and $\Lambda = 3.7$ μm, $\Lambda = 3.33$ μm, $\Lambda = 2.96$ μm, $\Lambda = 2.59$ μm, $\Lambda = 2.22$ μm, $\Lambda = 1.85$ μm, $\Lambda = 1.48$ μm, and $\Lambda = 1.11$ μm corresponding to the fiber tapered to 90 %, 80 %, 70 %, 60 %, 50 %, 40 %, and 30 %.

Three other series with constant pitch but varying relative holesize are also presented. The pitches of these are 3.7 μm, 2.22 μm, and 1.11 μm corresponding to 100 %, 60 %, and 30 %, of the tapered fiber but parameters are calculated for the relative holesizes $d/\Lambda = 0.79$, $d/\Lambda = 0.75$, $d/\Lambda = 0.65$, $d/\Lambda = 0.55$, $d/\Lambda = 0.45$, and $d/\Lambda = 0.35$. Comparison between the curves presented here gives some basic understanding of the way in which the various fiber parameters change as the fiber structure is altered.

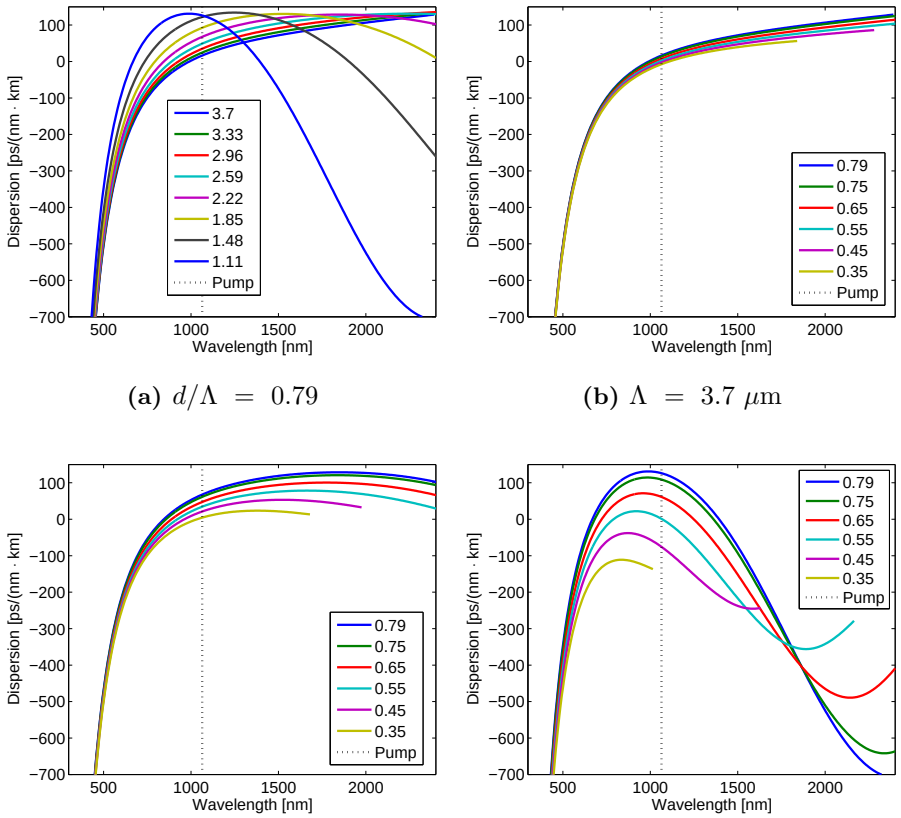

(a) $d/\Lambda = 0.79$ **(b)** $\Lambda = 3.7$ μm

(c) $\Lambda = 2.22$ μm **(d)** $\Lambda = 1.11$ μm

Figure A.1: Dispersion profiles. (a) d/Λ = 0.79 with varied pitch. (b) Λ = 3.7 μm with various relative hole sizes. (c) Λ = 2.2 μm with various relative hole sizes. (d) Λ = 1.1 μm with various relative hole sizes.

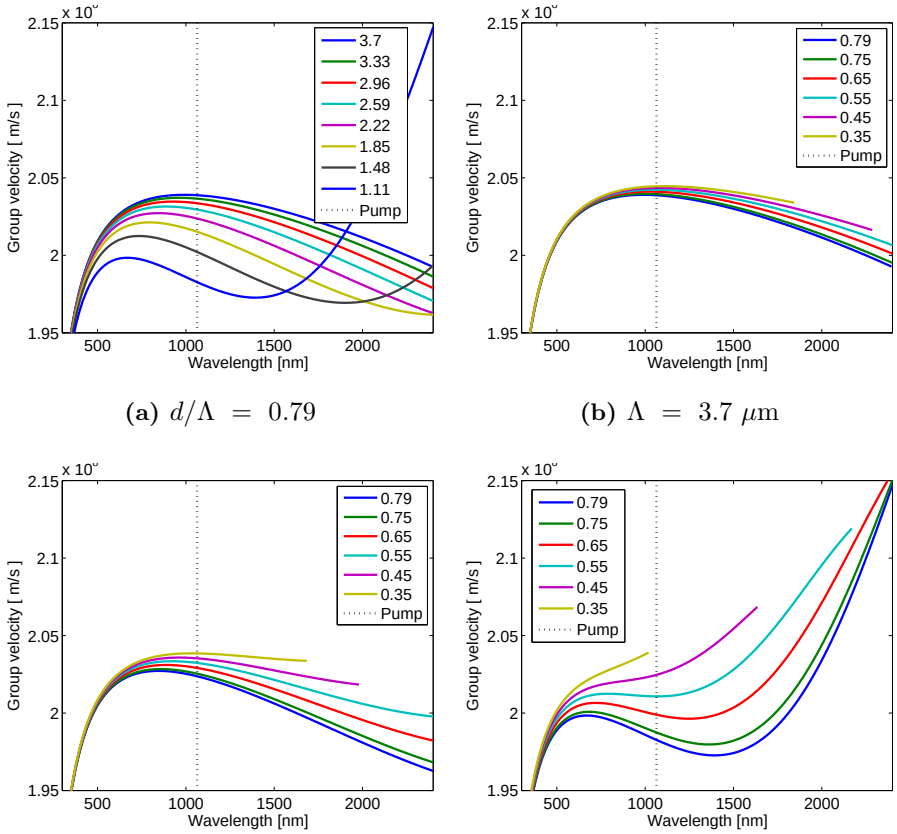

(a) $d/\Lambda = 0.79$ **(b)** $\Lambda = 3.7$ μm

(c) $\Lambda = 2.22$ μm **(d)** $\Lambda = 1.11$ μm

Figure A.2: Group velocity profiles. (a) d/Λ = 0.79 with varied pitch. (b) $\Lambda = 3.7$ μm with various relative hole sizes. (c) $\Lambda = 2.2$ μm with various relative hole sizes. (d) $\Lambda = 1.1$ μm with various relative hole sizes.

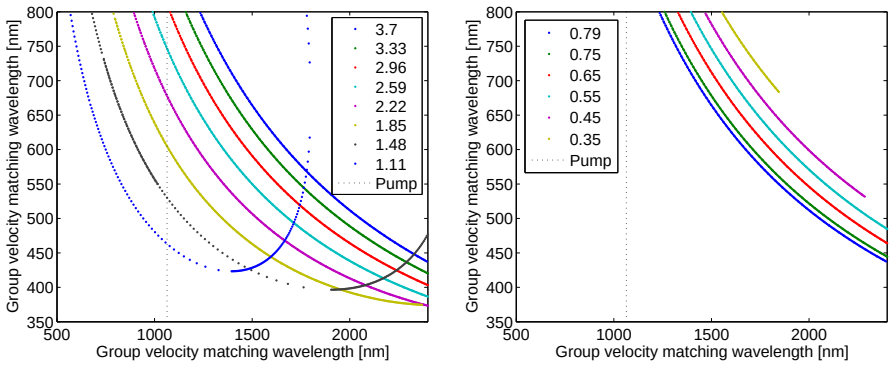

(a) $d/\Lambda = 0.79$

(b) $\Lambda = 3.7\ \mu$m

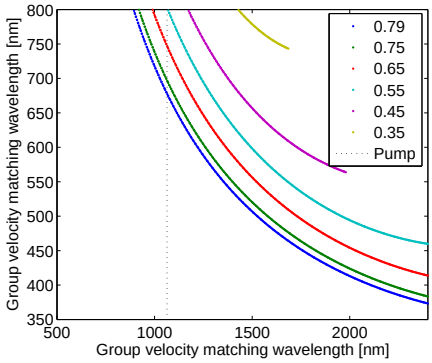

(c) $\Lambda = 2.22\ \mu$m

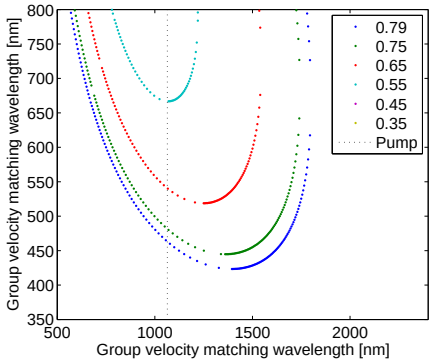

(d) $\Lambda = 1.11\ \mu$m

Figure A.3: Group velocity matching profiles. (a) d/Λ = 0.79 with varied pitch. (b) $\Lambda = 3.7\ \mu m$ with various relative hole sizes. (c) $\Lambda = 2.2\ \mu m$ with various relative hole sizes. (d) $\Lambda = 1.1\ \mu m$ with various relative hole sizes.

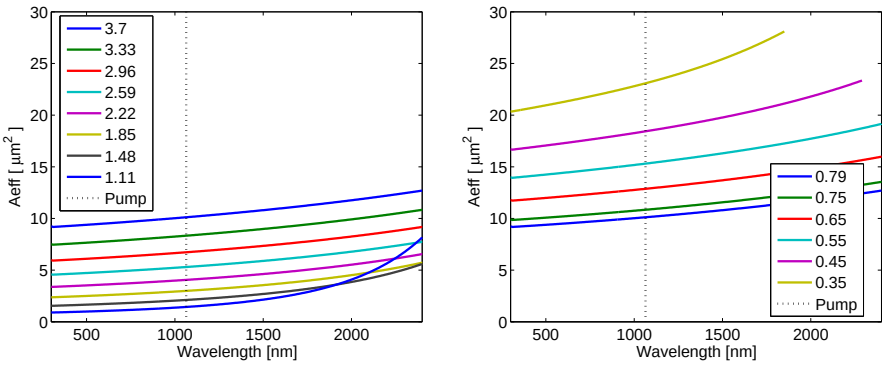

(a) $d/\Lambda = 0.79$

(b) $\Lambda = 3.7\ \mu$m

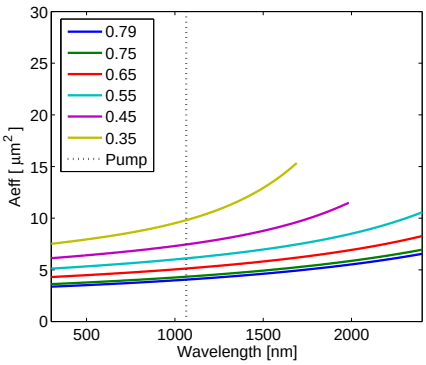

(c) $\Lambda = 2.22\ \mu$m

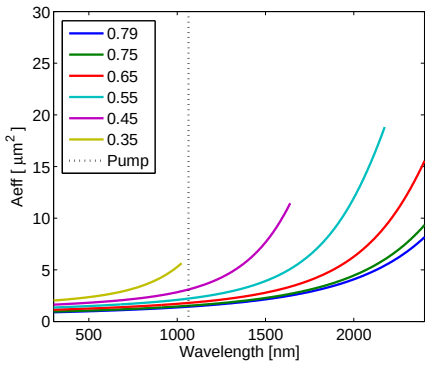

(d) $\Lambda = 1.11\ \mu$m

Figure A.4: Effective area. (a) d/Λ = 0.79 with varied pitch. (b) Λ = 3.7 μm with various relative hole sizes. (c) Λ = 2.2 μm with various relative hole sizes. (d) Λ = 1.1 μm with various relative hole sizes.

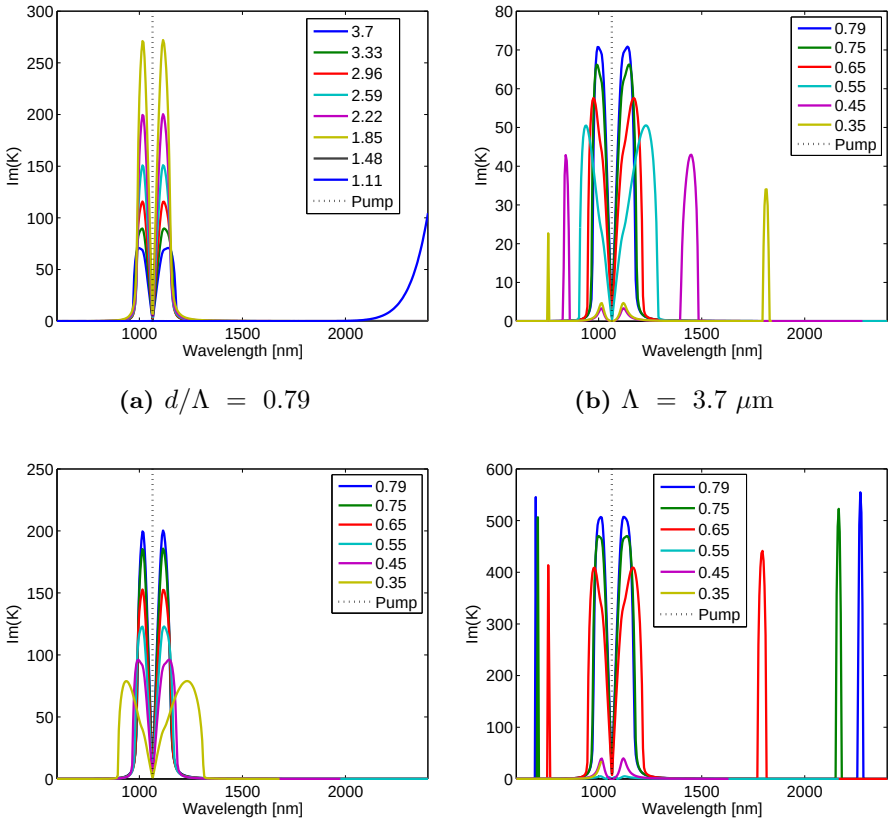

(a) $d/\Lambda = 0.79$ **(b)** $\Lambda = 3.7$ μm

(c) $\Lambda = 2.22$ μm **(d)** $\Lambda = 1.11$ μm

Figure A.5: Modulation instability of four-wave mixing gain calculated with a 10 kW peak power. (a) d/Λ = 0.79 with varied pitch. (b) $\Lambda = 3.7$ μm with various relative hole sizes. (c) $\Lambda = 2.2$ μm with various relative hole sizes. (d) $\Lambda = 1.1$ μm with various relative hole sizes.

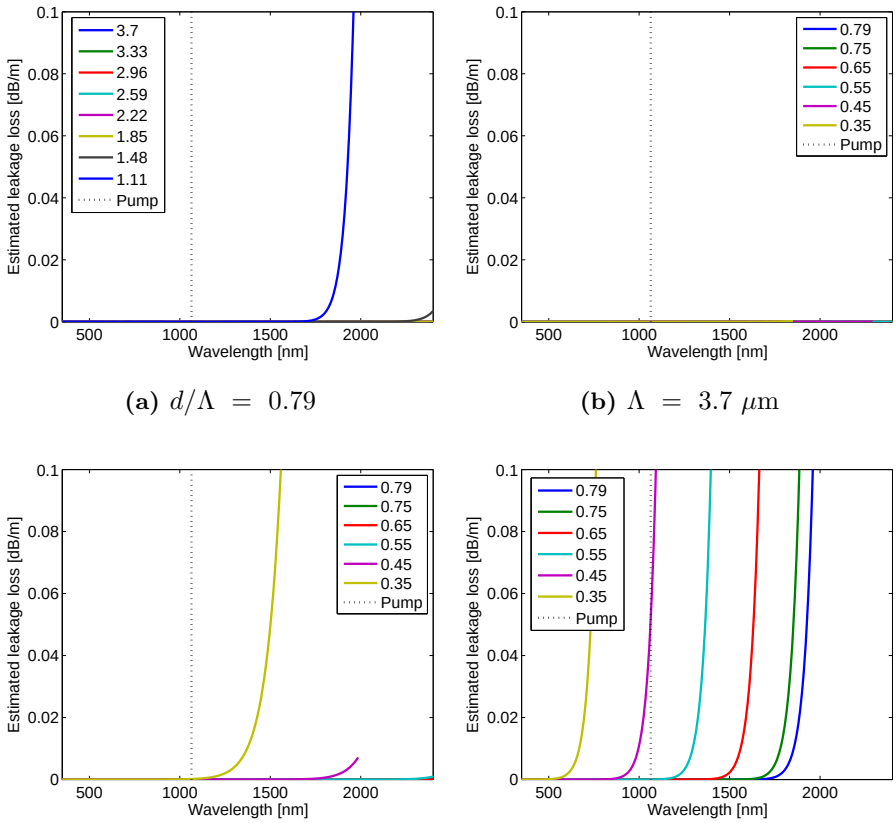

(a) $d/\Lambda = 0.79$ **(b)** $\Lambda = 3.7$ μm

(c) $\Lambda = 2.22$ μm **(d)** $\Lambda = 1.11$ μm

Figure A.6: Leakage loss. (a) d/Λ = 0.79 with varied pitch. (b) Λ = 3.7 μm with various relative hole sizes. (c) Λ = 2.2 μm with various relative hole sizes. (d) Λ = 1.1 μm with various relative hole sizes.

List of Acronyms

A_{eff} effective core area (see 2.1.4)

ASE amplified spontaneous emission

DW dispersive wave

CW continuous-wave

D dispersion (see sec. 2.1.2)

DCA double clad fiber amplifier

DW dispersive waves (see sec. 2.2.4)

ESM endlessly single mode

FBG fiber Bragg grating

fs femtosecond

FIR far-infrared

FWHM full width half maximum

FWM four-wave mixing(see sec. 2.2.3)

GV group velocity

GVD group velocity dispersion (see sec. 2.1.2)

IR infrared

LPG long period grating

MI modulation instability (see sec. 2.2.3)

N soliton number of a pulse

NL nonlinear

NLSE generalized nonlinear Schrödinger equation

ns nanosecond

MPB MIT Photonic Bands

NSR non-solitonic radiation

OSA optical spectrum analyzer

PCF photonic crystal fiber

PM polarization maintaining

ps picosecond

RF radio frequency

SESAM semiconductor saturable absorber mirror

SPM self-phase modulation (see sec. 2.2.1)

SSFS soliton self frequency shift (see sec. 2.2.4)

SC supercontinuum

SCG supercontinuum generation

SEM scanning electron microscope

SMF single mode fiber

UV ultra-violet

XPM cross-phase modulation (see sec. 2.2.1)

ZDW zero dispersion wavelength (see sec. 2.1.2)

Abstracts of publications

The Abstracts of the papers which form the basis of this thesis are given here. A complete list of publications submitted can be found in on page xi. The abstracts are placed in chronological order based on the time that they were published.

[4] P. M. Moselund, M. H. Frosz, C. L. Thomsen, and, O. Bang, "Back seeding of picosecond supercontinuum generation in photonic crystal fibres", *SPIE Europe Photonics Europe* Proceedings of SPIE (2008), 6990–24.

Supercontinuum generation (SCG) has been the subject of intense investigation during the last few years and its main mechanisms are now well understood. Focus has shifted towards tailoring the spectrum of the supercontinuum for specific applications. We experimentally investigate SCG with picosecond pumping in photonic crystal fibers with two closely spaced zero dispersion wavelengths. We couple parts of the output spectrum of the supercontinuum source back to the input in order to produce a gain of over 15 dB at some wavelengths. We use a variable time delay to optimize the overlap between the pump and the back seeded pulses and investigate how the delay and spectrum of the back seeded pulse affects the resulting supercontinuum spectrum.

[5] P. M. Moselund, M. H. Frosz, C. Thomsen, and O. Bang, "Picosecond supercontinuum generation with back seeding of different spectral parts", *Australian Conference on Optical Fibre Technology* (2008).

We study supercontinuum generation with picosecond pumping and the spectrum obtained when coupling back the part of the output around 1200-1700 nanometres or the part around 700-900 nanometres with a variable time delay.

[1] P. M. Moselund, M. H. Frosz, C. L. Thomsen and O. Bang "Back-seeding of higher order gain processes in picosecond supercontinuum generation," Opt. Express **16**(16), 11,954–11,968 (2008).

In photonic crystal fibers with closely spaced zero dispersion wavelengths it is possible to have two pairs of four-wave mixing (FWM) gain peaks. Here, we demonstrate both numerically and experimentally how the outer four-wave mixing gain peaks can be used to produce a strong amplification peak in a picosecond supercontinuum. The method involves feeding back part of the output light of a SC source and time matching it with the pump light. In this way it is possible to produce a gain of over 20 dB near the FWM gain wavelengths.

[2] M. H. Frosz, P. M. Moselund, P. D. Rasmussen, C. L. Thomsen, and O. Bang, "Increasing the blue-shift of a supercontinuum by modifying the fiber glass composition," Opt. Express **16**(25), 21,076–21,086 (2008). Also included in Virtual J. Biomed. Opt. **4** 2, (2009).

Supercontinuum light sources spanning into the ultraviolet-visible wavelength region are highly useful for applications such as fluorescence microscopy. A method of shifting the supercontinuum spectrum into this wavelength region has recently become well understood. The method relies on a proper design of the group-velocity profile of the nonlinear fiber in which the supercontinuum is generated. The groupvelocity profile of a photonic crystal fiber (PCF) can be engineered through the structure of the PCF, but this mostly modifies the group-velocity in the long-wavelength part of the spectrum. In this work, we first consider how the group-velocity profile can be engineered more directly in the short-wavelength part of the spectrum through alternative choices of the glass material from which the PCF is made. We then make simulations of supercontinuum generation in PCFs made of alternative glass materials. It is found that it is possible to increase the blue-shift of the generated supercontinuum through a careful choice of glass composition, provided that the alternative glass composition does not have a significantly higher loss than silica in the near-infrared.

[3] P. M. Moselund, C. L. Thomsen, T. V. Andersen, T. Feuchter, and O. Bang, "Raman seeding of high power picosecond supercontinuum generation," Optics Lett. Submitted.

The effect of Raman seeding high power picosecond supercontinuum generation is investigated under conditions where the Raman gain coincides with the modulation instability gain. It is shown that the presence of a Raman seed from the pump system can significantly degrade the efficiency of supercontinuum generation in the visible region. In addition it is shown that the modulation instability gain and Raman gain spectra typically overlap for photonic crystal fibers made for generating high power visible supercontinuum and that this reduces the efficiency of the modulation instability gain.

P. M. Moselund, M. H. Frosz, C. L. Thomsen and O. Bang "Supercontinuum generation in short PCF tapers", Opt. Express (2009). To be submitted.

Supercontinuum generation in PCF tapers with a length of a few centimeters is investigated for different taper waist widths and different taper lengths. It is shown that these short tapers can generate SC spectra reaching down to 400 nm when pumped with a 1064 nm 14 ps pump. The noise characteristics of the generated SC is remarkably different from that of SC generated in a long untapered PCF and the output pulses are in addition much shorter than from a conventional supercontinuum source. A comparison with simulations is used to show how the soliton dynamics involved in the SC generation process in these tapers is different from those normally observed in ps SC generation in long fibers.

Bibliography

[1] P. M. Moselund, M. H. Frosz, C. Thomsen, and O. Bang, "Back-seeding of higher order gain processes in picosecond supercontinuum generation," Opt. Express **16**(16), 11,954–11,968 (2008). http://www.opticsinfobase.org/abstract.cfm?URI=oe-16-16-11954.

[2] M. H. Frosz, P. M. Moselund, P. D. Rasmussen, C. L. Thomsen, and O. Bang, "Increasing the blue-shift of a supercontinuum by modifying the fiber glass composition," Opt. Express **16**(25), 21,076–21,086 (2008). http://dx.doi.org/10.1364/OE.16.021076.

[3] P. M. Moselund, C. L. Thomsen, T. V. Andersen, T. Feuchter, and O. Bang, "Raman seeding of high power picosecond supercontinuum generation," Optics Lett. (2009). To be submitted.

[4] P. M. Moselund, M. H. Frosz, O. Bang, and C. L. Thomsen, "Back seeding of picosecond supercontinuum generation in photonic crystal fibres," SPIE Europe Proceedings pp. 6990–24 (2008).

[5] P. M. Moselund, M. H. Frosz, C. Thomsen, and O. Bang, "Picosecond supercontinuum generation with back seeding of different spectral parts," in *Procedings of ACOFT* (2008).

[6] P. M. Moselund, M. H. Frosz, C. L. Thomsen, and O. Bang, "Noise Reduction of High-power Supercontinuum sources by Back Seeding," in *Proceedings of CLEO*, p. CD4.2.

[7] R. Alfano and S. Shapiro, "Emission in the region 4000 to 7000 Å via four-photon coupling in glass," Physical Review Letters **24**(11), 584–587 (1970).

[8] J. Ranka, R. Windeler, and A. Stentz, "Visible continuum generation in air-silica microstructure optical fibers with anomalous dispersion at 800 nm," Optics Letters **25**(1), 25–27 (2000).

[9] J. M. Dudley, G. Genty, and S. Coen, "Supercontinuum generation in photonic crystal fiber," Rev. Mod. Phys. **78**(4), 1135–1176 (2006).

[10] A. D. Aguirre, N. Nishizawa, J. G. Fujimoto, W. Seitz, M. Lederer, and D. Kopf, "Continuum generation in a novel photonic crystal fiber for ultrahigh resolution optical coherence tomography at 800 nm and 1300 nm," Opt. Express **14**(3), 1245–1160 (2006). http://www.opticsinfobase.org/abstract.cfm?URI=oe-14-3-1145.

[11] A. Bassi, L. Spinelli, A. Giusto, J. Swartling, A. Pifferi, A. Torricelli, and R. Cubeddu, "Feasibility of white-light time-resolved optical mammography," Journ. of Biomedical Optics **11**(5), 54,035 (2006).

[12] J. H. Frank, A. D. Elder, J. Swartling, A. R. Venkitaraman, A. D. Jeyasekharan, and C. F. Kaminski, "A white light confocal microscope for spectrally resolved multidimensional imaging," Journ. of Microscopy **227**(3), 203–215 (2007).

[13] D. Wildanger, E. Rittweger, L. Kastrup, and S. W. Hell, "STED microscopy with a supercontinuum laser source," Optics Express **16**(13), 9614–9621 (2008).

[14] E. Auksorius, B. Boruah, C. Dunsby, P. Lanigan, G. Kennedy, M. Neil, and P. French, "Stimulated emission depletion microscopy with a supercontinuum source and fluorescence lifetime imaging," Optics Letters **33**(2), 113–115 (2008).

[15] J. H. Lee, K. Lee, Y.-G. Han, S. B. Lee, and C. H. Kim, "Single, Depolarized, CW Supercontinuum-Based Wavelength-Division-Multiplexed Passive Optical Network Architecture With C-Band OLT L-Band ONU, and U-Band Monitoring," Journ. of Lightwave Technology **25**(10), 2891–2897 (2007). http://www.opticsinfobase.org/abstract.cfm?URI=JLT-25-10-2891.

[16] D. J. Jones, S. A. Diddams, J. K. Ranka, A. Stentz, R. S. Windeler, J. L. Hall, and S. T. Cundiff, "Carrier-Envelope Phase Control of Femtosecond Mode-Locked Lasers and Direct Optical Frequency Synthesis," Science **288**(5466), 635–639 and 3075,055 (2000).

[17] R. Holzwarth, T. Udem, T. Hansch, J. Knight, W. Wadsworth, and P. Russell, "Optical frequency synthesizer for precision spectroscopy," Physical Review Letters **85**(11), 2264–2267 (2000).

[18] N. Savage, "Supercontinuum sources," Nature Photonics **3**(2), 114 (2009).

[19] "NKT Annual Report for 2007," (2008).

[20] M. Colladon, "Sur le réflexions d'un rayon de lumière à l'intériure d'une veine liquide parabolique," Hebd. Seances Acad. Sci. (15), 800–

802 (1842). URL http://gallica.bnf.fr/ark:/12148/bpt6k2974q.image.f800.langFR.

[21] M. Barbinet, "Note sur la transmission de la lumière pas de canaux sinueux," Hebd. Seances Acad. Sci. (15), 802 (1842). URL http://gallica.bnf.fr/ark:/12148/bpt6k2974q.image.f802.langFR.

[22] J. Knight, T. Birks, P. St.J. Russell, and D. Atkin, "All-silica single-mode optical fiber with photonic crystal cladding," Optics Letters **21**(19), 1547–1549 (1996).

[23] G. P. Agrawal, *Nonlinear Fiber Optics*, 3rd ed. (Academic Press, San Diego, California, 2001).

[24] I. H. Malitson, "Interspecimen Comparison of the Refractive Index of Fused Silica," J. Opt. Soc. Am. **55**(10), 1205–1210 (1965).

[25] K. Okamoto, *Fundamentals of Optical Waveguides*, 2nd ed. (Academic Press, 2005).

[26] D. Mogilevtsev, T. A. Birks, and P. S. J. Russell, "Group-velocity dispersion in photonic crystal fibers," Opt. Lett. **23**(21), 1662–1664 (1998). URL http://ol.osa.org/abstract.cfm?URI=ol-23-21-1662.

[27] S. G. Leon-Saval, T. A. Birks, W. J. Wadsworth, P. S. Russell, and M. W. Mason, "Supercontinuum generation in submicron fibre waveguides," Optics Express **12**(13), 2864–2869 (2004). http://www.opticsinfobase.org/abstract.cfm?URI=oe-12-13-2864.

[28] S. Johnson and J. Joannopoulos, "Block-iterative frequency-domain methods for Maxwell's equations in a planewave basis," Opt. Express **8**(3), 173–190 (2001). http://www.opticsinfobase.org/abstract.cfm?URI=oe-8-3-173.

[29] J. Zhou, K. Tajima, K. Nakajima, K. Kurokawa, C. Fukai, T. Matsui, and I. Sankawa, "Progress on low loss photonic crystal fibers," Optical Fiber Technology **11**, 101–110 (2005).

[30] "NKT Photonics A/S, product specifications," (2009). http://www.nktphotonics.com/files/files/datasheet_nl-1060-list.pdf.

[31] J. Gowar, *Optical Communication Systems*, 2nd ed. (Prentice Hall Europe, Hertfordshire, UK, 1993).

[32] J. sheng Li and J. rui Li, "Study on Rayleigh scattering of photonic crystal fiber," vol. 6781, p. 678156 (SPIE, 2007). URL http://link.aip.org/link/?PSI/6781/678156/1.

[33] K. Tajima, J. Zhou, K. Nakajima, and K. Sato, "Ultralow Loss and Long Length Photonic Crystal Fiber," J. of Lightwave Tech. **22**(1), 7–10 (2004).

[34] J. Kobelke, K. Gerth, J. Kirchhof, K. Schuster, K. Mörl, and C. Aichele, "Mechanical and optical behavior of index guiding photonic crystal fibers (PCF)," vol. 5360, pp. 287–298 (2004).

[35] J. C. Travers, R. E. Kennedy, S. V. Popov, J. R. Taylor, H. Sabert, and B. Mangan, "Extended continuous-wave supercontinuum generation in a low-water-loss holey fiber," Opt. Letters **30**(15), 1938–1940 (2005). http://www.opticsinfobase.org/abstract.cfm?URI=ol-30-15-1938.

[36] P. Kaiser, "Drawing-induced coloration in vitreous silica fibers," J. Opt. Soc. Am. **64**(4), 475–481 (1974).

[37] V. Finazzi, T. M. Monro, and D. J. Richardson, J. Opt. Soc. Am. B .

[38] V. Finazzi, T. M. Monro, and D. J. Richardson, "The Role of Confinement Loss in Highly Nonlinear Silica Holey Fibers," IEEE Photonics tech. let. **15**(9), 1246–1248 (2003).

[39] K. Saitoh, M. Koshiba, T. Hasegawa, and E. Sasaoka, "Chromatic dispersion control in photonic crystal fibers: application to ultra-flattened dispersion," Opt. Express **11**(8), 843–852 (2003). URL http://www.opticsexpress.org/abstract.cfm?URI=oe-11-8-843.

[40] N. A. Mortensen, J. R. Folkenberg, M. D. Nielsen, and K. P. Hansen, "Modal cutoff and the V parameter in photonic crystal fibers," Opt. Lett. **28**(20), 1879–1881 (2003). URL http://ol.osa.org/abstract.cfm?URI=ol-28-20-1879.

[41] T. A. Birks, J. C. Knight, and P. S. Russell, "Endlessly single-mode photonic crystal fiber," Opt. Lett. **22**(13), 961–963 (1997). URL http://ol.osa.org/abstract.cfm?URI=ol-22-13-961.

[42] K. Kim, R. Stolen, W. Reed, and K. Quoi, "Measurement of the nonlinear index of silica-core and dispersion-shifted fibers," Optics Letters **19**(4), 257–259 (1994).

[43] D. Milam, "Review and assessment of measured values of the nonlinear refractive-index coefficient of fused silica," Applied Optics **37**(3), 546–550 (1998).

[44] C. V. Raman, "A new Radiation," Indian J. Phys **2**, 387–398 (1928).

[45] R. H. Stolen, E. P. Ippen, and A. R. Tynes, "Raman oscillation in glass optical Waveguide," Appl. Phys. Lett. **20**(2), 62–64 (1972).

[46] K. Rottwitt, "Raman Amplifiers in Optical Fibers: Principles and Applications," Dr.techn thesis, Technical University of Denmark, DTU Fotonik, Building 343, 2800 Lyngby, Denmark (2008). http://www.fotonik.dtu.dk/English/Service/Phonebook.aspx?lg=showcommon&id=234444.

[47] K. Furusawa, Z. Yusoff, F. Poletti, T. Monro, N. Broderick, and D. Richardson, "Brillouin characterization of holey optical fibers," Optics Letters **31**(17), 2541–2543 (2006).

[48] K. Furusawa, Z. Yusoff, F. Poletti, T. M. Monro, N. G. R. Broderick, and D. J. Richardson, "Brillouin characterization of holey optical fibers," Opt. Lett. **31**(17), 2541–2543 (2006). URL http://ol.osa.org/abstract.cfm?URI=ol-31-17-2541.

[49] T. Benjamin and J. Feir, "The disintegration of wave trains on deep water. I. Theory," Journal of Fluid Mechanics **27**, 417–430 (1967).

[50] A. Hasegawa, "Observation of self-trapping instability of a plasma cyclotron wave in a computer experiment," Physical Review Letters **24**(21), 1165–1168 (1970).

[51] K. Tai, A. Hasegawa, and A. Tomita, "Observation of modulation instability in optical fibers," Physical Review Letters **56**(2), 135–138 (1986).

[52] A. Hasegawa and W. Brinkman, "Tunable coherent IR and FIR sources utilizing modulational instability," IEEE Journal of Quantum Electronics **16**(7), 694–697 (1980).

[53] M. H. Frosz, T. Soerensen, and O. Bang, "Nanoengineering of photonic crystal fibers for supercontinuum spectral shaping," J. Opt. Soc. Am. B **23**(8), 1692–1699 (2006). http://www.opticsinfobase.org/abstract.cfm?URI=josab-23-8-1692.

[54] J. M. Dudley, G. Genty, and B. J. Eggleton, "Harnessing and control of optical rogue waves in supercontinuum generation," Opt. Express **16**(4), 3644–3651 (2008). http://www.opticsinfobase.org/abstract.cfm?URI=oe-16-6-3644.

[55] G. Genty, J. M. Dudley, and B. J. Eggleton, "Modulation control and spectral shaping of optical fiber supercontinuum generation in the picosecond regime," Appl. Phys. B **94**(2), 187–194 (2009).

[56] D. R. Solli, C. Ropers, and B. Jalali, "Active Control of Rogue Waves for Stimulated Supercontinuum Generation," Phys. Rev. Lett. **101**(23), 233902 (2008). URL http://link.aps.org/abstract/PRL/v101/e233902.

[57] J. Herrmann and A. Nazarkin, "Soliton self-frequency shift for pulses with a duration less than the period of molecular oscillations," Optics Letters **19**(24), 2065–2067 (1994).

[58] N. Akhmediev and M. Karlsson, "Cherenkov radiation emitted by solitons in optical fibers," Physical Review A (Atomic, Molecular, and Optical Physics) **51**(3), 2602–2607 (1995).

[59] D. V. Skryabin, F. Luan, J. C. Knight, and P. S. J. Russell, "Soliton Self-Frequency Shift Cancellation in Photonic Crystal Fibers," Science **301**, 1705–1708 (2003).

[60] O. Bang and M. Peyrard, "Generation of high-energy localized vibrational modes in nonlinear Klein-Gordon lattices," Phys. Rev. E **53**(4), 4143–4152 (1996).

[61] M. Islam, G. Sucha, I. Bar-Joseph, M. Wegener, J. Gordon, and D. Chemla, "Femtosecond distributed soliton spectrum in fibers," J. Opt. Soc. Am. B **6**(6), 1149–1158 (1989).

[62] F. Luan, D. Skryabin, A. Yulin, and J. Knight, "Energy exchange between colliding solitons in photonic crystal fibers," Opt. Express **14**(21) (2006).

[63] M. H. Frosz, O. Bang, and A. Bjarklev, "Soliton collision and Raman gain regimes in continuous-wave pumped supercontinuum generation," Opt. Express **14**(20), 9391–9407 (2006). http://www.opticsinfobase.org/abstract.cfm?URI=oe-14-20-9391.

[64] D. R. Solli, C. Ropers, P. Koonath, and B. Jalali, "Optical rogue waves," Nature **450**, 1054–1058 (2007).

[65] A. V. Gorbach and D. V. Skryabin, "Light trapping in gravity-like potentials and expansion of supercontinuum spectra in photonic-crystal fibres," Nature Photonics **1**(11), 653 (2007).

[66] A. V. Gorbach and D. V. Skryabin, "Theory of radiation trapping by the accelerating solitons in optical fibers," Physical Review A (Atomic, Molecular, and Optical Physics) **76**(5), 053803 (pages 10) (2007). URL http://link.aps.org/abstract/PRA/v76/e053803.

[67] T. P. Goldsmith, S. Coen, J. D. Harvey, and F. Vanholsbeeck, "Cancellation of Raman soliton self-frequency shift by cross-phase modulation," p. 231 (2005).

[68] J. Koplow, "Fused-silica damage threshold established at 1064 nm," Laser Focus World (2008). http://www.laserfocusworld.com/display_article/328494/12/none/none/NBrea/Fused-silica-damage-threshold-established-at-1064-nm.

[69] L. A. Siiman, J. Lumeau, and L. B. Glebov, "Nonlinear photosensitivity of photo-thermo-refractive glass by high intensity laser irradiation," J. of Non-Crystalline Solids **354**, 4070 (2008).

[70] B. C. Stuart, M. D. Feit, A. M. Rubenchik, B. W. Shore, and M. D. Perry, "Laser-Induced Damage in Dielectrics with Nanosecond to Subpicosecond Pulses," Phys. Rev. Lett. **74**(12), 2248–2252 (1995).

[71] I. M. Azzouz, "Investigation of photoionization processes in ultrashort laser induced damage in optical materials," J. Phys. B **37**, 3259 (2004).

[72] Y. Kodama and A. Hasegawa, "Nonlinear Pulse Propagation in a Monomode Dielectric Guide," IEEE J. of Quantum Elec. **23**(5), 510–524 (1987).

[73] J. C. Travers, S. V. Popov, and J. R. Taylor, "Extended blue supercontinuum generation in cascaded holey fibers," Opt. Letters **30**(23), 3132–3134 (2005). http://www.opticsinfobase.org/abstract.cfm?URI=ol-30-23-3132.

[74] R. B. Ettlinger and P. M. Moselund, "Superkontinuum - et glimt fra en eksperimentel ph.d," Gamma (150), 18–29 (2008). http://www.gamma.nbi.dk/Galleri/gamma150/superkontinuum.ps.gz.

[75] P. M. Moselund, M. H. Frosz, C. L. Thomsen, and O. Bang, "Back-seeded Higher-Order Parametric Gain in Supercontinuum Generation," Optics and Photonics News : Optics In 2008, Nonlinear Optics **19**(12), 35 (2008).

[76] J. H. Lee, K. Katoh, and K. Kikuchi, "Experimental investigation of continuous-wave supercontinuum ring laser composed of clad-pumped Er/Yb codoped fiber and highly-nonlinear optical fiber," Opt. Commun. **266**, 281–286 (2006).

[77] J. H. Lee and K. Kikuchi, "Experimental performance comparison for various continuous-wave supercontinuum schemes: ring cavity and single pass structures," Opt. Express **13**(13), 4848–4853 (2005). http://www.opticsinfobase.org/abstract.cfm?URI=oe-13-13-4848.

[78] W. Zhang, Y. Wang, J. Peng, and X. Liu, "Broadband high power continuous wave fiber Raman source and its applications," Opt. Commun. **231**, 371–374 (2004).

[79] M. Feng, Y. G. Li, J. Li, J. F. Li, L. Ding, and K. C. Lu, "High-Power Supercontinuum Generation in a Nested Linear Cavity Involving a CW Raman Fiber Laser," IEEE Photonics Technology Letters **17**(6), 1172–1174 (2005).

[80] Y. Deng, Q. Lin, F. Lu, G. P. Agrawal, and W. H. Knox, "Broadly tunable femtosecond parametric oscillator using a photonic crystal fiber," Opt. Letters **30**(10), 1234–1236 (2005). http://www.opticsinfobase.org/abstract.cfm?URI=ol-30-10-1234.

[81] D.-I. Yeom, J. A. Bolger, G. D. Marshall, D. R. Austin, B. T. Kuhlmey, M. J. Withford, C. M. de Sterke, and B. J. Eggleton, "Tunable spectral enhancement of fiber supercontinuum," Opt. Letters **32**(12), 1644–1646 (2007). http://www.opticsinfobase.org/abstract.cfm?URI=ol-32-12-1644.

[82] K. Iizuka, *Elements of Photonics, Volume I*, 1st ed. (John Wiley & Sons, New York, N.Y., 2002).

[83] B. A. Cumberland, J. C. Travers, S. V. Popov, and J. R. Taylor, "29 W High power CW supercontinuum source," Opt. Express **16**(8), 5954–5962 (2008). http://www.opticsinfobase.org/abstract.cfm?URI=oe-16-8-5954.

[84] T. T. Alkeskjold, "Personal communication," NKT Photonics A/S .

[85] K. M. Hilligsøe, T. V. Andersen, H. N. Paulsen, C. K. Nielsen, S. Keiding, K. Moelmer, R. Kristiansen, K. P. Hansen, and J. J. Larsen, "Supercontinuum generation in a photonic crystal fiber with two zero dispersion wavelengths," Opt. Express **12**(6), 1045–1054 (2004). http://www.opticsinfobase.org/abstract.cfm?URI=oe-12-6-1045.

[86] G. Genty, M. Lehtonen, and H. Ludvigsen, "Effect of cross-phase modulation on supercontinuum generated in microstructured fibers with sub-30 fs pulses," Opt. Express **12**(19), 4614–4624 (2004). http://www.opticsinfobase.org/abstract.cfm?URI=oe-12-19-4614.

[87] T. Schreiber, T. V. Andersen, D. Schimpf, J. Limpert, and A. Tünnermann, "Supercontinuum generation by femtosecond single and dual wavelength pumping in photonic crystal fibers with two zero dispersion wavelengths," Opt. Express **13**(23), 9556–9569 (2005). http://www.opticsinfobase.org/abstract.cfm?URI=oe-13-23-9556.

[88] A. Efimov, A. J. Taylor, F. G. Omenetto, A. V. Yulin, N. Y. Joly, F. Biancalana, D. V. Skryabin, J. C. Knight, and P. S. Russell, "Time-spectrally-resolved ultrafast nonlinear dynamics in small-core photonic crystal fibers: Experiment and modelling," Opt. Express **12**(26), 6498–6507 (2004). http://www.opticsinfobase.org/abstract.cfm?URI=oe-12-26-6498.

[89] M. H. Frosz, P. Falk, and O. Bang, "The role of the second zero-dispersion wavelength in generation of supercontinua and

bright-bright soliton-pairs across the zero-dispersion wavelength," Opt. Express **13**(16), 6181–6192 (2005). http://www.opticsinfobase.org/abstract.cfm?URI=oe-13-16-6181 + Erratum, Opt. Exp. **15**, pp. 5262–5263 (2007), http://www.opticsinfobase.org/abstract.cfm?URI=oe-15-8-5262.

[90] M. H. Frosz, P. Falk, and O. Bang, "Supercontinuum generation in a photonic crystal fiber with two zero-dispersion wavelengths tapered to normal dispersion at all wavelengths," Opt. Express **13**(19), 7535–7540 (2005). http://www.opticsinfobase.org/abstract.cfm?URI=oe-13-19-7535.

[91] M. L. V. Tse, P. Horak, F. Poletti, N. G. R. Broderick, J. H. V. Price, J. R. Hayes, and D. J. Richardson, "Supercontinuum generation at 1.06 μm in holey fibers with dispersion flattened profiles," Opt. Express **14**(10), 4445–4451 (2006). http://www.opticsinfobase.org/abstract.cfm?URI=oe-14-10-4445.

[92] P. Falk, M. H. Frosz, O. Bang, L. Thrane, P. E. Andersen, A. O. Bjarklev, K. P. Hansen, and J. Broeng, "Broadband light generation around 1300 nm through spectrally recoiled solitons and dispersive waves," Opt. Letters **33**(6), 621–623 (2008). http://www.opticsinfobase.org/abstract.cfm?URI=ol-33-6-621.

[93] G. Genty, S. Coen, and J. M. Dudley, "Fiber supercontinuum sources," J. Opt. Soc. Am. B **24**(8), 1771–1785 (2007).

[94] A. Kudlinski, G. Bouwmans, Y. Quiquempois, and A. Mussot, "Experimental demonstration of multiwatt continuous-wave supercontinuum tailoring in photonic crystal fibers," Appl. phys. lett. **92**(14), 141,103 (2008).

[95] A. Mussot, M. Beaugeois, M. Bouazaoui, and T. Sylvestre, "Tailoring CW supercontinuum generation in microstructured fibers with two-zero dispersion wavelengths," Opt. Express **15**(18), 11,553–11,563 (2007). http://www.opticsinfobase.org/oe/abstract.cfm?URI=oe-15-18-11553.

[96] S. Martin-Lopez, L. Abrardi, P. Corredera, M. Gonzalez-Herraez, and A. Mussot, "Spectrally-bounded continuous-wave supercontinuum generation in a fiber with two zero-dispersion wavelengths," Opt. Express **16**(9), 6745–6755 (2008). http://www.opticsinfobase.org/abstract.cfm?URI=oe-16-9-6745.

[97] M. H. Frosz, "Supercontinuum Generation in Photonic Crystal Fibres," Phd thesis, Technical University of Denmark, DTU Fotonik, Building 343, 2800 Lyngby, Denmark (2006).

[98] K. P. Hansen, J. R. Jensen, C. Jacobsen, H. R. Simonsen, J. Broeng, P. M. Skovgaard, A. Petersson, and A. Bjarklev, "Highly nonlinear photonic crystal fiber with zero-dispersion at 1.55 μm," Conference on Optical Fiber Communication **70**, FA91–FA93 (2002).

[99] N. Akhmediev and M. Karlsson, "Cherenkov radiation emitted by solitons in optical fibers," Phys. Rev. A **51**, 2602–2607 (1995).

[100] D. R. Solli, C. Ropers, and B. Jalali, "Stimulated supercontinuum generation: Acceleration, stabilization and control," LEOS 2008 - 21st Annual Meeting of the IEEE Lasers and Electro-Optics Society (LEOS 2008) Proceedings pp. 733–734 (2008).

[101] D. R. Solli, C. Ropers, and B. Jalali, "Demonstration of Stimulated Supercontinuum Generation - An Optical Tipping Point," (2008). URL http://www.citebase.org/abstract?id=oai:arXiv.org:0801.4066.

[102] J. M. Stone and J. C. Knight, "Visibly "white" light generation in uniformphotonic crystal fiber using a microchip laser," Opt. Express **16**(4), 2670–2675 (2008). URL http://www.opticsexpress.org/abstract.cfm?URI=oe-16-4-2670.

[103] A. Kudlinski, A. K. George, J. C. Knight, J. C. Travers, A. B. Rulkov, S. V. Popov, and J. R. Taylor, "Zero-dispersion wavelength decreasing photonic crystal fibers for ultraviolet-extended supercontinuum generation," Opt. Express **14**(12), 5715–5722 (2006). http://www.opticsinfobase.org/abstract.cfm?URI=oe-14-12-5715.

[104] J. Ranka, R. Windeler, and A. Stentz, "Optical properties of high-delta air-silica microstructure optical fibers," Optics Letters **25**(11), 796–798 (2000).

[105] S. Yan, "Effect of stimulated- Raman-scattering on modulation instability in anomalous-dispersion regime of fiber," vol. 7136, p. 713646 (2008). URL http://link.aip.org/link/?PSI/7136/713646/1.

[106] W. Shuang-Chun, S. Wen-Hua, Z. Hua, F. Xi-Quan, Q. Lie-Jia, and F. Dian-Yuan, "Influence of Higher-Order Dispersions and Raman Delayed Response on Modulation Instability in Microstructured Fibres," Chin. Phys. Lett. **20**(6), 852–854 (2003).

[107] F. Vanholsbeeck, P. Emplit, and S. Coen, "Complete experimental characterization of the influence of parametric four-wave mixing on stimulated Raman gain," Opt. Lett. **28**(20), 1960–1962 (2003).

[108] H. N. Paulsen, K. M. Hilligsøe, J. Thøgersen, S. R. Keiding, and J. J. Larsen, "Coherent anti-Stokes Raman scattering microscopy with a photonic crystal fiber based light source," Opt. Lett

28(13), 1123–1125 (2003). http://www.opticsinfobase.org/abstract.cfm?URI=ol-28-13-1123.

[109] R. Bhattacharya and S. Konar, "Design of a photonic crystal fiber with zero dispersion wavelength near 0.65 μm," Fiber and Integrated Optics **27**(2), 89–98 (2008).

[110] J. C. Travers, "Controlling nonlinear optics with dispersion in photonic crystal fibres," Phd thesis, Imperial College London, Imperial College London, South Kensington Campus, London SW7 2AZ (2008). https://155.198.5.37:8443/handle/10044/1/1362.

[111] J. C. Travers and J. R. Taylor, "Soliton trapping of dispersive waves in tapered optical fibers," Opt. Lett. **34**(2), 115–117 (2009). URL http://ol.osa.org/abstract.cfm?URI=ol-34-2-115.

[112] Y. Mazhirina, A. Konyukhov, and L. Melnikov, "Pulse Spectral Broadening in Microstructured Optical Fiber with Periodically Modulated Core Diameter," vol. 4, pp. 241–244 (2006).

[113] J. Cascante-Vindas, A. Diez, J. Cruz, M. Andrés, E. Silvestre, J. Miret, and A. Ortigosa-Blanch, "Tapering photonic crystal fibres for supercontinuum generation with nanosecond pulses at 532 nm," Opt. Commun. **281**, 433–438 (2008).

[114] C. Xiong, A. Witkowska, S. G. Leon-Saval, T. A. Birks, and W. J. Wadsworth, "Enhanced visible continuum generation from a microchip 1064 nm laser," Optics Express **14**(13), 6188–6193 (2006). http://www.opticsinfobase.org/abstract.cfm?URI=oe-14-13-6188.

[115] J. Laegsgaard, "Mode profile dispersion in the generalised nonlinear Schrödinger equation," Opt. Express **15**(24), 16,110–16,123 (2007). URL http://www.opticsexpress.org/abstract.cfm?URI=oe-15-24-16110.

[116] J. Lægsgaard, N. A. Mortensen, and A. Bjarklev, "Mode areas and field-energy distribution in honeycomb photonic bandgap fibers," J. Opt. Soc. Am. B **20**(10), 2037–2045 (2003). http://www.opticsinfobase.org/abstract.cfm?URI=josab-20-10-2037.

[117] K. J. Blow and D. Wood, "Theoretical description of transient stimulated Raman scattering in optical fibers," IEEE J. Quantum Electron. **25**, 2665–2673 (1989).

[118] O. V. Sinkin, R. Holzlöhner, J. Zweck, and C. R. Menyuk, "Optimization of the Split-Step Fourier Method in Modeling Optical-Fiber Communications Systems," J. Lightwave Technol. **21**(1), 61–68 (2003). http://dx.doi.org/10.1109/JLT.2003.808628.

[119] S. B. Cavalcanti, G. P. Agrawal, and M. Yu, "Noise amplification in dispersive nonlinear media," Phys. Rev. A **51**(5), 4086–4092 (1995). http://dx.doi.org/10.1103/PhysRevA.51.4086.

[120] A. Mussot, E. Lantz, H. Maillotte, T. Sylvestre, C. Finot, and S. Pitois, "Spectral broadening of a partially coherent CW laser beam in single-mode optical fibers," Opt. Express **12**(13), 2838–2843 (2004). http://www.opticsexpress.org/abstract.cfm?URI=OPEX-12-13-2838.

[121] J. R. Folkenberg, N. A. Mortensen, K. P. Hansen, T. P. Hansen, H. R. Simonsen, and C. Jakobsen, "Experimental investigation of cutoff phenomena in nonlinear photonic crystal fibers," Opt. Lett. **28**(20), 1882–1884 (2003). URL http://ol.osa.org/abstract.cfm?URI=ol-28-20-1882.

[122] H. C. Nguyen, B. T. Kuhlmey, M. J. Steel, C. L. Smith, E. C. Mägi, R. C. McPhedran, and B. J. Eggleton, "Leakage of the fundamental mode in photonic crystal fiber tapers," Opt. Lett. **30**(10), 1123–1125 (2005). URL http://ol.osa.org/abstract.cfm?URI=ol-30-10-1123.

[123] B. Kuhlmey, R. McPhedran, C. de Sterke, P. Robinson, G. Renversez, and D. Maystre, "Microstructured optical fibers: where's the edge?" Opt. Express **10**(22), 1285–1290 (2002). URL http://www.opticsexpress.org/abstract.cfm?URI=oe-10-22-1285.

[124] B. Kuhlmey, R. McPhedran, and C. Martijn de Sterke, "Modal cutoff in microstructured optical fibers," Optics Letters **27**(19), 1684–1686 (2002).